SURFACE AND BULK PROPERTIES OF MAGNETICALLY DOPED GaN AND THEIR DEPENDENCE ON THE GROWTH CONDITIONS

A dissertation presented to
the faculty of
the College of Arts and Sciences of Ohio University

In partial fulfillment
of the requirements for the degree
Doctor of Philosophy

Muhammad Baseer Haider
November 2005

This dissertation entitled

SURFACE AND BULK PROPERTIES OF MAGNETICALLY DOPED GaN AND THEIR DEPENDENCE ON THE GROWTH CONDITIONS

by

MUHAMMAD BASEER HAIDER

has been approved
for the Department of Physics & Astronomy
and the College of Arts and Sciences by

Arthur R. Smith
Associate Professor of Physics & Astronomy

Benjamin M. Ogles
Interim Dean, College of Arts and Sciences

Haider, Muhammad. Ph.D. November 2005. Physics & Astronomy

Surface and Bulk Properties of Magnetically Doped GaN and Their Dependence on the Growth Conditions (123pp.)
Director of Dissertation: Arthur R. Smith

MnGaN and CrGaN thin films were grown by molecular beam epitaxy on MOCVD GaN(0001)/sapphire(0001) and sapphire(0001) substrates respectively. Dependence of structural and magnetic properties of MnGaN and CrGaN samples on Ga/N flux ratios were investigated. Scanning tunneling microscopy studies of c-GaN(001) were performed to understand the surface reconstructions of this material, as Mn doped c-GaN has been predicted to have a Curie temperature about 6% higher compared to Mn-doped wurtzite GaN.[1]

MnGaN samples were grown on MOCVD GaN(0001)/sapphire(0001) at substrate temperature of 550 °C under different Ga/N flux ratios leading to 4 different growth regimes: N-rich, slight metal-rich, metal-rich, and Ga-rich. Mn incorporation and hence magnetic properties clearly depend on the growth conditions. The N-rich grown sample exhibits much larger magnetization compared to the other samples. Ga-rich magnetization is attributed to accumulates, but N-rich magnetization is attributed to carrier-mediated ferromagnetism and/or ferromagnetism due to clusters.

Influence of the growth conditions on structural and magnetic properties of CrGaN on sapphire(0001) has been investigated. CrGaN samples are grown under different Ga/N flux ratio of 65% to 100% at substrate temperatures of 650 and 700 °C by rf N-plasma molecular beam epitaxy. The Cr/Ga flux ratio is set to either 3% or 5%. These growth parameters allow to vary over a range of growth conditions from N-rich to Ga-rich. Surface conditions during growth influence the surface morphology and magnetic properties of CrGaN films. In particular, we show that N-rich and metal-rich growth conditions result in room temperature ferromagnetism.

Scanning tunneling microscopy studies have been performed on c-GaN(001) grown by rf N-plasma molecular beam epitaxy. Scanning tunneling microscopy studies of c-GaN (001) reveal several surface reconstructions including 4×11, c(4×20), 4×9, c(4×16), 4×7, and c(4×12). These reconstructions depend on the surface Ga coverage with 4×11 having the highest Ga coverage and c(4×12) having the lowest Ga coverage per unit area. The reconstruction which is most commonly found on the surface is c(4×16). Scanning tunneling spectroscopy results suggest that c(4×16) reconstruction is in metallic state.

Approved:

Arthur R. Smith
Associate Professor of Physics & Astronomy

To my parents, my wife,
and my brothers

Acknowledgments

"By the name of Allah, Most merciful Most beneficial".

First I would like to thank my advisor Dr. Arthur R. Smith for his guidance and help in the completion of this work, without whom I may not be able to accomplish this. I would also like to thank my parents Haji Ghulam Haider and Parveen Haider who worked really hard through out their life for me to reach at this position. Also I would like to thank my wife Adiba Maryum for her patience and encouragement during my PhD and thanks to my brothers for their well wishes for me. I would also like to thank my collaborators Dr. David C. Ingram and Dr. Eugene Trifan for Rutherford backscattering measurements. Also, I would like to thank Dr. Charles J. O'Connor and Dr. Gabriel Caruntu for their help in measuring magnetic properties of our samples. Also I would like to extend my thanks to my committee members Dr. Saw W. Hla, Dr. David C. Ingram and Dr. P. Gregory Van Patten for reviewing the dissertation. I would also like to extend my thanks to all of my colleagues in the lab: Dr. Hamad Al-Brithen, Dr. Haiqian Yang, Dr. Costel Constantin, and Rong Yang for their help and support in this work. Finally I would like to thank the staff of department of Physics and Astronomy for their help and kindness through out my stay here at Ohio University.

Table of Contents

List of Tables

List of Figures

Chapter 1

Introduction

Spintronics has attracted a lot of interest in past several decades, where not only charge property of electrons but spin can also be used. A recent example in the field of spintronics is the creation of Giant Magnetoresistive effect (GMR) where resistance of certain materials is dropped dramatically in the presence of a magnetic field. The GMR is formed by a junction of two magnetic materials where the direction of spin of one of the magnetic material can be reversed by applying a strong magnetic field. The GMR is now being used in practical devices like magnetic read head for hard drives and magnetoresistive random access memory (MRAM). The great success of GMR strengthened the idea of injecting highly polarized spins into well established semiconductor heterostructures to form spin field effect transistors, spin light emitting diodes, and quantum bits for quantum computing. Spin injection can be achieved by growing magnetic materials on top of the semiconductor heterostructures. But one of the problems with this approach is that ferromagnetic materials like Fe, Co and Ni do not grow epitaxially on the semiconductors and may form some magnetically dead layers at the ferromagnetic/semiconductor interface. These magnetic dead layers act as spin scattering centers and highly polarized spins in the ferromagnetic material do not remain as polarized in the semiconducting materials.[2, 3, 4]

Another approach is to grow transition metal doped semiconductors, which can be used as semiconductors as well as ferromagnetic materials. The advantage of using this approach is that the material can be grown epitaxially on the semiconductor heterostructures and hence spin injection can be much more polarized compared to the ferromagnetic/semiconductor structures.

Dietl *et al.* proposed that Mn doped GaN can be grown as a dilute magnetic semiconductor with a Curie temperature higher than room temperature.[1] There are many reports of the experimental study of Mn doped GaN. Some of these reports show ferromagnetic behavior but with different Curie temperatures ranging from 10K to 940K.[5, 6, 7, 8, 9] Some report a change in the lattice constant of GaN due to Mn doping but again some show increase in the lattice constant and some show decrease in the lattice constant. Similar discrepancies exist for the RHEED patterns, some report streaky RHEED and some report not so streaky RHEED pattern of MnGaN films. As streaky RHEED pattern is an indication of smooth two dimensional growth whereas spotty RHEED pattern is an indication of rough three dimensional growth. These two different kind of RHEED patterns indicate different growth modes and the properties of the films grown under two different growth modes can be quite different from each other. We think that there was a need for a systematic growth study where one can grow the samples under different growth conditions and then study the properties of the films and their correlation with the growth modes.

We have performed a systematic growth study of wurtzite MnGaN to address the discrepancies in the structural and magnetic properties of this material. Our goal is not only to find the optimal MnGaN sample which gives best magnetic properties but to completely understand the growth of this material and how the growth is affected by different parameters like Ga/N flux ratio. To understand the growth of MnGaN, it is important to understand the growth of its binary components MnN and GaN. It is known that in case of Mn_xN_y, Mn prefers octahedral bonding with N, leading to tetragonal rock-salt type phases.[10, 11, 12, 13, 14] In case of GaN, Ga prefers tetrahedral bonding with N and forms mainly wurtzite phase. GaN can be grown under two different growth conditions Ga-rich and N-rich. A rough three dimensional growth is observed under N-rich growth conditions and a spotty RHEED pattern is observed during and after the growth. Whereas under Ga-rich growth conditions a smooth two dimensional growth is achieved and a streaky RHEED pattern is observed. As well as after the growth and after cooling down to below 300 °C, surface reconstructions are observed formed by Ga ad-atoms. Richness of the GaN film depends on the Ga/N flux ratio. If the flux ratio is less than 100% then the film is N-rich and if the Ga/N flux ratio is equal and above 100% then Ga-rich film is formed. GaN can be grown under two different polarities namely Ga-polar and N-polar. GaN grown on MOCVD GaN(0001)/sapphire(0001) substrate leads to Ga-polar GaN(0001) film and the polarity of the MBE grown GaN is N-polar [GaN(000$\bar{1}$] if it is grown on sapphire(0001) substrate. In case of Ga-polar GaN, Ga form three back bonds with N whereas in case of N-polar GaN, N form three back bonds with Ga. Moreover, in case of Ga-polar Ga-rich GaN, a Ga bi-layer exists on the surface as shown in Fig. 1.1 and the typical surface reconstructions observed after the growth and after cooling the sample below 300 °C are 2×2, 5×5, 6×4 and ”1×1” formed by Ga ad-atoms.[15, 16, 17, 18] In case of N-polar Ga-rich GaN, a Ga ad-layer exists on the surface as is shown in Fig. 1.1 and the surface reconstructions observed after the growth and after cooling the sample below 300 °C are 1×1, 3×3, 6×6 and c6×12, which are also formed by Ga ad-atoms.[16]

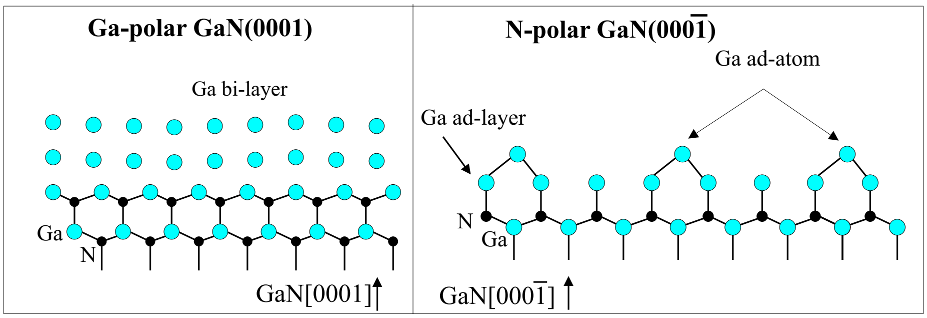

Figure 1.1: Schematic atomic models of Ga-rich Ga-polar and N-polar GaN

We have performed the growth of MnGaN by changing the Ga/N flux ratios and have observed that depending on the Ga/N flux ratios, MnGaN can be grown under three different growth conditions namely N-rich, Ga-poor but metal-rich and Ga-rich growth conditions. Samples grown under these three growth conditions have totally different surface structures and magnetic properties.

By using the *ab initio* electronic structure calculations within the local spin density approximations, Sato *et al.* predicted that Mn and Cr doped GaN have stable ferromagnetic states as compared to the spin glass state.[19] In the case of Mn, they have predicted that the ferromagnetic state is stable at lower concentrations of Mn (e.g 5%), whereas at higher concentration of Mn (e.g 25%), the spin glass state becomes more stable and the material is no longer ferromagnetic. Whereas in the case of Cr, the ferromagnetic state becomes even more stable with the increasing concentration of Cr. In the case of Cr, the minimum concentration of Cr is proposed to be above 2%.

Recently a few results have been reported about the growth and bulk properties of CrGaN. Lee *et al.* have used ion implantation of Cr on Mg doped MOCVD grown GaN on sapphire substrate.[20] Park *et al.* performed the growth of Cr doped GaN single crystal by sodium flux method.[21] Hashimoto *et al.* reported the growth and above room temperature ferromagnetism in CrGaN samples which were grown on sapphire(0001) by electron-cyclotron plasma-assisted molecular beam epitaxy (MBE).[22] Liu *et al.* have reported the observation of ferromagnetism in Cr-GaN above 900K which was grown by reactive molecular beam epitaxy.[23]

We have performed the growth studies using rf N-plasma MBE for wurtzite CrGaN on sapphire substrate to understand the growth of this material and not just to grow a sample that exhibits ferromagnetic properties. We have found that depending on the Ga/N flux ratio wurtzite N-polar CrGaN can also be grown under three different growth conditions N-rich, metal-rich, and Ga-rich growth conditions. These growth conditions also affect the surface structure and the magnetic properties of CrGaN.

The Curie temperature(T_C) for Mn doped zinc-blende GaN (c-GaN) is predicted to be about 6% higher compared to the T_C for Mn doped wurtzite GaN.[1] To understand the growth and behavior of ternary c-MnGaN, it is important to understand the growth and surface structure of its binary host lattice c-GaN. Since the surface reconstructions of c-GaN are not well understood, we have performed extensive STM studies of c-GaN surface. We have found a family of intrinsic surface reconstructions on c-GaN surface which helped us to better understand this material.

The work in this dissertation is divided into four main parts. The first part is an introduction to wurtzite and zinc-blende GaN and STM studies of zinc-blende GaN. The second part consists of the growth and analysis of MnGaN on MOCVD GaN(0001) / sapphire(0001) grown by rf plasma MBE. The third part consists of growth and analysis of CrGaN on sapphire(0001) grown by rf plasma MBE. In the fourth part, results of the STM studies of CrGaN are presented.

Chapter one is an overall introduction of the work presented in this dissertation. Chapter two includes a brief description of the instruments, which are used in the laboratory to study MnGaN, CrGaN and c-GaN systems.

Chapter three includes a brief introduction of both N-polar and Ga-polar wurtzite GaN surfaces and also the STM studies of zinc-blende GaN surface are discussed.

Chapter four includes the surface and bulk properties of MnGaN grown on MOCVD GaN(0001)/sapphire(0001). Growth conditions, polarity, and Mn incorporation are discussed in this chapter.

Chapter five includes the dependence of magnetic properties of MnGaN system on the growth conditions.

Chapter six includes the surface and bulk properties of CrGaN samples grown on Sapphire(0001) substrates, including the surface morphology during and after the growth, and effect of Cr on the GaN surface. Growth conditions are also discussed and how they affect the surface morphology of N-polar CrGaN surface.

Chapter seven includes the results of STM studies of the CrGaN surface. We have found that at least on the surface, Cr substitutes the Ga lattice position.

Chapter eight is a summary of the MnGaN, CrGaN and c-GaN results.

There are two appendices at the end, first includes the list of published work in refereed journals, and second appendix includes the list of talks and posters presented in the conferences.

Chapter 2

Instruments

2.1 Molecular Beam Epitaxy Chamber

The molecular beam epitaxy chamber is an ultra high vacuum custom designed chamber with four ports for the sources (e.g gallium, manganese, chromium and iron), and radio frequency (rf) plasma is used for nitrogen. The growth chamber pressure is kept in the order of 10^{-11} Torr, and the pressure is monitored by an ion gauge which can function in the range of 10^{-4}-10^{-11} Torr. A closed cycle ^{4}He cryo pump is used to achieve the ultra high vacuum in the growth chamber. The growth chamber is attached to an analysis chamber, which houses a home built, room temperature scanning tunneling microscope (STM). We can transfer the grown samples from the MBE growth chamber to the analysis chamber for STM studies without exposing them to air. Shown in Fig. 2.1 is a photograph of our MBE chamber.

Effusion cells are used for gallium, manganese, and chromium sources, whereas electron beam evaporation cell is used for the iron source. Sources are held in the effusion cell inside a ceramic crucible, and the fluxes of the sources are controlled by adjusting the temperatures of the effusion cells. Whereas in the case of e-beam cells, a tungsten filament is heated and electrons are bombarded onto the solid rod shaped source, which is kept at a potential difference of about 1.5-2.0 kV with respect to the filament.

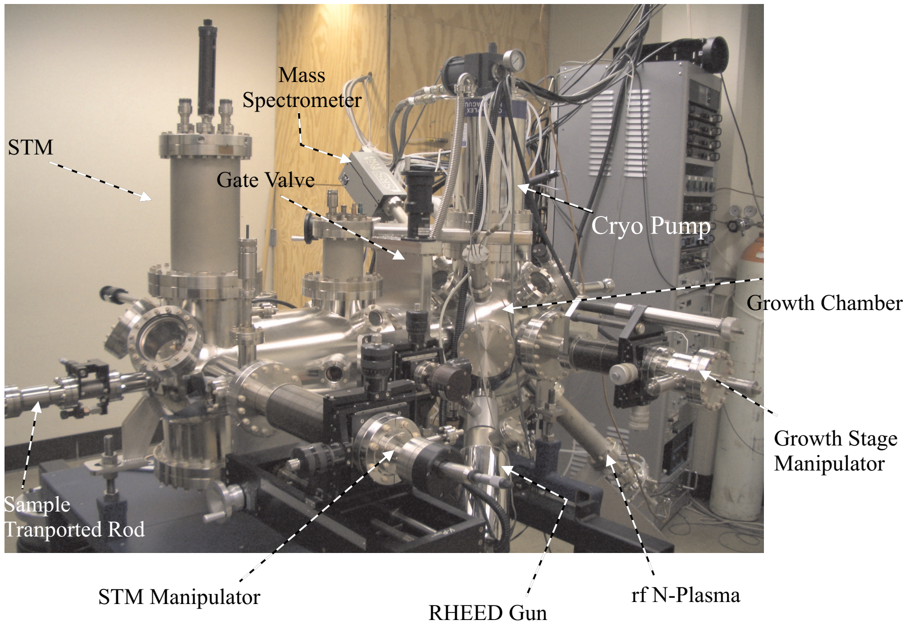

Figure 2.1: A photograph of the MBE chamber. Different parts of the chamber are indicated by arrows.

E-beam cells are used for the sources which have very low vapor pressure and are not easy to evaporate thermally by using effusion cells. Recently we have started using an e-beam cell for the Cr source instead of an effusion cell. As the vapor pressure of Cr is several orders of magnitude lower than Mn and Ga and the temperature must be set very high (about 1600 °C) to evaporate Cr by using effusion cell, the flux carries contaminants from out gasing at this temperature. This contamination can be eliminated by using an e-beam cell for the Cr source. The flux is measured *in situ* by a crystal thickness monitor, which is kept at room temperature. We measure the flux of different sources by using quartz crystal thickness monitor, which is kept at room temperature. We can estimate the N flux by growing GaN and at the transition point between N-rich GaN growth and Ga-rich GaN growth, where the RHEED pattern turns streaky from spotty, the Ga to N flux ratio is equal to 1.

For MnGaN and CrGaN growth, MOCVD grown GaN(0001)/Sapphire(0001) and Sapphire(0001) substrates were used respectively. For c-GaN samples, MgO(001) substrates were used. All of our substrates have a surface area of 1×1 cm^2 and are held by a sample holder made of molybdenum. Samples are transferred in the chamber by using transfer rods and the motion of these rods are controlled by magnets which are attached outside the casing of the transfer rods. For growth, samples are mounted on a growth stage which can be manipulated in X, Y, and Z directions and can be rotated in both θ and ϕ angular directions. The growth stage is equipped with a graphite heater to set the growth temperature or the annealing temperature for the samples. A thermocouple is attached at approximately the same distance behind the filament as is the distance of the sample from the filament in the front direction. The sample temperature is also measured by an optical pyrometer attached outside the chamber.

2.2 Reflection High Energy Electron Diffraction

Growth is monitored by reflection high energy electron diffraction (RHEED). An electron gun is used with an energy of 20 keV. These electrons impinge upon the sample surface at a glazing angle of about 1° and are diffracted. The diffracted electron beam from a diffraction pattern on the phosphorus screen and the pattern is acquired in real time by a CCD camera as shown in a schematic diagram in Fig. 2.2

RHEED is an important tool to investigate the sample surface during and after the growth. A spotty RHEED pattern is an indication of rough three dimensional growth, whereas a streaky RHEED pattern is an indication of smooth two dimensional growth. RHEED can be used to calculate the in-plane lattice constant of the grown film. RHEED patterns also give information about the in-plane symmetry of the crystal structure and can also show the reconstructions on the sample surface. Atoms on the surface rearrange themselves in a different periodicity compared to the bulk arrangement to reduce the total free energy of the system. This rearrangement of the atoms on the surface is referred to as surface reconstruction. Normally the separation between the atoms in surface reconstruction is bigger than the separation between the

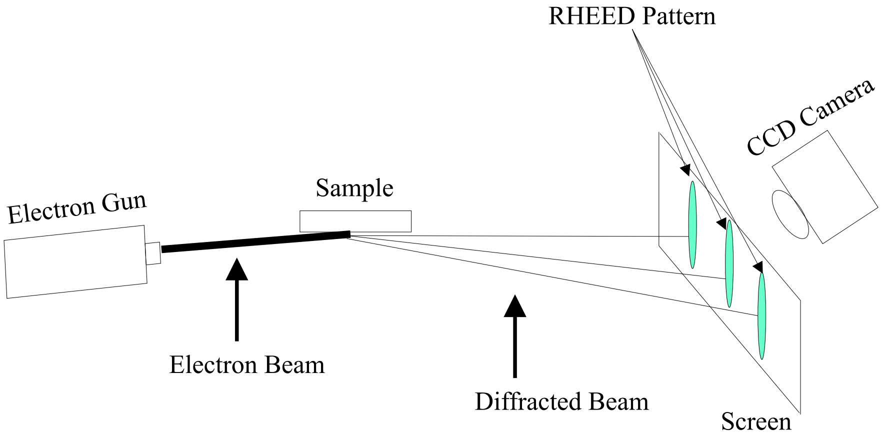

Figure 2.2: A schematic drawing of reflection high energy electron diffraction.

atoms in the bulk (e.g. 3×3 surface reconstructions of N-polar GaN means that the separation between the Ga atoms on the surface is 3 times larger than the separation between bulk Ga atoms).

2.3 Scanning Tunneling Microscopy

After the growth, the sample can be transferred *in situ* to the analysis chamber, where scanning tunneling microscopy(STM) is performed on the sample surface. The analysis chamber has a base pressure of the order of $\approx 10^{-10}$ Torr. An ion pump is used to pump down the analysis chamber and also a titanium sublimation pump is used to get the ultra high vacuum in the analysis chamber.

STM is a tool used to image the surface of the sample in real space with atomic resolution. Shown in Fig. 2.3 is the schematic drawing of our STM setup. The average scanning size of the sample surface by using STM is of the order of a few hundred Å. The STM is used to determine the surface morphology with atomic resolution, surface reconstructions, and also the surface electronic states can be determined using scanning tunneling spectroscopy(STS).

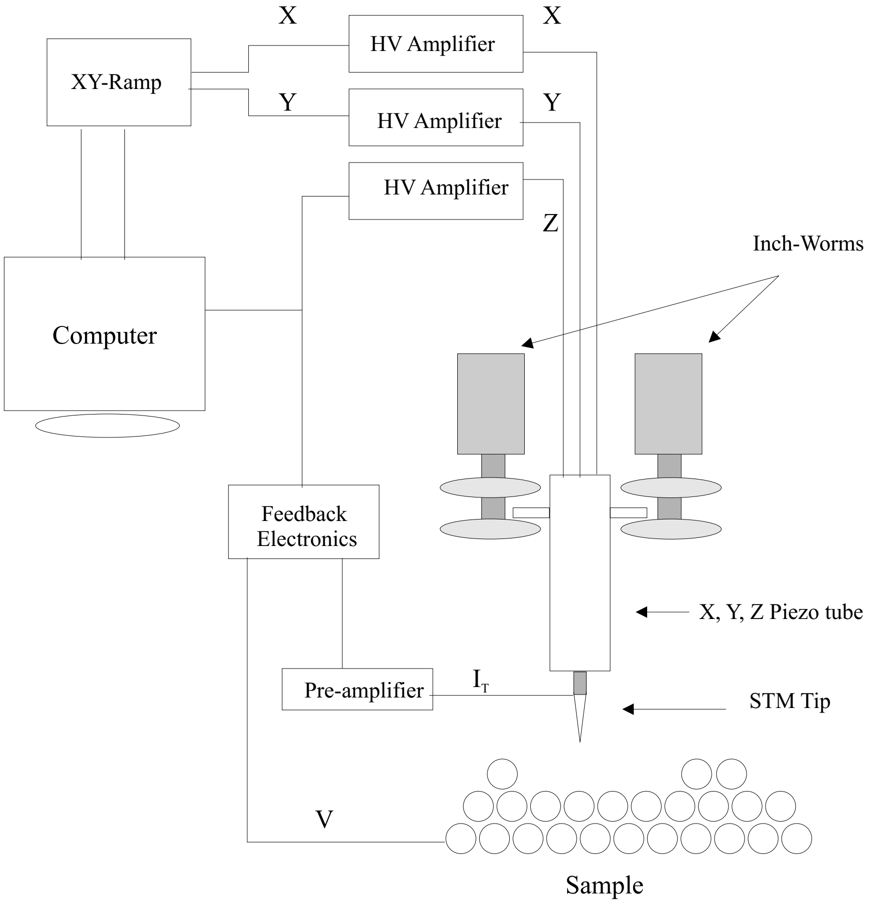

Figure 2.3: A schematic drawing of the scanning tunneling microscope and related electronics

A sharp tungsten tip is used for STM. The STM tips are sharpened *ex situ* using electro chemical etching. Then tips are cleaned by electron bombardment in the UHV analysis chamber. The STM tip is mounted on the scanner as is shown in Fig. 2.3. First the STM tip is approached towards the sample manually using "inch-worms" and then a sample voltage and tunneling current value is set and a computer controlled automatic approach is performed. The STM tip is stopped at a certain distance from the sample surface when it senses the set tunneling current value. Then scanning is started in constant current mode and the tip height(Z direction) is adjusted automatically by an electronic feedback control. The STM tip is pulled back when it senses higher tunneling current than the set tunneling current value in order to maintain the constant current value and similarly the tip comes towards the surface when tunneling current is smaller than the set tunneling current value which is of the order of about 0.1 nano Amperes. The STM tip scans in X and Y directions and the Z position of the tip is plotted that gives the image of the surface.

Information about the surface electronic structure can be obtained using STS. In this case, the feedback electronics is disabled so that the position of the STM tip stays at constant height during the acquisition of the STS spectra. At constant STM height, variable voltage is applied and the tunneling current is plotted as a function of the voltage. This provides the I-V curve, which can be used to determine the filled and empty surface states with zero current values in the band-gap range. Differential conductance (dI/dV), which is numerically calculated from the I-V curve, provides the information about the local density of states (LDOS). Normalized conductance, (dI/dV)/$(I\bar{/}V)$, is directly proportional to the LDOS,[24] and when plotted against voltage, provides information about the surface bandgap of the material.

2.4 Atomic Force Microscopy

Atomic Force Microscopy (AFM) is another surface imaging technique. We use AFM *ex situ* to determine the surface morphology at relatively larger sizes compared to the STM scanning sizes. AFM can provide us with the information of the surface morphology at micron length scales. Shown in Fig. 2.4 is a schematic drawing of our AFM system.

The AFM imaging is performed in the contact mode using the repulsive Van der waal force between the atoms of the tip and those of the surface. The AFM tip is attached to an optically reflecting cantilever, and the cantilever is deflected according to the amount of Van der Waal force experienced by the AFM tip. A laser

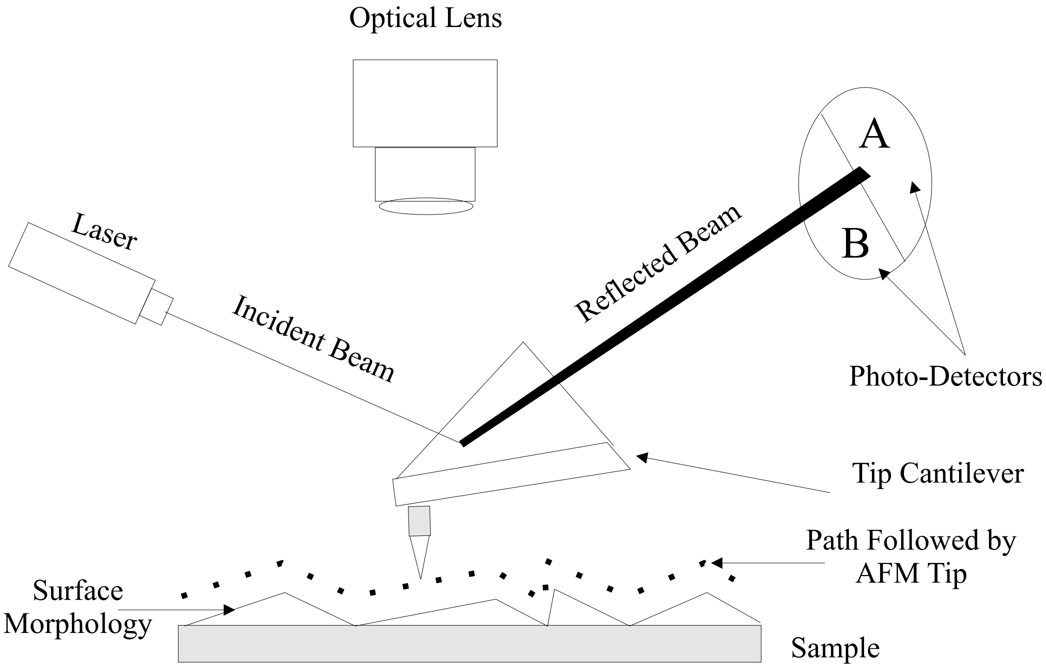

Figure 2.4: A schematic drawing of atomic force microscope.

beam is focused onto the cantilever and reflection of the beam from the cantilever is collected by a photodetector consisting of two photo-diodes. The difference between the signals of two photo-diodes detects the position of laser spot on the photodetector and consequently the amount of deflection of the cantilever is detected.

2.5 X-ray Diffraction

X-ray diffraction (XRD) is used to determine the bulk lattice constant and bulk crystal symmetry of the sample. We use a Rigaku θ-2θ x-ray diffractometer using Cu $K\ \alpha$ radiation as a probe beam with a wavelength of 1.542 Å. We can use θ-2θ scanning from 10°-140°. A schematic drawing of the XRD system is shown in Fig.

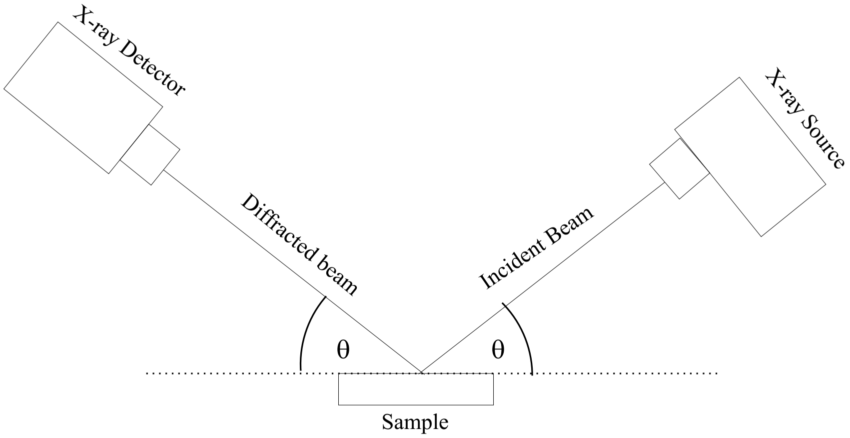

Figure 2.5: A schematic drawing of the X-ray diffractometer.

2.5. We can determine d (the interplanar spacing) using Bragg's law, after finding out the 2θ value of the peak position. Following is Bragg's law:

$$\lambda_{hkl} = 2dsin(\theta) \tag{2.1}$$

$$\lambda_{hkl} = \frac{1}{((h/a)^2 + (k/b)^2 + (l/c)^2)^{\frac{1}{2}}} \tag{2.2}$$

Chapter 3

An Overview of Wurtzite GaN and Scanning Tunneling Microscopy Studies of Zinc-Blende GaN/MgO(001)

3.1 Introduction

To understand the growth of ternary alloy MnGaN and CrGaN, it is very important to understand the host semiconductor GaN growth and surface reconstructions. GaN can be grown in both wurtzite and zinc-blende crystal structures. Wurtzite GaN has been studied intensively for past several decades and the growth and surface reconstructions are well understood.[15, 16, 17, 18, 25, 26, 27, 28, 29] It has been well known that wurtzite GaN can be grown as Ga-polar and N-polar.

GaN grown by rf N-plasma MBE on MOCVD GaN(0001)/Sapphire(0001) leads to Ga-polar growth. Depending on the Ga/N flux ratios Ga-polar GaN can be grown under N-rich and Ga-rich growth conditions. N-rich growth conditions lead to rough growth whereas under Ga-rich growth conditions a liquid Ga bi-layer exists on the surface and a smooth growth is observed. Several different kind of reconstructions are formed on the Ga-rich grown Ga-polar GaN(0001)namely: Pseudo 1×1 ("1×1"), 2×2, 5×5, and 6×4.[25]

GaN grown on Sapphire(0001) using rf N-plasma MBE leads to N-polar growth. Like Ga-polar GaN, N-polar GaN($000\bar{1}$) can also be grown under Ga-rich and N-rich growth conditions. N-rich growth conditions lead to rough 3D growth whereas Ga-rich growth conditions lead to atomically smooth surface. Unlike Ga-rich Ga-polar GaN, there is no Ga bi-layer on the surface; instead there is a terminating Ga ad-layer on the surface. Under Ga-rich growth conditions several different reconstructions are formed on the N-polar GaN($000\bar{1}$) namely: 1×1, 3×3, 6×6, and c(6×12).[30]

Unlike w-GaN, zinc-blende GaN (c-GaN) surface reconstructions have not been well understood yet. There has been some controversy in the past experimental studies of the surface reconstructions of c-GaN(001). A number of different atomic reconstructions were observed on c-GaN(001) surface depending on the growth conditions and the substrate. For growth of c-GaN on GaAs(001), the surface showed 1×1, 2×2, and c(2×2) reconstructions.[31, 32, 33, 34] A $\sqrt{10} \times \sqrt{10}$ -R18.4° reconstruction was also reported.[35, 36]

The growth of c-GaN on SiC/Si(001), by contrast, shows that c-GaN(001) has 1×1 and 4×1 reconstructions and they are correlated with the sample temperature and the Ga flux during growth.[33, 34, 37, 38, 39] However, when an arsenic background was applied, the surface showed an irreversible transition to 2×2 under slight N-rich conditions, and an irreversible transition to c(2×2), near stoichiometric conditions.[38, 39]

A recent study by Kim *et al.* showed that under Ga-rich conditions, growth of GaN on GaP(001) leads to single crystal c-GaN with a 2×2 surface reconstruction. However, under N-rich growth conditions, a wurtzite GaN layer grew preferentially.[40]

Kikuchi *et al.* reported the growth of GaN on MgO(001), and they showed that the surface has a 1×1 reconstruction.[33] Moreover, Powell *et al.* reported that the surface of c-GaN on MgO(001) has a two-domain 4×1 structure when the growth temperature is above 600 °C.[41]

Neugebauer *et al.*, by employing first principles total energy calculations, reported that 4×1, consisting of linear Ga tetramers, is the intrinsic reconstruction. Whereas, 2×2 is an arsenic related reconstruction.[42] Neugebauer *et al.* found that 2×2 is stable if the reconstruction involves As ad-atoms, and similar behavior is expected for the other group V surface ad-atoms, in agreement with the 2×2 reconstruction reported for c-GaN grown on GaAs(001) and GaP(001).

To understand the c-GaN(001) reconstructions, we have performed the STM studies on the Ga-rich grown GaN(001) on MgO(001) substrate. We have found that these reconstructions are due to Ga ad-atoms. Our MBE growth chamber is As and P free, and hence the reconstructions observed on the c-GaN(001) are not As or P related. Moreover, we have not observed any 2×2 reconstructions, which according to Neugebauer *et al.* are formed due to As or other group V ad-atoms on c-GaN(001). We have observed a series of reconstructions on c-GaN(001) surface, which differ slightly from each other in terms of Ga coverage per unit area, and we believe these are the intrinsic reconstructions of c-GaN(001).

Scanning Tunneling Spectroscopy (STS) has been employed to determine the electronic state of the surface reconstructions.

3.2 Experimental Procedure

c-GaN layers are grown by MBE on MgO(001), using a radio frequency rf N-plasma source and an effusion cell for Gallium. MgO(001) substrates were chemically cleaned with acetone and isoprapanol before introducing them into the chamber. GaN growth takes place with the substrate temperature set in the range of $\sim$ 550-700 °C and the base pressure of nitrogen and the plasma source power are set at $0.9\text{-}1.1 \times 10^{-5}$ Torr and 500 Watts respectively.

The growth starts when the Ga shutter is opened. Gallium rich growth conditions occur at a certain threshold of Ga flux. This threshold depends on the N flux. The Ga-rich growth conditions occur in our system at an average Ga flux of $\sim 3 \times 10^{14}\ /cm^2 sec$. The growth is ended by closing the Ga shutter and turning off the plasma power simultaneously. The Ga flux has been determined by a crystal thickness monitor at room temperature.

The growth is monitored in real time using reflection high energy electron diffraction (RHEED). Following growth, samples are transferred under UHV to the adjoining analysis chamber for room temperature STM studies. We have mostly used W tips to acquire the STM images with an exception of the first STM image shown in this chapter which was acquired with Fe coated W tip, which was available at that time. We have not intended to perform any comparative studies of STM images acquired with different kinds of tips. Although, this could be an interesting study.

3.3 Results and Discussion

Shown in Fig. 3.1 are the RHEED patterns and their horizontal line profiles of the GaN film along $[1\bar{1}0]$ direction of MgO(001). Shown in Fig. 3.1(a) is the RHEED pattern of the GaN film during the growth. Shown in Fig. 3.1(b) is the RHEED pattern after the growth and after cooling to below 200° C. RHEED patterns show 4-fold symmetry for both MgO substrate and GaN film.

RHEED patterns of the substrate(not shown here) indicate the smoothness of the surface, suggesting that nitridation and annealing the surface prior to the growth result in smoothness of the MgO(001) surface. In Fig. 3.1(a), the RHEED pattern of c-GaN(001) grown under Ga-rich growth condition shows that the surface is grown smoothly with 1×1 reconstruction. After growth the RHEED pattern also shows similar reconstructions at temperatures $T_s > 200°$ C. The ratio of the spacing between the main streaks for MgO(001), to c-GaN(001) equals the inverse ratio of their lattice constants, $(a_{MgO}/a_{c-GaN})^{-1}$. This indicates that $\langle 110 \rangle$ of c-GaN(001) are parallel to $\langle 110 \rangle$ of MgO(001).

After the sample is cooled below 200° C, the RHEED pattern of c-GaN(001) shows 2× and 8× reconstructions, as can be seen in the line profile of Fig. 3.1(b). In fact, if the sample temperature is raised above 200 °C, the RHEED pattern will again show 1× reconstructions, suggesting a reversibility ($2\times \,/\, 8\times \longleftrightarrow 1\times$). The surface reconstructions observed by STM on c-GaN(001) are not only 8× but also 6×, 7×, 9×, 10× and 11×, which will be explained in detail later. These other reconstructions do not appear very well in the RHEED because either they are so

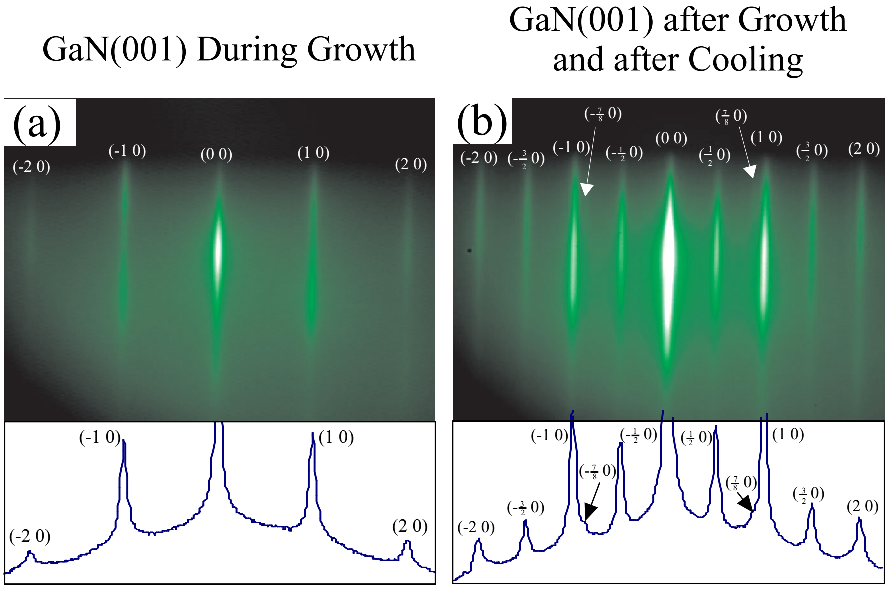

Figure 3.1: RHEED patterns for (a) c-GaN(001) during growth, (b) c-GaN(001) after growth below 200° C with a horizontal line profile attached underneath

close to the main 1×1 streaks that they are not as visible or their intensity is much lower than the 8× streaks and so it is not easy to observe them in the RHEED pattern. As in STM images we have observed that most of the surface was covered by c(4×16) reconstructions, which appears as 8× streaks in the RHEED pattern.

The 2× reconstruction observed for our sample is different than all previously reported 2× reconstructions, as observed when using GaAs(001) or GaP(001) substrates, or when having an As background for SiC(001) substrates.[32, 34, 35, 36, 38, 40] Three observations support this statement. First, MgO(001) is used as a substrate which dose not have As or P, and our chamber is free of other group V elements or compounds except for N. Second, the 2× observed for our sample does not occur during the growth or even at sample temperatures higher than 200° C, whereas the previously reported 2× does occur even during the growth. Third, our 2× observed below 200° C is accompanied with 8×; however, the previously reported 2× is not accompanied by 8×. Therefore, this is the first time, to our knowledge, that an intrinsic 2×8 reconstruction has been observed for c-GaN(001).

Since c-GaN(001) has been grown under Ga-rich conditions, it is expected to have excess Ga on the surface. Moreover, due to the order-disorder transition observed at $T_s \sim 200$ °C for c-GaN(001)-2×8 reconstruction, it can be inferred that Ga adatoms form a 2×8 reconstruction on Ga-terminated c-GaN(001).

An analogy of c-GaN(001) reconstructions with wurtzite GaN surface reconstructions will be helpful to understand the reversible 2× and 8× reconstructions. Smith *et al.* have reported the formation of 3×3 Ga adatom reconstructions on 1×1 Ga adlayer for wurtzite GaN(000$\bar{1}$) grown by rf N-plasma MBE under Ga-rich growth conditions.[16] The 3×3 reconstruction is formed with reversibility at $T_s \leq 300°$ C, and it is associated with an order-disorder transition of the Ga adatoms atop the 1×1 Ga adlayer. Even higher order reconstructions with order-disorder transitions have been reported by Smith *et al.* for GaN(000$\bar{1}$) for higher Ga coverage, such as 6×6 and c(6×12) reconstructions. These reversible order-disorder transitions are attributed to weak Ga-Ga bonding between Ga adatoms and the Ga adlayer, compared to the strong Ga-N bonding.

This analogy supports our hypothesis that 2×8 reconstruction on c-GaN(001) is formed by Ga adatoms. However, a complete theoretical study will be important to understand the exact nature of the reconstructions, which we have discovered in this study.

STM studies were performed to observe the surface reconstructions in real space. Shown in Figs. 3.2(a-d) are some large scale STM images of the Ga-rich c-GaN surface. Shown in Fig. 3.2(a) is the STM image of an area 2200 Å × 2200 Å ($V_s = +2$V; $I_t = 0.08$nA). The surface consists of terrace-step structure. Shown in Fig. 3.2(b) is a zoom-in STM image of size 1200 Å × 1200 Å ($V_s = +2$V and $I_t = 0.08$nA). Shown in Fig. 3.2(c) and 3.2(d) are STM images of smaller zoom-in areas of the surface with sizes of 450 Å × 450 Å and 600 Å × 600 Å ($V_s = +1.5$V and +2V; $I_t = 0.08$nA respectively). We find that similar row-type structures are found everywhere on the surface, in 2 different domains at 90° to each other.

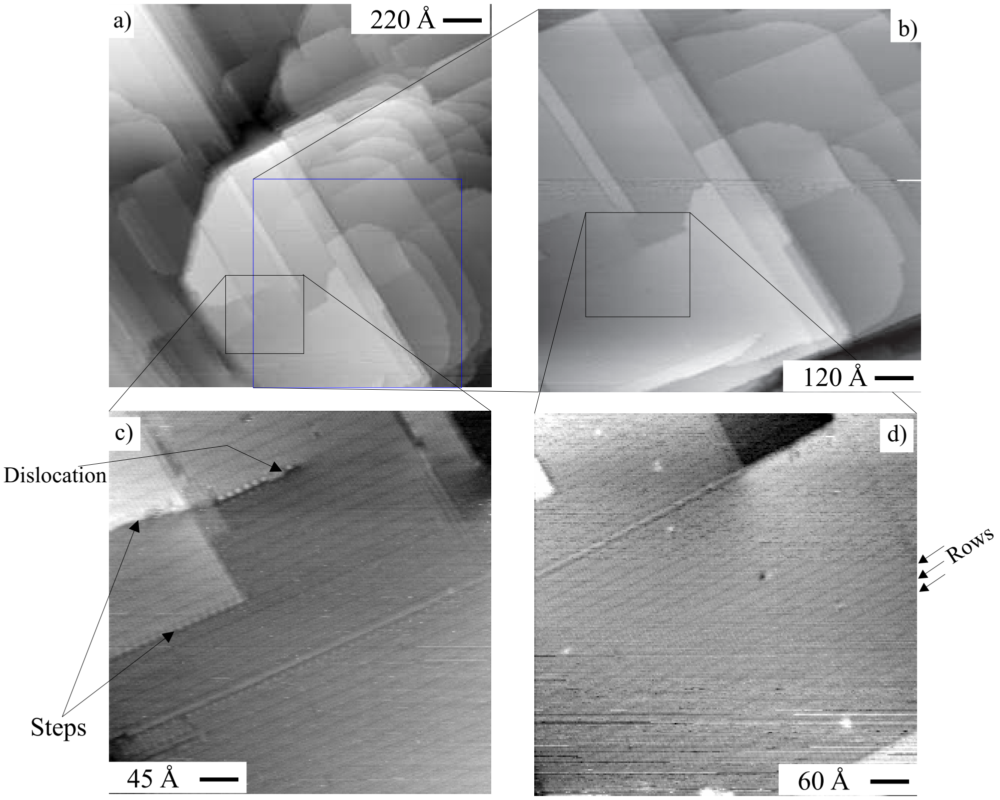

Figure 3.2: STM images of c-GaN surface a) STM image of 2200 Å by 2200 Å surface area, sample voltage (V_s) = +2V and tunneling current (I_t) = 0.08nA. b) STM image of 1200 Å by 1200 Å surface area obtained at V_s = +2V and I_t = 0.08nA. c) STM image of 450 Å by 450 Å surface area obtained at V_s = +1.5V and I_t = 0.08nA. d) STM image of 600 Å by 600 Å surface area obtained at V_s = +2V and I_t = 0.08nA.

Shown in Figs. 3.3(a) is the STM image (V_s = -0.4V and I_t = 0.1nA) of the c-GaN(001). This STM image contains three different reconstructions. Schematic models of these reconstructions are presented in Fig. 3.3(b-d), filled circles with bigger diameter represent Ga adatoms whereas small circles represent underlying Ga layer. Each reconstruction consists of row-type structures.

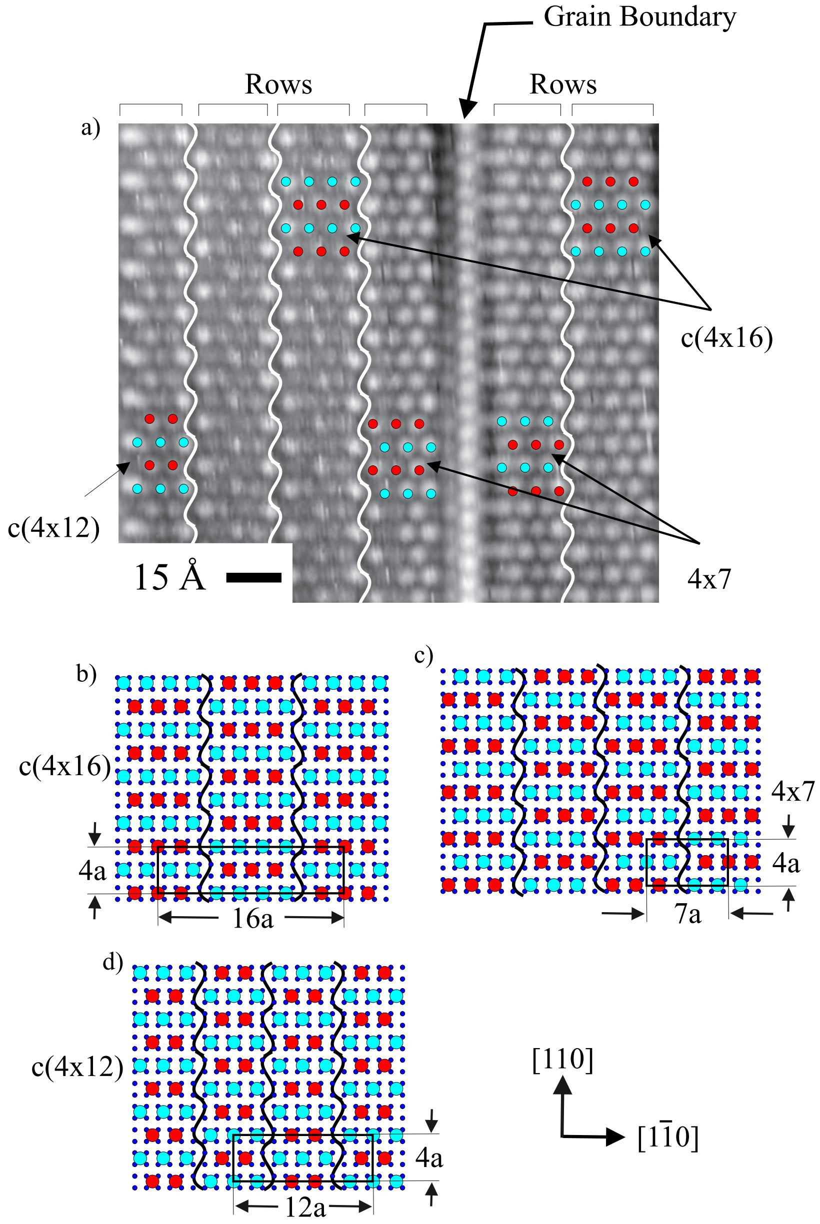

Figure 3.3: STM image of c-GaN(001)-c(4×12), 4×7 and c(4×16) reconstructions: (a) STM image acquired at V_s = -1.5 V and tunneling current, I_t = 0.07 nA, and Schematic atomic model of (b) c(4×12), (c) 4×7, and (d) c(4×16) surface reconstructions.

First reconstruction shown in the STM image is labeled as c(4×12) consisting of row-type features. The periodicity of rows along $[1\bar{1}0]$ is about 19.2 Å which is 6 times Ga-Ga spacing of c-GaN(001), which is 3.2 Å = a.

Each row consists of linearly aligned either 3 or 2 Ga adatoms alternating along [110]. The spacing between these Ga adatoms along [110] is 6.4 Å which equals 2a. The spacing between the last Ga adatom in one row and the first Ga adatom in the adjacent row along $[1\bar{1}0]$ is 9.6 Å which equals 3a. From the symmetry of the atomic arrangement, the structural model is presented in Fig. 3.3(b). The conventional unit cell of the surface reconstruction is c(4×12). Each unit cell consists of 10 Ga adatoms with Ga adatom coverage of 0.208 monolayer(ML).

Second reconstruction shown in the STM image is labeled as 4×7 consisting of row-type feature and there are 3 linearly aligned Ga adatoms in the row-type structure as shown in Fig. 3.3(a and c). Rows have a periodicity of 7a along $[1\bar{1}0]$ and Ga adatoms in each row have a periodicity of 4a along [110]. Each unit cell contains 6 Ga adatoms. The Ga adatoms coverage is 0.214 ML.

Third reconstruction shown in this image is the c(4×16) reconstruction. This reconstruction is most commonly found on c-GaN(001), which is why we can see 1/8th order streaks in the RHEED more clearly than any other streaks due to other reconstructions. Same reconstructions is Shown in Figs. 3.4(a-d). A schematic model is presented in Fig. 3.4(d). The dashed circles determine the same point in each Figure. The periodicity of rows along $[1\bar{1}0]$ is 8a and linearly aligned either 3 or 4 Ga adatoms alternating along [110] have a periodicity of 2a along [110]. The conventional unit cell of the surface reconstruction is c(4×16). The density of Ga adadoms is 14 per c(4×16) unit cell; therefore, the coverage of Ga adadoms is 0.219ML.

Shown in Figs. 3.5(a-b) are the STM image (V_s = -0.4V and I_t = 0.1nA) and a schematic atomic model of the 4×9 reconstruction observed on c-GaN(001). This reconstruction also consists of row-type structure. Each row in this reconstruction consists of linear structures of equal length. Each rectangular feature contains 4 Ga adatoms. Row-type structures have a periodicity of 9a along $[1\bar{1}0]$ and the rectangular features in the rows have a periodicity of 4a hence forming a 4×9 reconstruction. This 4×9 reconstruction has 8 Ga adatoms per unit cell as is shown in the schematic

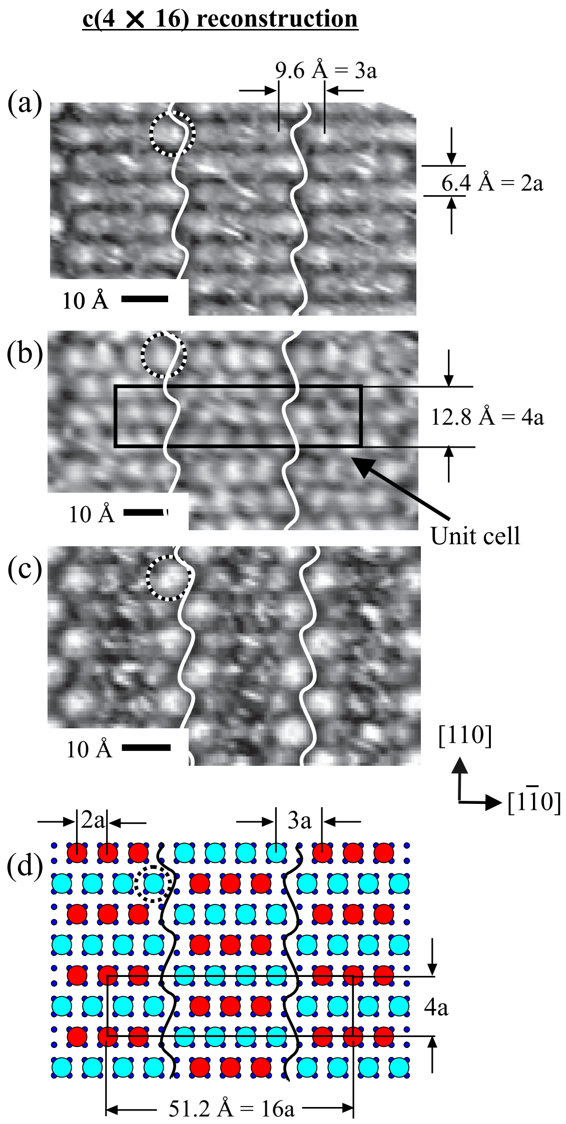

Figure 3.4: STM images of c-GaN-c(4×16) reconstruction acquired at: (a) $V_s = +0.5$ V, $I_t = 0.6$ nA; (b) $V_s = +0.1$ V, $I_t = 0.9$ nA; and (c) $V_s = -1.0$ V, $I_t = 0.2$ nA. (d) Schematic atomic model of c(4×16) atomic reconstruction. The gray scales of a, b, and c are 0.82 Å, 0.96 Å, and 1.43 Å, respectively.

atomic model [Fig. 3.5(b)]. There are 0.222ML of Ga adatoms coverage on the 4×9 reconstruction.

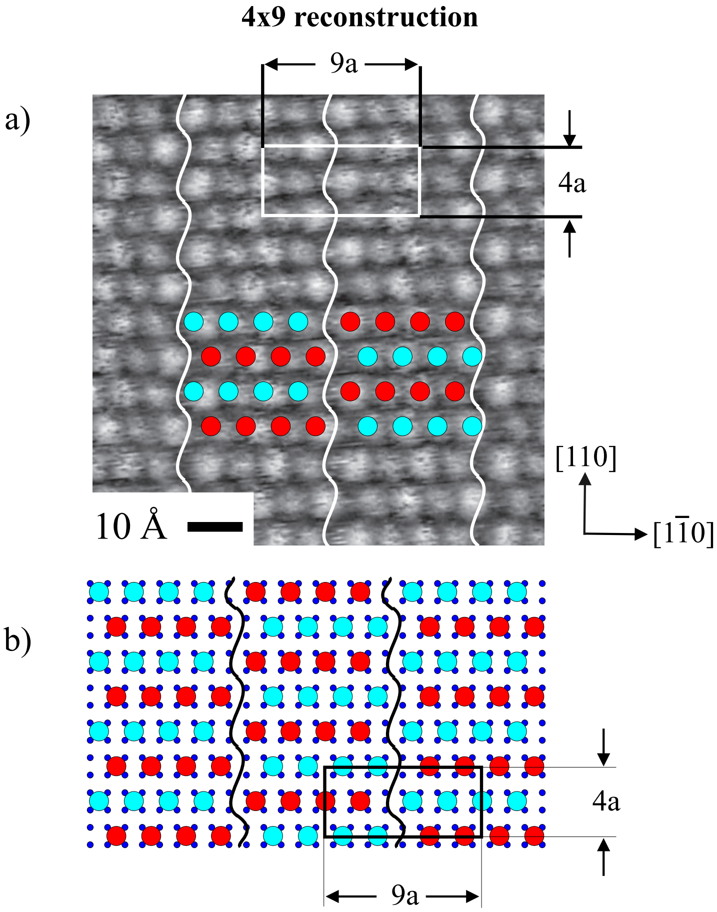

Figure 3.5: STM image of c-GaN(001)-4×9 reconstruction: (a)STM image acquired at V_s = -0.8 V and tunneling current, I_t = 0.07 nA, (b) Schematic model of 4×9 atomic reconstruction.

Shown in Figs. 3.6(a,b) are the STM image (V_s = -0.4V and I_t = 0.1nA) and a schematic atomic model of this reconstruction observed on c-GaN(001). This reconstruction also consists of row-type structures. These rows have a periodicity of 20a along [1$\bar{1}$0] and the linear structures in each row have a periodicity of 4a along

[110] hence a c(4×20) reconstruction is formed. A unit cell is drawn as a rectangle, as shown in Fig. 3.6(b). Each unit cell contains 18 Ga adatoms. The c(4×20) reconstruction contains 0.225ML of Ga adatoms coverage.

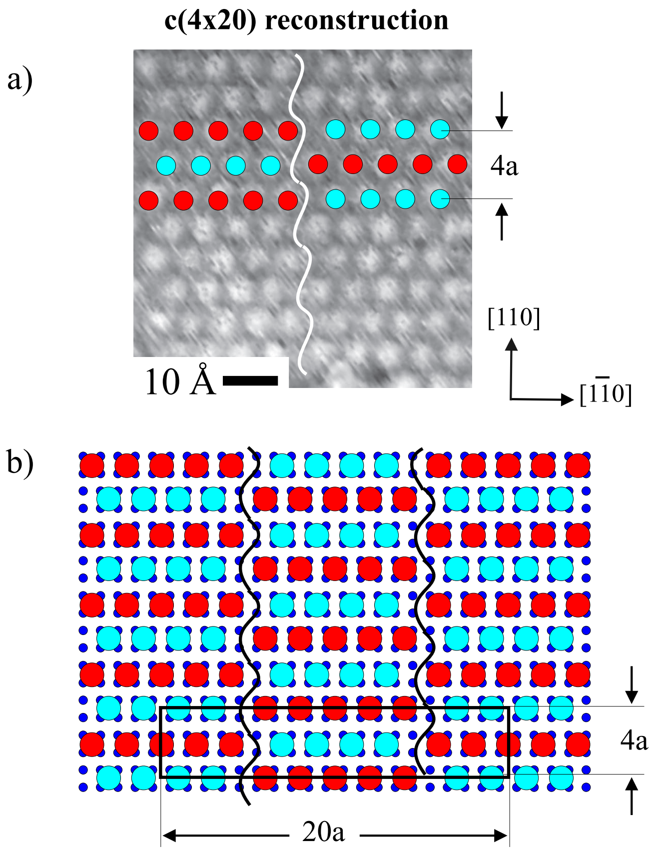

Figure 3.6: STM image of c-GaN(001)-c(4×20) reconstruction: (a)STM image acquired at V_s = -0.4 V and tunneling current, I_t = 0.1 nA, (b) Schematic model of c(4×20) atomic reconstruction.

Shown in Figs. 3.7(a,b) are the STM image (V_s = -1V and I_t = 0.1nA) and a schematic atomic model of the c(4×11) reconstruction. This STM image also consists of row-type structures similar to the STM image of c(4×16) reconstruction. Each row in this reconstruction consists of linear structures, which are made up of five Ga adatoms instead of alternating 4-3-4-3 Ga adatoms sequence along [110]. There is a periodicity of 4a along [110] and a periodicity of 11a along [1$\bar{1}$0] direction hence it is a 4×11 reconstruction. Shown in Fig. 3.7(b) is the schematic atomic model of this reconstruction and unit cell of this reconstruction is shown. There are 10 Ga adatoms in each unit cell. This reconstruction has Ga adatoms coverage of 0.227ML. This reconstruction has the highest Ga adatom coverage out of all the six reconstructions discussed here.

From the discussion above it can be summarized that six different intrinsic reconstructions were found on the c-GaN surface in the present study. These reconstructions are labeled as c(4×12), 4×7, c(4×16), 4×9, c(4×20), and 4×11. These reconstructions are formed at low temperature ($\leq$ 200°C) after the growth and disorder if the temperature is raised. So these reconstructions are formed with reversibility at $T_s \leq 200°$ C, which is an indication that these reconstructions are formed by Ga adatoms. These reconstructions depend on the amount of Ga on the surface i.e. c(4×12) contains the lowest Ga adatoms coverage (0.208ML), at a little higher Ga coverage of 0.214ML 4×7 reconstruction is formed, c(4×16) contains 0.219ML of Ga coverage, at 0.222ML of Ga coverage 4×9 reconstruction is formed, at 0.225 ML of Ga coverage c(4×20) reconstruction is formed, and at 0.227ML of Ga coverage 4v11 reconstruction is formed, which has the highest Ga coverage. These can be called as a family of reconstructions as they differ slightly from each other in terms of Ga coverage.

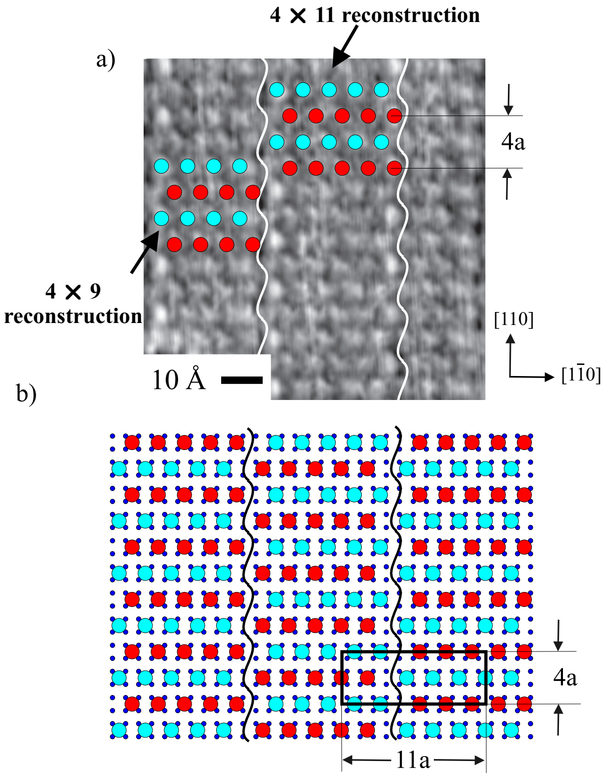

Figure 3.7: STM image of c-GaN(001)-4×11 reconstruction: (a)STM image acquired at V_s = -1.0 V and tunneling current, I_t = 0.1 nA, (b) Schematic model of 4×11 atomic reconstruction.

We have constructed simple schematic atomic models for these reconstructions, however, we strongly encourage a complete theoretical study of these reconstructions formed on c-GaN(001)/MgO(001).

3.3.1 Electronic Properties

Shown in Figs. 3.8(a-d) are the STM images of c-GaN(001)-c(4×16) reconstructions and STS spectra of the sruface. The sample biases of STM images in Figs. 3.8(a) and 3.8(b) are +0.3 V and -0.3 V, respectively.

As can be seen in both Figs. 3.8(a) and 3.8(b), even though the sample biases are opposite in polarities for the two images, corrugation of the atoms is not flipped. Being able to image the surface at small sample biases, V$_s$ = +0.3 V and -0.3 V, suggests that the surface has a narrow or even zero bandgap.

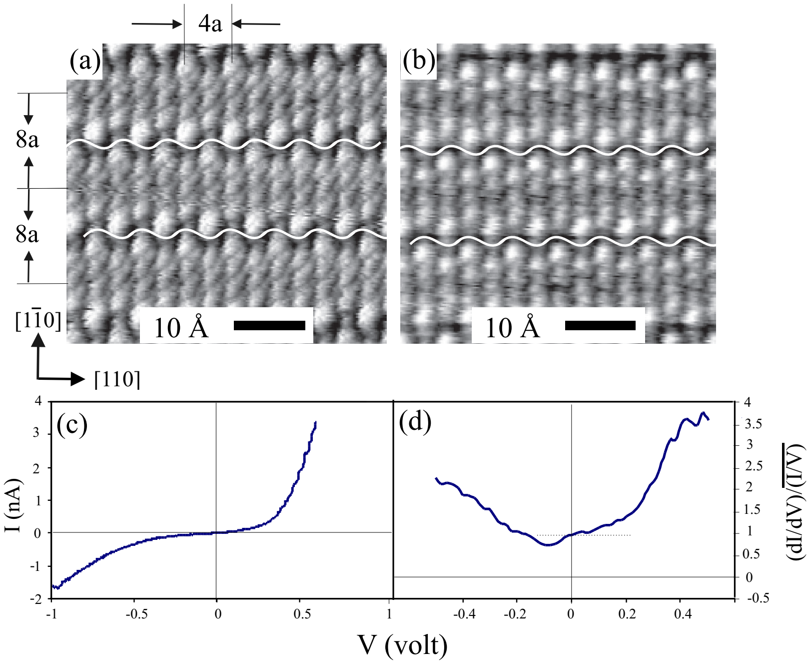

Figure 3.8: STM and STS of c-GaN(001)-c(4×16) reconstruction: (a) and (b) STM images acquired at V$_s$ = +0.3 V and -0.3 V, respectively, with the same tunneling current, I$_t$ = 0.08 nA, (c) and (d) tunneling current vs. voltage, I-V, curve and normalized tunneling current, NC-V, curve, respectively.

STM images with V$_s$ = +0.3 V and -0.3 V cannot be conclusive to determine the electronic properties of the surface reconstructions. STS can provide useful information about the surface electronic states.

Figure 3.8(c) shows the Tunneling current vs. voltage (I-V) curve, and Fig. 3.8(d) displays the normalized conductance, $(dI/dV)/\overline{(I/V)}$ vs. Voltage, (NC-V) curve, which is numerically calculated from the I-V data in Fig. 3.8(c). The horizontal dashed lines in the NC-V panel indicate the zero and unity position of NC. The bar over the $\overline{I/V}$ indicates broadened I/V values are used to avoid divergence near the band edges.[24] Both I-V and NC-V are the averages of 16 spectra.

The I-V curve in Fig. 3.8(c) shows a smoothly continuous variation of the tunneling current with a change in the sample bias. Even in the range between $V_s = +0.3$ V and -0.3 V, the plot shows non-zero values of the current. The plot in Fig. 3.8(d), NC-V, dose not go to zero in the vicinity of $V_s = 0$. Instead, NC passes through unity at zero voltage.

Clear non-zero current in the I-V curve, except the vicinity of the zero-voltage, indicates that the surface has states in all energies. The NC-V plot shows also non-zero density of states for all energies confirming the observation of the I-V plot and indicating metallic surface. Therefore, it is concluded that c(4×16) has a metallic surface. As all the other five reconstructions differ a little in terms of Ga coverage and also we were able to image those surface reconstructions at smaller voltage biases so we can infer that all the other five reconstructions discussed above are also metallic.

3.4 Summary

Cubic GaN(001) has been grown smoothly under Ga-rich growth conditions on MgO(001) using rf N-plasma MBE. A family of surface reconstructions c(4×12), 4×7, c(4×16), 4×9, c(4×20), and 4×11, with Ga adatoms coverage of 0.208ML, 0.214ML, 0.219ML, 0.222ML, 0.225ML, and 0.227Ml respectively, were observed on Ga-rich grown c-GaN(001). Due to the fact that our MBE chamber is free of group V elements except N, these are intrinsic c-GaN(001) reconstructions. STM and STS shows that c-GaN(001)-c(4×16) and other reconstructions have metallic surface.

Chapter 4

Ga/N Flux Ratio Influence on Mn Incorporation, Surface Morphology, and Lattice Polarity During rf Molecular Beam Epitaxy of MnGaN

4.1 Introduction

The formation of magnetic semiconductors is of widespread interest due to the possibility of making highly efficient spin injectors for spintronics applications. According to the prediction of Dietl, ferromagnetic MnGaN is very promising since it should have a Curie temperature above room temperature (300 K).[1] Therefore, the formation of a uniform MnGaN alloy is a crucial issue which needs to be explored.

There are many challenges to the formation of a uniform MnGaN alloy film. For example, Mn-N growth results in films in which Mn has octahedral bonds with N, whereas Ga prefers tetrahedral bonding.[14] In the case of alloy growth, it may also be relevant that the vapor pressure of Mn metal is about 100 times greater than that of Ga metal. Generally, the challenges combined with the great technological possibilities render the MnGaN system quite interesting to study, as also evident by the appearance of several new theoretical works.[43, 44, 45]

Already, many experimental efforts have been reported regarding the preparation and magnetic properties of MnGaN layers.[46, 47, 48] There have been a number of reports on the use of molecular beam epitaxy (MBE) to grow MnGaN using either radio frequency (rf)-plasma[46, 49, 8, 7], electron-cyclotron-resonance (ECR) plasma[9], or ammonia[5] for the nitrogen source. Despite many promising results, the reported growth conditions, as revealed by reflection high energy electron diffraction (RHEED), appear to vary widely. For example, Kuwabara *et al.* who used rf N-plasma, showed a streaky RHEED pattern and reported Mn incorporation as high as 11% without macroscopic precipitation for a substrate temperature of 600 °C. On the other hand, Overberg *et al.* who also used rf N-plasma reported a partially spotty RHEED pattern and a Mn concentration of 7.0 at%.[8] Sonoda *et al.*, who used ammonia, reported a sample which was apparently grown with a streaky RHEED pattern and without precipitation.[5] Yet, Cui and Li reported that ECR MBE using a nitrogen-hydrogen plasma resulted in a spotty RHEED pattern and a $Mn_xGa_{1-x}N$ alloy without precipitation.[9] Thus, while it is therefore unclear whether streaky or spotty RHEED patterns are preferable for incorporation, it is well known that a spotty RHEED pattern implies rough 3-Dimensional growth whereas a streaky RHEED pattern, implying smooth 2-Dimensional growth, is much more desirable from the point of view of forming smooth interfaces for heterostructures. In addition, to our knowledge few reports have mentioned lattice constant changes for MnGaN with respect to GaN, except for those cases involving growth in the presence of hydrogen.[9, 50] Thus it is also unclear whether growth with hydrogen is necessary for incorporation on substitutional sites.

Therefore, it is important to investigate the growth conditions without hydrogen which may result in both Mn incorporation *and* smooth surface morphology *and* to provide compelling evidence that the Mn incorporation is occurring on Ga sites. To achieve these goals requires systematic investigations of the effects of various growth conditions on the film properties. One of the most important variables in the growth of $Mn_xGa_{1-x}N$ is the Ga/N flux ratio. Here, we present a study of the effects of the

Ga/N flux ratio on the afore-mentioned properties using rf N-plasma MBE. It will be shown that this parameter is critical in determining both incorporation and film morphology, and it will be shown what is the growth condition which can optimize these two properties. In addition, it is also shown that the Ga/N flux ratio affects the resulting film polarity. The results are explained in terms of three separate regimes of growth, each corresponding to a certain type of surface structure.

4.2 Experimental

The growth experiments are performed in a custom MBE system utilizing gallium and manganese effusion cells and a rf plasma source with N_2 as the source gas. The substrates are wurtzite Ga-polar GaN(0001) grown by metal-organic chemical vapor deposition (MOCVD) on sapphire and are either Si-doped *n*-type at 1–3×10^{18} cm^{-3} or unintentionally-doped *n*-type at 5×10^{16} – 5×10^{17} cm^{-3}. The substrates are loaded into the MBE chamber and heated up to 550 °C which is maintained throughout the entire growth. The N plasma source is applied using 500 W with a N_2 flow rate of 1.1 standard cubic centimeters per minute (sccm). The chamber background pressure $= 9\times10^{-6}$ Torr. The Ga and Mn fluxes, J_{Ga} and J_{Mn}, are measured by a crystal thickness monitor held at room temperature. The Ga/N flux ratio (J_{Ga}/J_N) is set in the range from 0.7 (N-rich) to 1.46 (Ga-rich) with constant N flux. The Mn/N flux ratio (J_{Mn}/J_N) is set to $\sim$ 0.07. The growth begins with a 30 nm thick GaN buffer layer (no intentional doping), and then the Mn shutter is opened to grow the MnGaN layer with thickness in the range $0.3-0.6$ μm. Finally, a 30 nm thick GaN cap layer is grown.

The growth is monitored *in-situ* by RHEED, and the films are studied *ex-situ* by Scanning Electron Microscopy (SEM), Energy Dispersive X-ray Spectroscopy (EDX), X-Ray Diffraction (XRD), Atomic Force Microscopy (AFM), Rutherford Backscattering (RBS), and Vibrating Sample Magnetometry (VSM). The XRD machine uses Cu $K\alpha$ X-rays, and the RBS uses an incident beam of 3.05 Mev He ions.

4.3 Results and Discussion

4.3.1 Surface Structure

In the case of binary GaN growth, there are two growth regimes - namely, N-rich and Ga-rich.[15, 27, 26, 17] The line between these two regimes is the point at which the net Ga flux is equal to the net N flux, and this line is easy to determine experimentally. For a dilute ternary alloy like MnGaN, there are three growth regimes - namely, N-rich, metal-rich, and Ga-rich, as indicated by the growth map for MnGaN shown in Fig. 4.1. We should expect that the MnGaN film properties will be different in these three regimes as they are quite different for the two regimes of GaN growth.

Yet, it is not a simple matter to define these three conditions quantitatively based upon the measured Ga, Mn, and N fluxes since the surface sticking coefficients for these atoms vary with surface structure. However, we find that these three regimes can be defined qualitatively as follows: 1) N-rich: surface N atoms more than surface metal atoms; 2) metal-rich: surface metal atoms (Ga plus Mn) more than surface N atoms; and 3) Ga-rich: surface Ga atoms more than surface N atoms. The ratio of the chemical species present on the surface (e.g. Ga/N) is a function of the Ga, Mn, and N fluxes, but it is certainly not directly equal to the ratio of those flux values. This is because the sticking coefficient S for each species varies as a function of the chemical potential of the surface, which in turn is a function of the flux ratios. And, the chemical potential of the surface in turn determines the surface structure which affects the growth mode. For example, under Ga-rich growth conditions in which the interaction is mainly between Ga and weakly-bound Ga on the surface, S_{Ga} will be smaller than S_{Ga} under Ga-poor conditions in which there is not only a Ga–Ga interaction but also a stronger Ga–N interaction between the incident Ga and the surface. Thus it is difficult to determine *a priori* where the lines should be drawn between these separate growth regimes just based on the flux ratios.

However, in the following we shall describe the results in terms of the Ga/N flux ratio, which we define equal to unity at the metal-rich/Ga-rich transition point. We find this transition point to be identical, within uncertainty, to the transition point for binary GaN growth, for reasons to be explained later. Setting the Ga flux at this

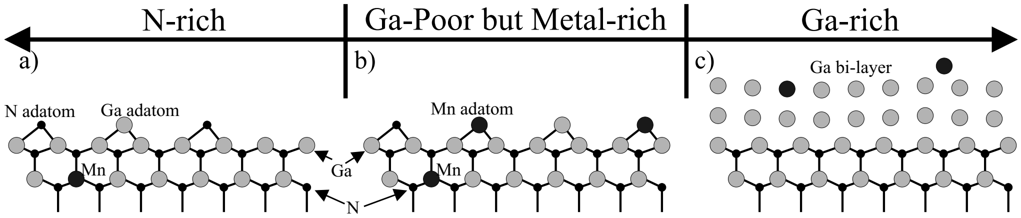

Figure 4.1: Growth map for MnGaN showing three growth regimes and the corresponding schematic surface structure models.

transition point equal to the N flux allows us to define the Mn/N flux ratio, and for this study, that has been held constant at $J_{Mn}/J_N = 0.07$.

Shown in Fig. 4.2(a–e) are RHEED patterns during MnGaN growth as a function of the Ga/N flux ratio as seen along [11$\bar{2}$0]. Results for the first sample are presented in Fig. 4.2(a) for $J_{Ga}/J_N = 0.76$ ($J_{metal}/J_N = 0.83$). The RHEED pattern is very spotty, indicating a 3D growth mode. For the case of $J_{Ga}/J_N = 0.84$ ($J_{metal}/J_N = 0.91$), as shown in Fig. 4.2(b), the pattern is much less spotty, indicating smoother growth. In Fig. 4.2(c) is the case for $J_{Ga}/J_N = 0.92$ ($J_{metal}/J_N = 0.99$), in which the RHEED pattern shows distinct nodes. Shown in Fig. 4.2(d) is the case for $J_{Ga}/J_N = 0.98$ ($J_{metal}/J_N = 1.05$), and here the RHEED pattern is more streaky. Finally, shown in Fig. 4.2(e) is the case for $J_{Ga}/J_N = 1.01$ ($J_{metal}/J_N = 1.08$). The RHEED pattern is very streaky, indicating a very smooth growth surface. This is also seen even at very high Ga/N flux ratios(e.g. $J_{Ga}/J_N = 1.46$). All of the RHEED patterns during growth are 1×1 without any fractional streaks. The samples of Figs. 4.2(a), 4.2(b), 4.2(c), and 4.2(d) are all shiny with a slight tan color, whereas the sample of Fig. 4.2(e) has a hazy appearance.

AFM images were acquired to measure the morphology of the films and to correlate with the RHEED patterns. In these AFM studies, special samples were grown under the same conditions but without the GaN cap layer so that the MnGaN surface could be studied directly.

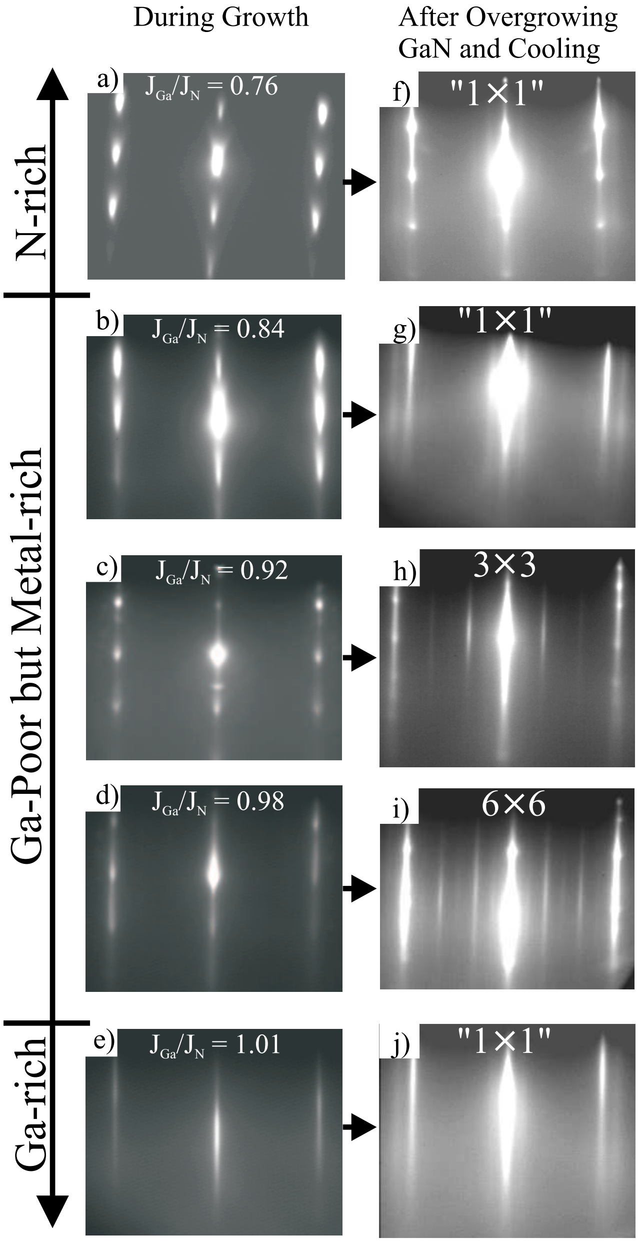

Figure 4.2: (a–e) RHEED patterns during MnGaN growth as a function of Ga/N flux ratio along $[11\bar{2}0]$; f-j) RHEED patterns after Ga-rich GaN overgrowth and cooling to below 200°C.

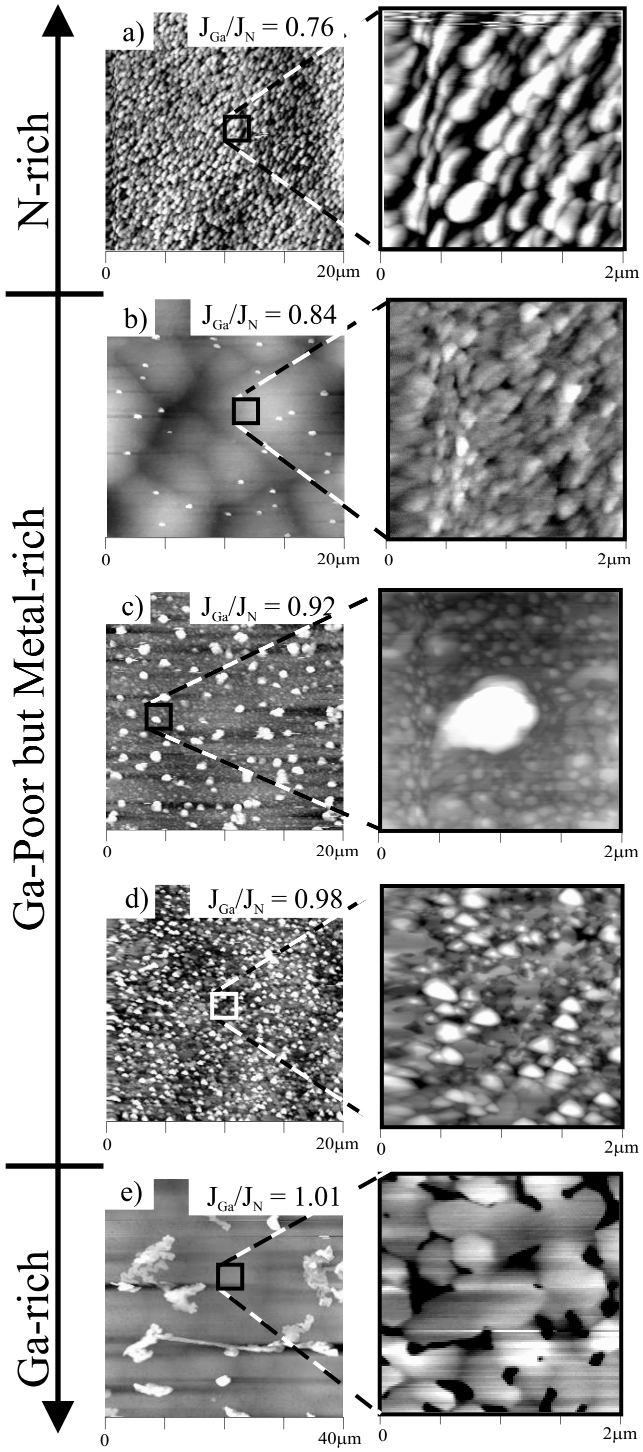

Figure 4.3: AFM images following MnGaN growth as a function of Ga/N flux ratio.

Shown in Fig. 4.3(a) is the AFM image of the MnGaN film grown under the condition $J_{metal}/J_N = 0.83$. This image shows a very rough surface, correlating well with the spotty RHEED pattern of Fig. 4.2(a). A zoom-in AFM image of the same surface is shown to the right. The surface consists of small hillocks of about 0.25 μm in lateral dimension, and these are spaced closely together. The root–mean–square (RMS) surface roughness is 81 Å with peak-to-valley height of 685 Å. Thus, a 3-D growth mode is observed. We find that this surface is consistent with growth under N-rich conditions.

Rough 3-D growth is well known to occur under N-rich conditions in the case of GaN grown by rf N-plasma MBE.[15, 27, 26, 17] Here, we find that the Mn atoms make little difference to this behavior, and a schematic model of the surface during growth is shown in Fig. 4.1(a). Under N-rich conditions, it is understood that the N accumulates on the GaN surface, resulting in dramatically reduced surface diffusion for both Ga and N atoms.[29] Although the diffusion barrier for Mn atoms on such a N-rich surface has not been reported to our knowledge, we expect it to be similarly high. This will prevent Mn from accumulating in precipitates, but will result in a rough 3-D growth.

Shown in Fig. 4.3(b) is the AFM image of the film surface for $J_{metal}/J_N = 0.91$ together with a zoom-in. In contrast to the surface of Fig. 4.3(a), this surface is clearly smoother, correlating well with the RHEED pattern of Fig 2(b). The RMS surface roughness of the zoom-in region is ~ 12 Å, substantially less than for N-rich growth. Such a strikingly smoother growth morphology indicates a major change in the growth mode; thus we conclude that this sample was not grown in N-rich conditions but rather in slightly metal-rich conditions.

The smoothening behavior for this sample suggests that the surface diffusion is substantially increased compared to N-rich conditions. This could well be explained as being due to the effect of the excess surface metal, as indicated schematically in the surface model shown in Fig. 4.1(b). Since metal atoms are dominant on the surface, N atoms are prevented from accumulating on the surface. This results in larger surface diffusion length, and the surface is smoother compared to N-rich growth.

Further evidence that the surface is metal rich is given by the appearance of tiny dots, as seen in the AFM image of Fig. 4.3(b). Their lateral dimension is about 0.5 μm with height of 0.01–0.03 μm, and there are ~ 0.1 dots μm^{-2}. Since such dots are not observed for the case of binary GaN growth, they are evidently caused by the Mn at the surface. The excess metal which is not used up eventually forms metallic precipitates. We emphasize that the metal-rich conditions refers to the surface and is therefore a function of the atom sticking coefficients as well as the flux ratio, which is why a metal/N flux ratio of 0.91 is entirely consistent with metal-rich conditions. The lack of any other good explanation for the growth mode transition we observe near $J_{metal}/J_N = 0.91$ further supports our conclusion.

Shown in Fig. 4.3(c) are AFM images of the surface grown with $J_{metal}/J_N = 0.99$. Clearly, we observe an increased density of the tiny dots on the surface. This increased density is attributed to the increased metal-rich surface conditions. The dots themselves have lateral dimension of about 1 μm with a height of about 0.1–0.2 μm, and we observe ~ 0.3 dots μm^{-2}. The areas between the tiny dots are somewhat rougher in comparison to Fig. 4.3(b), having RMS roughness of ~ 90 Å. This rough surface correlates well with the RHEED pattern of Fig. 4.2(c).

Shown in Fig. 4.3(d) are AFM image of the MnGaN film grown with $J_{metal}/J_N = 1.05$. Here we observe a further increase of the dot-like features. They have typical lateral dimension of ~ 0.25 μm with height of 0.05–0.1 μm and a density of ~ 7 dots μm^{-2}. Therefore, about 33% of the total surface area is covered by the dots. However, some areas between the dots appear somewhat smooth, which agrees well with the fairly streaky RHEED pattern of Fig. 4.2(d).

Thus we find over the range of metal-rich conditions clear evidence for tiny dot-like precipitates which increase in density as the conditions become more metal rich. As conditions become closer to N-rich, the dot size decreases. These tiny dots do not significantly affect the RHEED pattern, probably because they have a random crystalline alignment with the substrate. We also find that when the density of the dots becomes small (going towards N-rich conditions), the surface shows much improved smoothness. This implies that the less excess metal there is on the surface, the better will be the surface morphology. Beyond this, when the conditions become

N-rich, the dots no longer appear since there is no excess surface metal, N atoms accumulate on the surface,[29], and 3-D growth occurs.

Shown in Fig. 4.3(e) is the AFM image for a sample grown with J_{Ga}/J_N= 1.01 ($J_{metal}/J_N = 1.08$) and the zoom-in image of that surface. This image clearly reveals a qualitatively different type of surface morphology characterized by very smooth areas and some large precipitates. These precipitates have irregular shapes, some being more compact and some having a linear shape. The compact ones have lateral dimensions ranging from 2–10 μm, heights varying from 0.1–0.9 μm, and we see ∼ 5×10^{-3} $\mu\mathrm{m}^{-2}$. The linear islands can be very long; in some SEM images they go on for several hundred μm or more.

The zoom-in image of the smooth area between the large precipitates shows the typical morphology of a smooth GaN surface grown under Ga-rich conditions by rf MBE.[17] A further zoom-in (not shown) of this smooth surface reveals individual atomic-height steps.

The precipitates contain large amounts of Mn as revealed by EDX (see below). To understand why the Ga-rich conditions lead to large Mn precipitation with atomically smooth regions in between the precipitates, it is useful to consider the structure of the GaN surface under Ga-rich conditions. As has been previously reported in several different places, it is now well understood that the Ga-rich surface of Ga-polar GaN consists of a liquid Ga bilayer.[17, 51, 18] This liquid layer of Ga metal at growth temperature is like a "sea" of atoms all moving rapidly. Based on the strong similarity of the growth behavior in Ga-rich conditions for MnGaN and GaN, we conclude that the surface structure is nearly the same for the two cases. For MnGaN, Mn dopants added to this liquid Ga bilayer are evidently not able to penetrate it. This is reasonable considering the high energetic stability of the Ga bilayer and the fact that the vapor pressure of Mn is of order 10^2 larger than Ga at the growth temperature. Therefore the Mn dopants are carried along on top of the layer or within the top monolayer.

The schematic picture of the surface during growth is shown in Fig. 4.1(c). Since most likely it is the lower monolayer of Ga atoms which mainly participate in GaN growth (at step edges for example), the Mn atoms are never able to come into contact with the top-most GaN bi-layer (growth sites). Thus the Mn is not incorporated. The Mn atoms are carried along the surface until Mn-rich islands begin to form. The liquid Ga "sea" continues to bring new Mn to these islands and they grow, resulting in the observed precipitates seen in Fig. 4.3(e). The linear features are presumably caused by anisotropic growth of the Mn-containing islands. The tallest islands also correspond to the ones having smaller lateral dimensions. Finally, the fact that Mn atoms are evidently swept away by the Ga bilayer is also the explanation for why the Ga-rich transition point is little changed compared to growth without Mn. Shown in table 4.1 is a summary of the Ga/N flux ratios and richness of the samples.

$R_{Ga:N}$	$R_{metal:N}$	T_s	Growth Condition
0.76	0.83	550 °C	N-rich
0.84	0.91	550 °C	slight metal-rich
0.92	0.99	550 °C	metal-rich
0.98	1.05	550 °C	metal-rich
1.01	1.08	550 °C	Ga-rich

Table 4.1: Summary of the MnGaN samples with their growth parameters and growth mode.

4.3.2 Effect of Flux Ratio on Film Polarity

Now we address the issue of the film polarity. RHEED patterns have been shown to be identifiers of the polarity of GaN by Smith *et al.*[52] To verify the polarity of our MnGaN films, they were overgrown with GaN and then cooled to less than 200°C. It is known that if the film has Ga-polarity, a pseudo–1×1 ("1×1") pattern will be observed at low temperatures. On the other hand, if a 3×3 or 6×6 pattern emerges, then the film has N polarity.

As shown in Fig. 4.2(f) for the N-rich grown MnGaN film, the pattern after overgrowing and cooling clearly shows the 1×1 with faint outside additional streaks, the characteristic of the “1×1” surface, thus showing the Ga-polarity of the substrate was maintained.[52] Similarly, we observe the “1×1” pattern for the case of slightly metal-rich growth, as shown in Fig. 4.2(g), again proving the Ga-polarity of the substrate is maintained for the film.

When the conditions of growth become more metal-rich, however, we observe a different result. Namely, after cooling the Ga-rich overgrown layer, the RHEED pattern shows both 3×3 and 6×6 structure, as shown in Figs. 4.2(h) and 4.2(i), respectively. This indicates that the polarity of the MnGaN film, grown on a Ga-polar GaN substrate, has apparently flipped to become N-polar.[52]

Finally, the result of the polarity test for the case of Ga-rich growth of MnGaN is displayed in Fig. 4.2(j). Clearly, upon cooling, the RHEED pattern shows the characteristics of the “1×1” with no sign of 3×3 or 6×6. Thus, the MnGaN film grown under Ga-rich conditions remains Ga-polar.

Based on our previous discussions of the surface structure during growth for the three different regimes, the polarity dependence can be understood as follows. Under N-rich or slightly metal-rich conditions, Mn atoms at the surface do not build up much higher concentration than in the bulk ($\sim$ 5%). They are thus incorporated and do not modify the polarity. Under Ga-rich conditions, the Mn atoms are swept away by the liquid Ga bi-layer and also cannot modify the Ga-polarity. However, under substantially metal-rich conditions (but not Ga-rich), it may be that excess Mn accumulates at the surface, forming a Mn-rich surface monolayer. It has been reported that a magnesium rich surface layer causes polarity flipping from Ga-polar to N-polar.[53] We thus infer that a similar mechanism occurs for the case of manganese.

4.3.3 Bulk Structure and Chemical Content

The samples were analyzed using SEM, and EDX spectra were collected to assess the chemical content. Shown in Fig. 4.4(a) is the EDX spectrum of the N-rich grown sample ($J_{Ga}/J_N = 0.76$) corresponding to Figs. 4.2(a) and 4.2(a). The Ga $K_{\alpha 1}$ and Ga $K_{\alpha 2}$ peaks are evident, and also small Mn $K_{\alpha 1}$ and Mn $K_{\alpha 2}$ peaks are seen. The Mn/Ga peak area ratio is about 4.3%, which also samples the Ga of the GaN substrate. As the AFM image of this sample [Fig. 4.3(a)] indicates a homogeneous layer without any precipitates, we infer that the Mn is incorporated uniformly in the layer.

Shown in Fig. 4.4(b) is the EDX spectrum of the metal-rich grown sample (J_{metal}/J_N = 1.05) corresponding to Figs. 4.2(d) and 4.3(d). Both Mn and Ga peaks are observed, and the Mn/Ga peak area ratio is similar to that of the N-rich grown sample. The AFM image of Fig. 4.3(d) indicates a homogeneous surface at large scale but some inhomogeneities at smaller scale. However, the EDX spectrum averages over these small features, and therefore it only suggests the Mn is possibly incorporated in the layer for this metal-rich condition.

Shown in Fig. 4.4(c) are EDX spectra for a Ga-rich grown sample ($J_{Ga}/J_N = 1.21$) with a surface similar to that shown in Fig. 4.3(e). These spectra were acquired with the electron beam focused on particular regions. The lower spectrum is representative of the compact precipitates seen in the AFM image. It shows Mn peaks which are almost half as large as the Ga peaks, and the Mn/Ga peak area ratio is $\sim 43\%$ (Note: the Ga signal may also partly come from the GaN substrate). Thus the Mn content of these precipitates is quite large. Also, for the linear features, we observe a large Mn/Ga peak area ratio of $\sim 18\%$ (spectrum not shown). The upper spectrum is representative of the smooth areas in between the precipitates. These areas have quite different chemical content - the EDX spectrum shows no sign of Mn peaks. Therefore, these regions have little if any Mn. Thus for Ga-rich growth conditions, the resulting film has a highly non-uniform Mn incorporation. Indeed, it appears that most of the film is mainly GaN with the Mn precipitating into concentrated clumps and linear features. This is consistent with what Cui *et al.* observed for their growth without adding hydrogen. The crystalline structure of these microscopic precipitates has not been determined.

To provide an additional, independent measurement regarding Mn incorporation, RBS was performed on the films. Results for the N-rich, metal-rich, and Ga-rich MnGaN films are shown in Figs. 4.5(a), 4.5(b), and 4.5(c), respectively.

For N-rich growth, Fig. 4.5(a) shows the random (incident beam randomly aligned with sample normal) spectrum (dark dots), clearly revealing the presence of a Mn hump at an energy of $\sim$ 2.28 MeV. The data agrees well with the RUMP simulated

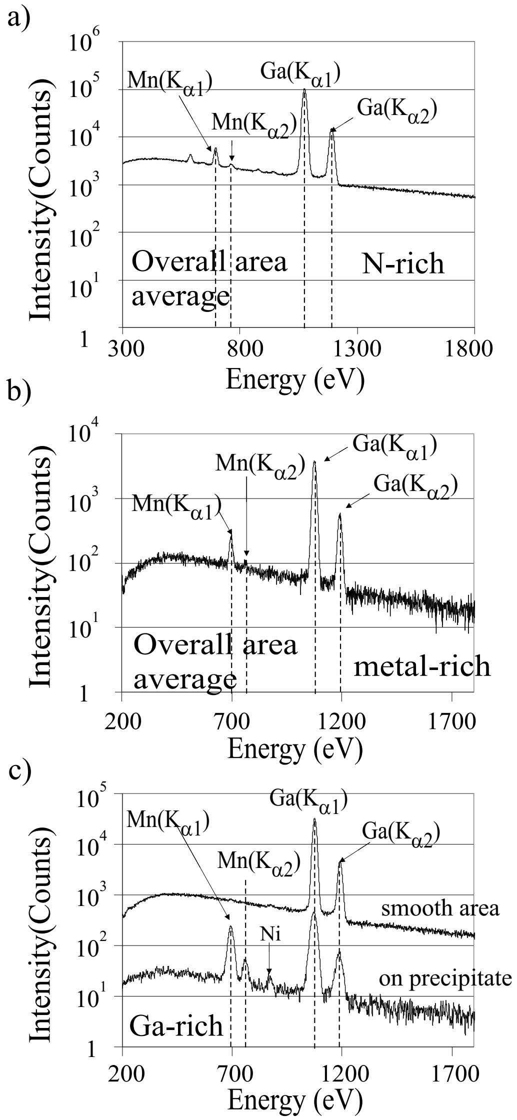

Figure 4.4: EDX spectra as a function of the Ga/N flux ratio: a) N-rich ($J_{Ga}/J_N = 0.76$); b) metal-rich ($J_{Ga}/J_N = 0.92$); c) Ga-rich ($J_{Ga}/J_N = 1.21$). For (c), upper spectrum is for region between the precipitates; lower spectrum is for one of the compact-shaped precipitates, showing a Mn/Ga peak area ratio of 43%.

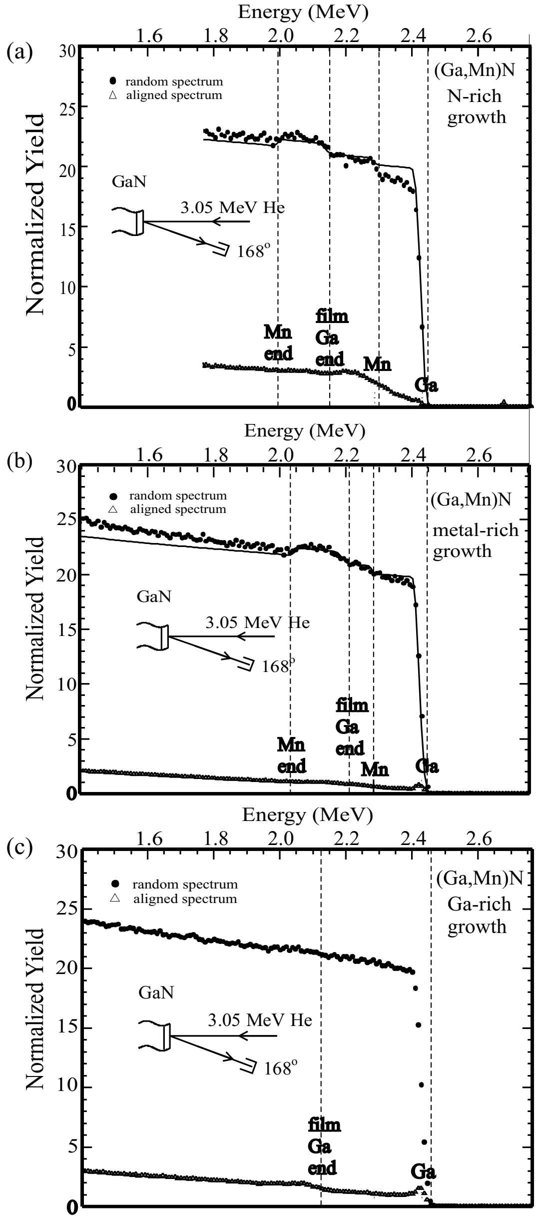

Figure 4.5: RBS spectra as a function of Ga/N flux ratio: a) N-rich ($J_{Ga}/J_N = 0.76$); b) metal-rich ($J_{Ga}/J_N = 0.92$); c) Ga-rich ($J_{Ga}/J_N = 1.21$). Dark dotted data points represent the randomly aligned data; light triangle points represent the aligned data (crystal axis aligned with He ion beam). The continuous black curves represent simulations using the RUMP code.

spectrum (black line) for a layer having $\sim$ 5% Mn/Ga.[54] The smaller data values compared to the model fit near the Ga onset (surface region) is due to the surface roughness shown in Fig. 4.3(a) not taken into account in the model. The aligned spectrum (light triangles) shows a rapidly rising signal, indicating poor channeling for the film, followed by a more slowly rising part, indicating good channeling for the substrate. A likely cause of the poor film channeling could be the presence of interstitial metal atoms; we also observed similar behavior for MBE-grown GaN under N-rich conditions.

For the case of metal-rich growth [Fig. 4.5(b)], the presence of Mn is also revealed by the Mn onset at energy $\sim$ 2.28 MeV in the random spectrum (dark dots). The data agrees well with the RUMP simulated spectrum (black line) for a layer having $\sim$ 5% Mn/Ga. In addition, the aligned spectrum (light triangles) in Fig. 4.5(b) shows a slowly rising signal, indicating good film channeling and no clear Mn hump. This suggests that the Mn atoms in the film are well aligned with the Ga atoms and that there are negligible interstitial atoms. This is strong evidence that the incorporated Mn is substitutional on the Ga sites. Thus, the slightly metal-rich growth regime has the attributes of a comparably smooth surface [indicated by the AFM image of Fig. 4.3(b)] as well as Mn incorporation and is thus a candidate for the ideal conditions for growing the highest quality MnGaN layers using rf N-plasma MBE.

For Ga-rich growth, the random (dark dots) spectrum in Fig. 4.5(c) indicates the presence of Ga only in the film, and there is no indication of any Mn signal. The aligned spectrum (light triangles) shows an interface between the film and MOCVD GaN at energy 2.1 MeV and also no evidence for any Mn. Although the EDX clearly reveals Mn on the surface in the form of precipitates, the RBS is sensitive to the total volume fraction of Mn, which is apparently very small.

The crystallinity of the layers was assessed using XRD. Shown in Fig. 4.6 are the XRD results for four films: 1) MBE-grown GaN on MOCVD GaN substrate (control sample in N-rich conditions, $J_{Ga}/J_N = 0.7$); 2) MnGaN under N-rich conditions ($J_{Ga}/J_N = 0.76$); 3) MnGaN under metal-rich conditions ($J_{Ga}/J_N = 0.92$); 4) MnGaN under Ga-rich conditions ($J_{Ga}/J_N = 1.21$). Shown is the third-order 0006 peak region for GaN near $2\theta = 126°$. Both the $K_{\alpha 1}$ and the $K_{\alpha 2}$ peaks are clearly resolved for all three films at 125.96° and 126.53°, respectively. Given that Cu $K_{\alpha 1} = 1.540$ Å and Cu $K_{\alpha 2} = 1.544$ Å, the known lattice constant of GaN, $c = 5.186$ Å, is obtained.[55]

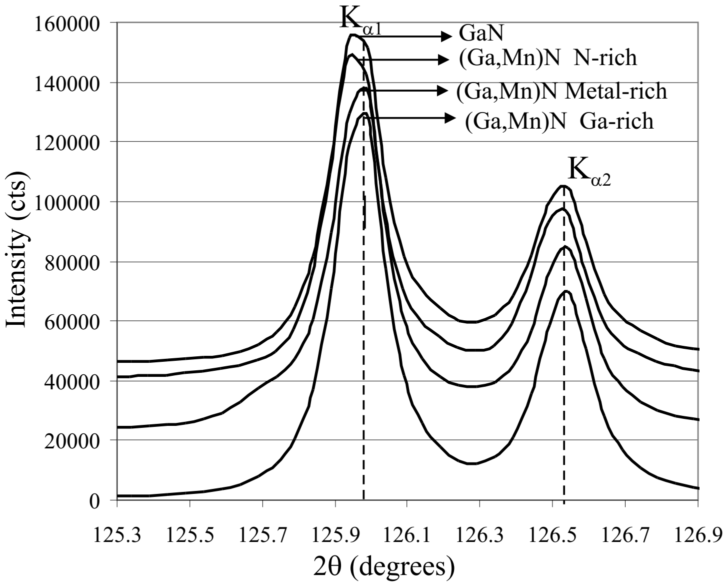

Figure 4.6: XRD 2θ spectra near 126° for MBE-grown GaN (control sample), N-rich grown MnGaN, metal-rich grown MnGaN, and Ga-rich grown MnGaN, showing the 0006 GaN peak region. Vertical offsets have been added for clarity.

Surprisingly, the positions of the peaks are the same for all 4 films to within 0.005°, implying a lattice constant change of < 0.0001 Å with respect to c of GaN. We also find little evidence for broadening of the 0006 peak for the three MnGaN films.

Only Cui *et al.* and Sonoda *et al.* reported lattice constant shifts for their GaMnN samples grown using N_2H_2 plasma and ammonia, respectively.[9, 50] In fact, we note that Cui *et al.* reported an increase in the c-axis lattice constant while Sonoda *et al.* reported a decrease in the c-axis lattice constant.

Our observations are consistent with many papers not reporting peak shifts for MnGaN samples grown using rf N-plasma MBE.[46, 49, 8, 7] And, our EDX and RBS results clearly show the incorporation of $\sim 5\%$ Mn in our N-rich and metal-rich grown films. Thus, we can only conclude that the bilayer spacing in wurtzite GaN is not very much affected by such small Mn concentrations.

4.3.4 Magnetic Properties

Lastly, we compare the magnetic properties of the films using VSM. The magnetic measurements have been done at room temperature and are shown in Figs. 4.7(a), 4.7(b) and 4.7(c).

The VSM measurement of the N-rich grown sample ($J_{Ga}/J_N = 0.76$) is shown in Fig. 4.7(a). After subtraction of the diamagnetic contribution from the sapphire substrate, the film shows a weak diamagnetic behavior with little indication of ferromagnetic (FM) behavior.

The VSM measurement of the metal-rich grown sample ($J_{Ga}/J_N = 0.92$) is shown in Fig. 4.7(b). Again, only a weak diamagnetic behavior is observed with little sign of FM behavior. However, we do note that both the N-rich and metal-rich grown films show a tiny separation in their hysteresis loops.

There are several probable explanations for the negligible FM behavior for N-rich and metal-rich growth. One reason could be that VSM lacks the sufficient sensitivity to observe it. A second possible explanation is that the sample needs to have the correct carrier type and concentration, whereas we have not yet attempted to specifically dope the film. The Mn may act as an acceptor in a film which would otherwise be *n*-type due to small concentrations of N-vacancies or other unintentional impurities. Thus the film could even be insulating. A third possibility is that the Mn concentration needs to be higher or lower, as indicated by a recent theory paper[56].

The VSM result for the Ga-rich grown sample ($J_{Ga}/J_N = 1.21$) is shown in Fig. 4.7(c). After subtraction of the diamagnetic contribution from the sapphire substrate, a small FM loop is observed, as shown in the inset. This small FM behavior cannot however be attributed to the MnGaN since the previously discussed RBS and EDX results show that very little Mn is incorporated into the GaN in the Ga-rich growth case. Ga-rich growth leads to microscopic precipitation of Mn-rich regions. It is known that both GaMn and Mn_4N have FM behavior (ferro and ferri,

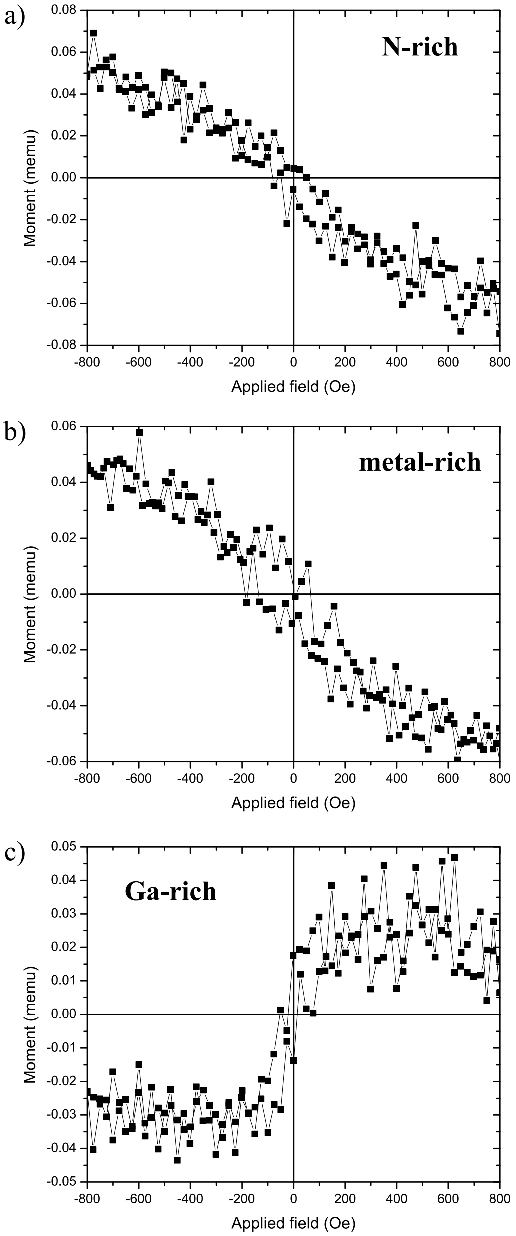

Figure 4.7: VSM measurements of a) N-rich grown film ($J_{Ga}/J_N = 0.76$); b) metal-rich grown film ($J_{Ga}/J_N = 0.92$); c) Ga-rich grown film ($J_{Ga}/J_N = 1.21$). The diamagnetic substrate background has already been subtracted from the original data.

respectively).[57, 58] Therefore, the small FM loop for this sample is attributed to such types of metallic precipitates.

Although we have not yet observed the FM behavior at room temperature in our MnGaN films in which the Mn is incorporated on the Ga sites, we have shown that by choosing the N-rich or metal-rich growth conditions, the FM behavior due to metallic precipitation is eliminated. This makes it possible to move to the next step of intentional doping. Thus these results imply that FM behavior is possible since Mn has been proven to be incorporated into the film on Ga sites, an important step to achieving the FM MnGaN dilute magnetic semiconductor.

4.4 Summary

The growth of MnGaN by rf N-plasma MBE under Ga-rich, metal-rich, and N-rich conditions has been investigated. RHEED shows a streaky, dim pattern for Ga-rich growth, a bright, spotty pattern for N-rich growth, and a partly streaky pattern for slightly metal-rich conditions. Ga-rich growth results in microscopic precipitation and chemical inhomogeneity while N-rich growth results in more uniform incorporation without microscopic precipitation. For metal-rich growth, Mn is incorporated but excess metal precipitates. RBS has shown that slightly metal-rich conditions result in Mn substituting for Ga at the level of $\sim 5\%$ in this study, and AFM confirms minimal precipitation. We also find that it is very difficult to determine incorporation of Mn based on XRD analysis; negligible 0006 peak shifts are observed in our experience.

We have thus shown that either metal-rich or N-rich conditions are necessary for achieving substitutional Mn incorporation on the Ga sites. Metal-rich conditions result in films with better crystallinity compared with N-rich conditions, as determined by RBS channeling. This is presumed to be related to increased surface diffusion for the metal-rich case. Moreover, our AFM study finds that the smoothest surface morphologies occur for either Ga-rich conditions (not including the precipitates) or for slightly metal-rich conditions. Therefore, in order to provide both Mn incorporation on Ga sites and the smoothest surface morphology, it is concluded that the optimal growth conditions for Ga-polar MnGaN by rf N-plasma MBE are in the slightly metal-rich regime.

We also found that the Ga-polarity is maintained for N-rich, slightly metal-rich, and Ga-rich conditions. However, for increasingly metal-rich conditions (but not Ga-rich), the polarity is flipped, resulting in N-polarity. This is attributed to Mn building up and forming a Mn-rich surface atomic layer which leads to the inversion.

Finally, we re-emphasize that the slightly metal-rich growth regime occurs for a metal/N incident flux ratio less than one in our definition due to fact that N-rich, metal-rich, and Ga-rich are surface properties. The surface concentration ratios depend on both the flux rates of metal and N atoms and also the sticking coefficients of metal and N atoms (which vary with the flux rates).

Chapter 5

Dependence of Magnetic Properties on the Growth Conditions of MnGaN Grown by rf N Plasma Molecular Beam Epitaxy

5.1 Introduction

Sato *et al.* have predicted, based on first-principles calculation in the mean field approximation, that MnGaN DMS can exhibit ferromagnetism above room temperature.[56] There are several reports about the growth and ferromagnetism of MnGaN DMS systems.[5, 6, 7, 8] But the reported Curie temperature of these materials varies from 10K to 940K. Moreover, there could be various configurations of Mn, including in the form of 1) magnetic accumulates (or precipitates); 2) $\mathrm{Mn}_x\mathrm{N}$ clusters; and 3) Mn ions. So this remains an open issue how the Curie temperature, accumulation (precipitation), $\mathrm{Mn}_x\mathrm{N}$ clustering, and Mn ion formation, depend on the growth conditions. In this chapter, we report a systematic growth study of MnGaN and discuss the effect of different growth conditions on the magnetic properties of MnGaN.

5.2 Experimental

Transition metal (TM) doped GaN growth was performed in a molecular beam epitaxy(MBE) chamber dedicated to the growth of nitrides. In the growth chamber, solid state effusion cells are used for Ga and Mn sources. RF plasma is used for nitrogen with N_2 as the source gas. During the MnGaN growth, chamber background pressure is set at 9.1×10^{-6} Torr. Growth is monitored *in situ* by reflection high energy electron diffraction (RHEED).

MnGaN samples were grown on MOCVD GaN(0001)/Sapphire(0001) substrates at sample temperature of 550 °C with different Ga/N flux ratios ($R_{Ga:N}$) ranging from 0.7 to 1.46 with constant N flux. Mn/N flux ratio ($R_{Mn:N}$) was kept constant at $\sim$ 0.07. First a 30 nm thick GaN buffer layer was grown, then $\sim$ 0.3-0.6 μm thick main MnGaN layer was grown, the growth was finished with a 30 nm thick GaN cap layer.

After removal from the growth chamber, the samples were characterized by a variety of techniques. Here we report on the results of *ex-situ* atomic force microscopy (AFM) measurements which are correlated very well with the RHEED patterns; furthermore, the magnetic properties of the samples were measured using a superconducting quantum interference device (SQUID). Zero field cooled and field cooled measurements were performed after demagnetizing the sample. Samples were cooled to a temperature of 5K under zero magnetic field then samples were heated slowly to room temperature under the magnetic field of 200 Oe applied parallel to the plane of the film and magnetization of the sample was recorded at each interval. Then samples were cooled down to 5K in a similar fashion in the presence of a magnetic field of 200 Oe and data was recorded.

5.3 Results and Discussions

5.3.1 Modes of Growth

We show that there are 4 distinguishable modes of growth as a function of Ga flux: N-rich, metal-rich, and Ga-rich. The Metal-rich growth mode can further be divided into slight metal-rich and heavy metal-rich growth modes. These modes are distinguished by their RHEED patterns and have distinctly different surface morphology as seen in AFM images. For comparison overall grey scale is shown on the right hand corners of the AFM images.

Qualitatively, these growth conditions can be defined as that under N-rich conditions, there are more surface N atoms than surface Ga and Mn atoms. Metal-rich growth conditions can be defined such that there are more surface metal atoms (Ga+Mn) than surface N atoms. Under Ga-rich conditions, there are more surface Ga atoms than surface N atoms. The ratio of the chemical species present on the surface (e.g., Ga/N) is a function of Ga, Mn and N fluxes, but it is not directly equal to the ratios of those flux values. The reason is that the sticking coefficient of different species varies as a function of the chemical potential of the surface, which in turn determines the surface structure which affects the growth mode. For example, under Ga-rich conditions in which the interaction is between Ga and weakly bound Ga on the surface, the sticking coefficient of Ga will be smaller than under Ga-poor conditions where the interaction of Ga adatoms is not only with surface Ga but also with other species (Mn and N) present on the surface. In the following discussion, we will describe the results in terms of the flux ratios. Interestingly, it is shown below that each of these modes also corresponds to different magnetic properties.

N-rich Growth Mode

Shown in Fig. 5.1(a,b) is the RHEED pattern and AFM image of the MnGaN(0001) sample (MnGaN-1) grown under N-rich conditions ($R_{Ga:N} = 0.76$). The RHEED pattern of the sample is spotty which is an indication of the 3D growth mode, and this is confirmed by the 5 μm × 5 μm AFM image (with gray scale of 326 Å and rms roughness of 57 Å inside the box area) which shows a rough surface consisting of small hillocks but no other noticeable features. This kind of rough surface/3D growth mode is also observed for growth under N-rich conditions without Mn.[15, 26, 17] The N-rich growth mode for GaN(0001) has been explained as due to N accumulation on the surface and loss of Ga, which reduces the surface diffusion for both Ga and N atoms. Mn does not appear to remove this effect. Rutherford backscattering (RBS) has shown that under N-rich growth, Mn is incorporated on the Ga lattice sites, but the de-channeling of 10% indicates defects, which could include some possible Mn and/or Ga interstitials.[60] The Ga-polarity of the lattice is maintained during MnGaN growth under N-rich conditions.[60] A schematic of the surface structure of N-rich MnGaN growth is shown in Fig. 5.2(a). For wurtzite GaN, the stacking sequence is ABABAB... If diffusion is limited, atoms may not find the correct site to maintain this sequence, which may result in stacking faults and other lattice defects. We note that, for the N-rich grown film, we did not observe any statistically significant change in the lateral or perpendicular lattice constants, which one might expect with interstitials. Therefore, the RBS de-channeling of 10% may be more likely attributed to stacking faults.

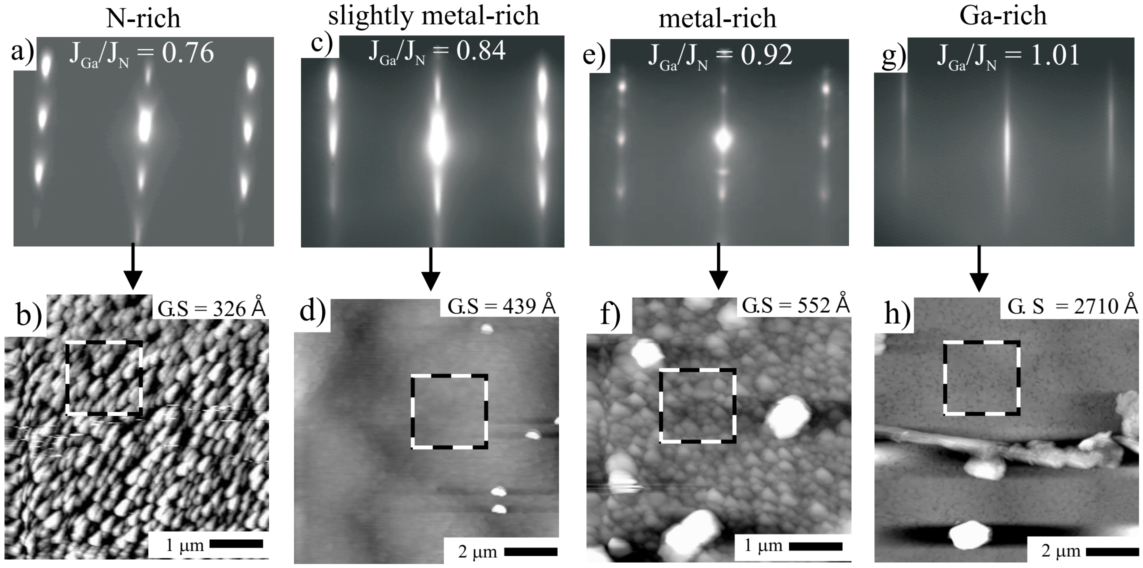

Figure 5.1: RHEED patterns obtained during the growth and AFM images, obtained *ex situ* after the growth, of the MnGaN samples grown at different Ga/N flux ratios. gray scale(GS) is shown on the right hand corner of the AFM images.

Slight Metal-rich Growth Mode

A qualitatively different mode of growth occurs when the Ga flux is increased to $R_{Ga:N} = 0.84$ (MnGaN-2), as shown in Figs. 5.1(c,d), which corresponds to slightly metal-rich growth. Although the RHEED pattern is only slightly less spotty as compared to N-rich growth, the 10 μm × 10 μm AFM image (with gray scale of 439 Å and rms roughness of 12 Å inside the box area) shows a significantly smoother-looking surface than MnGaN-1 (N-rich). The few small dots appearing in the image of Fig. 5.1(d) are due to the slight excess of metal (Ga and/or Mn).

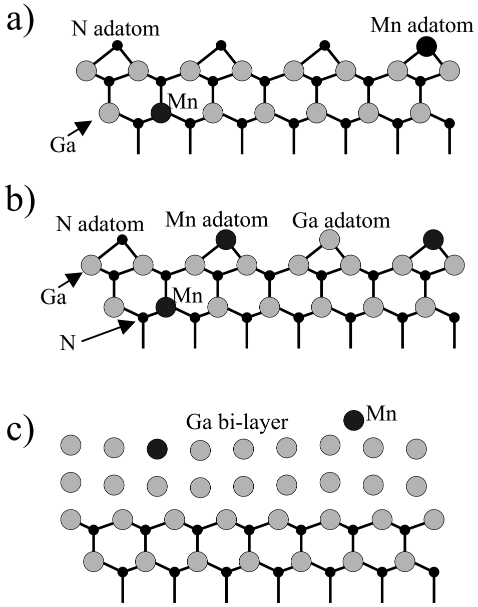

Figure 5.2: Schematic of surface structural models for a) N-rich b) metal-rich and c) Ga-rich growth of MnGaN

For slight metal-rich growth, RBS has shown incorporation of Mn into the GaN lattice as well as increased channeling compared to N-rich growth, suggesting better crystallinity. The polarity for slight metal-rich growth of MnGaN is also maintained from the starting Ga-polarity of the substrate.[60] A schematic surface structure of the metal-rich grown MnGaN sample is shown in Fig. 5.2(b).

Metal-rich Growth Mode

Increasing the Ga flux to $R_{Ga:N} = 0.92$ (MnGaN-3) results in increased metal-rich conditions, as shown in Figs. 5.1(e,f). The RHEED pattern is more spotty, and the 5 μm × 5 μm AFM image (with gray scale of 552 Å and rms roughness of 72 Å inside the box area) shows a rougher surface as well as an increased density of dots appearing on the surface. These dots are attributed to excess metal (Ga and/or Mn). In addition to the dots, we also found that, for highly metal-rich conditions, the polarity of the sample is reversed (from Ga-polar to N-polar).[60]

Ga-rich Growth Mode

For Ga-rich growth conditions, the mode of growth is completely different. The RHEED pattern obtained during the growth of MnGaN (MnGaN-4) under Ga-rich conditions [$R_{Ga:N} = 1.01$] and subsequent AFM image are shown in Figs. 5.1(g,h). Clearly the RHEED pattern is streaky, indicating a smooth growth, and the 10 μm × 10 μm AFM image (with gray scale of 2710 Å and rms roughness of 41 Å inside the box area) reveals the large smooth regions of the surface, similar to what is found for Ga-rich GaN growth.[17] Yet, some large dot-like as well as rod-like features are found at the surface. These are attributed to metal accumulation. Some of these (with rod-like shape) are up to hundreds of microns in length, whereas the dot-like features have lateral dimensions of only 2-10 μm. According to energy dispersive x-ray spectroscopy (EDX), these accumulates contain large amounts of Mn, whereas the smooth areas of the surface contain very little if any Mn.[60] The mechanism behind this distinctly 2-phase growth mode has been explained previously as being caused by the existence of a double Ga layer on the surface, which is known for Ga-rich GaN(0001).[51] RBS of the Ga-rich grown sample shows high crystallinity but no evident Mn incorporation. No reversal of the lattice polarity was found for Ga-rich growth. A schematic diagram of the surface structure of the Ga-rich MnGaN growth is shown in Fig. 5.2(c).

5.3.2 Magnetic Properties of MnGaN as Functions of the Growth Modes

The 4 modes of growth just described lead to distinctly different magnetic properties as measured by SQUID magnetometry. The Mn incorporated was estimated from RBS measurements for samples MnGaN-1, MnGaN-2, and MnGaN-4 to be 5%, 5%, and 0% respectively. It should be noted that the uncertainty of these estimates is $\sim 2\%$. For MnGaN-3, RBS was not performed; we assume that the total amount of Mn is still 5% although some is in the form of accumulates. For Ga-rich (MnGaN-4) we assume the Mn is all in the Mn-rich accumulates which is approximately 5% of total metal. Therefore, in the following, the magnetization/gMn were calculated for each film by estimating the total amount of Mn in the film as 5% of Ga, whether as incorporated or as accumulates.

Shown in Figs. 5.3(a-d) are plots of the temperature dependence of the field cooled (FC) and zero field cooled (ZFC) magnetization of the MnGaN samples for N-rich, slight metal-rich, metal-rich, and Ga-rich growth conditions. For all 4 cases, a low-temperature paramagnetic behavior becomes clearly apparent in the temperature range T < 20-30K.

Magnetization of the samples grown under N-rich, slight metal-rich, metal-rich and Ga-rich conditions is plotted as a function of applied field as shown in Figs. 5.4(a-d). A clear remnant magnetization can be seen in all 4 cases. Note that all the M-H loops were acquired at room temperature except for MnGaN-3, which was acquired at 30K. The coercive field in each case is also shown in Figs. 5.4(a-d).

Magnetic Properties: N-rich Growth

As seen in Fig. 5.3(a), in the case of N-rich growth (MnGaN-1) above about 20K, the magnetization becomes approximately constant (slowly decreasing for FC data) ($\sim$ 77 emu/g Mn at 200 Oe applied field) with temperature for both FC and ZFC curves up to $\sim$ 150K. Since there is not too much difference between FC and ZFC data, evidently the applied field (200 Oe) is strong enough to rotate the moments even at low temperatures. The behavior suggests a ferromagnetic state (region FM-

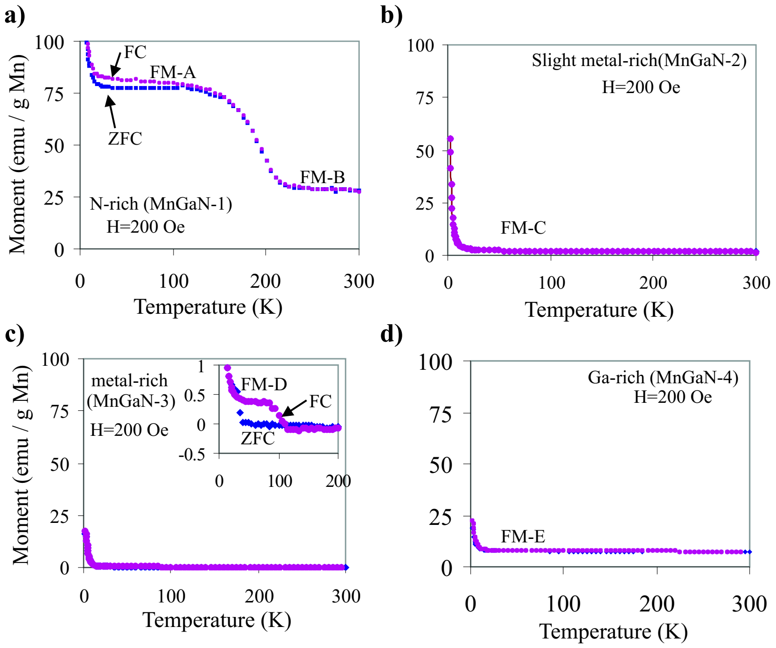

Figure 5.3: Magnetization (emu per grams of Mn) as a function of temperature of MnGaN samples grown under N-rich, slight metal-rich, metal-rich, and Ga-rich growth regimes

A) with a $T_C \approx$ 190K. As temperature increases further, there is another region of nearly constant magnetization ($\sim$ 29 emu/gMn at 200 Oe applied field) in the range above 220K (region FM-B). This FM-B region has ferromagnetic behavior, and the T_C is clearly above room temperature.

The magnetization vs. applied magnetic field (hysteresis loop) is plotted for MnGaN-1 in Fig. 5.4(a) for T=300K, which shows ferromagnetic behavior with a coercive field of H_C = 27 Oe. The magnetization reaches a value of $\sim$ 65 emu/gMn at 1000 Oe. Remnant magnetization of MnGaN-1 is 3.97 emu/gMn.

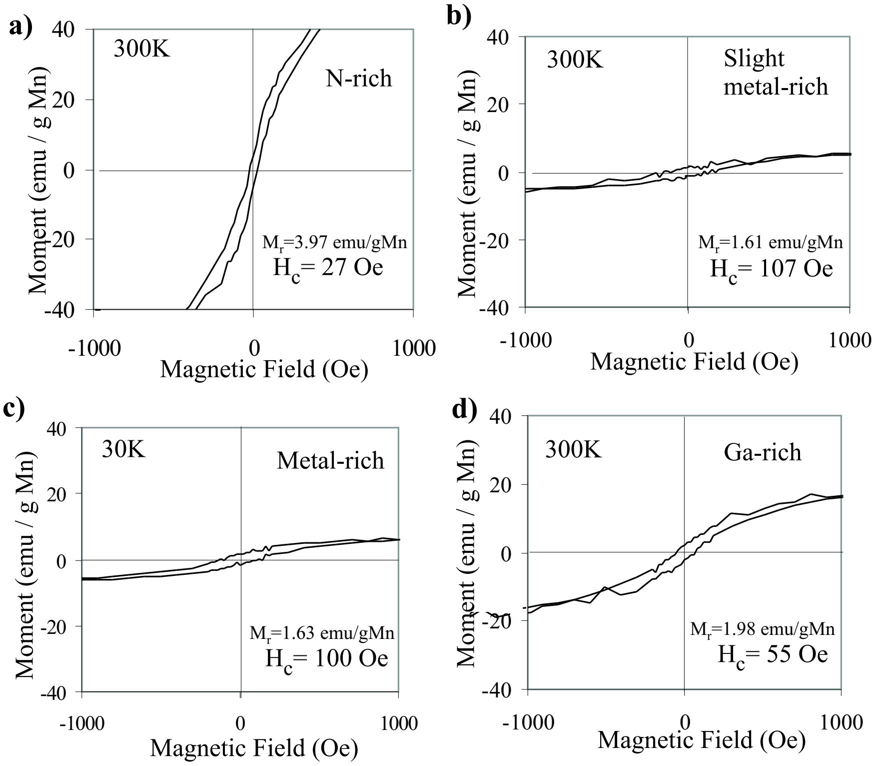

Figure 5.4: Magnetization vs. magnetic field (hysteresis loops) of MnGaN samples grown under N-rich, slight metal-rich, metal-rich, and Ga-rich growth regimes

Magnetic Properties: Slight Metal-rich Growth

A qualitatively different magnetic result is found for a slightly metal-rich grown sample (MnGaN-2), as shown in Fig. 5.3(b). The ZFC and FC curves follow very closely to each other. After the paramagnetic transition there is only a single ferromagnetic region (FM-C) up to room temperature. Within the FM-C region, the magnetization is very low ($\sim$ 2.1 emu/gMn at 200 Oe applied field) although T$_C$ is clearly above room temperature. This M vs. T curve is comparable to that reported in some earlier work.[7]

Shown in Fig. 5.4(b) is the M-H hysteresis curve for MnGaN-2 at T=300K. This sample shows a relatively large coercive field of 107 Oe but ~ 13× smaller magnetization (5.12 emu/gMn at 1000 Oe) compared to MnGaN-1 (N-rich). Remnant magnetization of slight metal-rich grown sample (MnGaN-2) is 1.61 emu/gMn.

Magnetic Properties: Metal-rich Growth

For the metal-rich grown sample (MnGaN-3), yet a different magnetic behavior is observed. As seen in Fig. 5.3(c) for the ZFC data, the magnetization drops sharply to nearly zero at ~ 30K. For the FC data, the paramagnetic region at the lowest temperatures gives way to a weak ferromagnetic region (FM-D) with a $T_C \sim 100$K, which can be seen more clearly in the inset shown in Fig. 5.3(c). We note that the magnetization for the FM-D region (~ 0.37 emu/gMn at 200 Oe applied field) is more than 2 orders of magnitude smaller than that of the FM-A region of N-rich-grown sample MnGaN-1 and ~ 80 times smaller than that of the FM-B region of sample MnGaN-1. Above this weak FM-D region, the magnetization drops to nearly zero as with the ZFC data.

The hysteresis loop is plotted in Fig. 5.4(c) for MnGaN-3 at T=30K. The coercive field at this temperature is relatively large (100 Oe) - about 4× the value for MnGaN-1 (N-rich) at 300K. However, the magnetization is only ~ 5.82 emu/gMn at 1000 Oe applied field. Remnant magnetization of metal-rich grown sample (MnGaN-3) is 1.63 emu/gMn at 30K.

Magnetic Properties: Ga-rich Growth

Finally, the magnetic property of the Ga-rich grown sample (MnGaN-4) is yet again very different compared to those of MnGaN-1, MnGaN-2, and MnGaN-3, as seen in Fig. 5.3(d). Little difference is seen between FC and ZFC data for the given applied field (200 Oe). Above the paramagnetic region, from about 20K and up, the magnetization is approximately constant (but slowly decreasing) all the way up to room temperature. This ferromagnetic region, denoted FM-E, has a T_C clearly above room temperature. We note that the magnitude of the magnetization is ~ 7.85 emu/gMn (at 200 Oe applied field) in region FM-E.

The hysteresis loop for MnGaN-4 is shown in Fig. 5.4(d) for T=300K. At this temperature, the coercive field is $\sim$ 55 Oe, more than twice as large as that for MnGaN-1. Yet, the magnetization at 1000 Oe applied field is $\sim$ 16.68 emu/gMn - about one fourth that of MnGaN-1. Remnant magnetization of Ga-rich grown sample (MnGaN-4) is 1.98 emu/gMn.

5.3.3 Interpretation of Magnetic Results and Correlation with Structural Properties

The results presented here show that for the 4 growth conditions studied, each corresponds to unique magnetic properties. Briefly, while the N-rich sample shows 2 magnetic regions with fairly large magnetization up to > 300K, the metal-rich and slightly metal-rich samples have very small magnetizations. For the Ga-rich sample, the magnetization is much larger than for the metal-rich case. These different regions can be interpreted in terms of different origins of ferromagnetism.

For the N-rich (MnGaN-1) sample, the calculated average magnetic moment per Mn atom at 300K is 1.13 μ_B. Below 190K, the average magnetic moment increases to $\sim 1.85\mu_B$. These calculated average magnetic moments/Mn atom are smaller than the theoretical value of 3.5 μ_B per Mn ion in MnGaN predicted by Das *et al.*[61] and also much smaller than the theoretical values for the Mn site in Mn_xN clusters calculated by Rao *et al.* which range from 4.12-4.54μ_B.[43]. One explanation could be that the number of Mn which are magnetically active is much less than the total number of Mn in the sample.

Shown in Fig. 5.5 is a plot of the remnant magnetization of MnGaN-1 versus temperature. For comparison, zero-field cooled data of MnGaN-1 is also shown in the graph. The remnant magnetization values are taken from hysteresis measurements which were obtained at different temperatures: 5K, 30K, 180K, and 300K. The trend of the remnant magnetization values at 30K, 180K, and 300K matches very well with the trend of the ZFC data. However, while the ZFC magnetization increases, the remnant magnetization decreases, as temperature decreases towards 5K. It is interesting to note that this kind of drop off in the remnant magnetization was not observed in other samples grown under different growth modes.

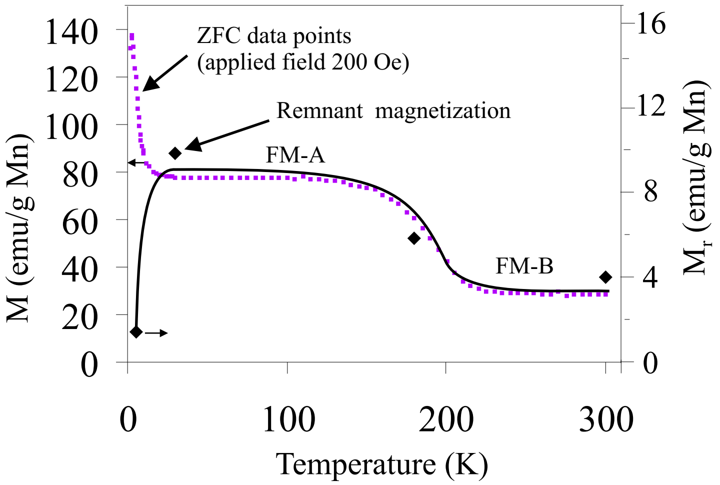

Figure 5.5: Remnant magentization and zero field cooled data as a function of temperature of N-rich MnGaN-1 sample. Solid curve is a guide to the eye.

As described previously, the N-rich sample has two ferromagnetic components as is evident from ZFC and FC data. One of the components (FM-B) has T_C above room temperature, and the other (FM-A) has T_C around 190K. To explain this behavior of the remnant magnetization, we consider that the magnetism is due to either large magnetic accumulates, small magnetic nano-clusters, or else magnetic ions (e.g. carrier-mediated ferromagnetism). If we rule out the accumulates based on the fact that none were seen on the N-rich growth surface, that leaves 2 possibilities. In the case of clusters, there would need to be 2 different types to explain the 2 regions FM-A and FM-B. This is certainly possible.[43] Still, the question is how could the remnant magnetization drop off to a value at 5K below the values at 30K and 300K? Such behavior for magnetic clusters has in fact been reported in the paper by Ploog *et al.*[62] But on the other hand, Ploog *et al.* have not observed a feature similar to the FM-A region shown here. In addition, so far we have no direct imaging or observation of such clusters in this sample.

The other possibility is that the ferromagnetism is due to isolated magnetic ions whose magnetic moments are aligned by mediating carriers (carrier-mediated ferromagnetism). To check the electronic properties of this N-rich grown sample, we performed resistivity measurements over the temperature range from 350K down to 77K. We found that the resistivity of MnGaN-1 (grown N-rich) is very small - about .008 ohm-cm - and is almost constant throughout the temperature range. We also found out that MnGaN-1 is *n*-type. This suggests that MnGaN-1 has a high density of extrinsic conduction electrons. Therefore, these results support the possibility of a carrier-mediated ferromagnetism in this sample.

The drop-off of remnant magnetization below 20K could be attributed to carrier freeze-out. Then the magnetic moments of the Mn ions will be oriented randomly, and the sample will become paramagnetic. However, it is challenging to explain both ferromagnetic regions (FM-A and FM-B) having different T_C's as both being carrier-mediated (although that might be possible if there existed 2 different types of magnetic species).

Third possible explanation is that the magnetic behavior of N-rich grown MnGaN-1 is a combination of carrier-mediated ferromagnetism (region FM-A) and ferromagnetic clusters (region FM-B). This is reasonable since the Curie temperature of large ferromagnetic clusters is expected to be much greater than 300K.[43] Moreover, if we compare the ZFC/FC measurements of MnGaN-1 with the results of Ploog *et al.*, it is evident that FM-A region is not observed in either of their samples, while FM-B region appears more like the magnetic results of their sample B, which was attributed to ferromagnetic clusters.[62] In addition, Ploog *et al.* reported that their samples were insulating, whereas MnGaN-1 sample was found to be conducting.

For the case of slight metal-rich growth conditions (MnGaN-2), the magnetic moment per Mn atom was calculated to be only about 0.084 μ_B at 300K. This very small value indicates that either very few of the Mn are magnetically active and/or there are significant antiferromagnetic interactions. The slight metal-rich regime has the advantage of avoiding the polarity reversal of metal-rich growth; the material remains Ga-polar. But although Mn is incorporated on Ga lattice sites as determined by RBS,[60] and there are very few and small metallic particles, large magnetic moments are still not achieved.

For the metal-rich conditions (MnGaN-3), the calculated magnetic moment per Mn atom in this film is only 0.082 μ_B at 30K. It suggests that few of the Mn are magnetically active and/or there are significant antiferromagnetic interactions. In any case, the metal termination of the surface in metal-rich growth can provide for some reasonable amount of diffusion on the surface. Mn is incorporated in the lattice, although some metallic accumulates are observed. Despite the likely Mn incorporation, a large magnetic moment is not achieved.

For the Ga-rich growth (MnGaN-4), the average magnetic moment/Mn atom is 0.23 μ_B at 300K. Although the T_C is above room temperature and the magnetic moment is larger than for metal-rich case, the magnetism can be attributed to metallic ferromagnetic accumulates,[57] which are shown in the AFM image [Fig. 5.1(h)]. Energy dispersive x-ray (EDX) analysis has previously shown that these accumulates contain significant concentrations of Mn.[60] They may be composed of ferromagnetic Mn_xGa_y compounds as well as ferrimagnetic Mn_4N, both of which have critical temperatures greater than room temperature. The origin of the ferromagnetic accumulation in Ga-rich conditions can be attributed to the presence of a double layer of Ga on Ga-polar GaN(0001) in Ga-rich conditions.[60, 51] This highly mobile layer can promote the fast diffusion and accumulation of Mn. Fast diffusion is consistent with the high crystalline quality of the Ga-rich grown film, but Mn is not incorporated into the lattice substitutionally.

5.4 Summary

It has been shown that the magnetic properties of the MnGaN samples strongly depend on the growth mode. N-rich growth results in two fairly large magnetic components, one of which has a transition temperature which exceeds 300K and the other is at ∼ 190 K. Slight metal-rich growth results in a single very small magnetic component with transition above 300K. Metal-rich growth results in a film with almost zero magnetization at 300K. Finally, Ga-rich growth results in a significant magnetization which is attributed to Mn_xGa_y or Mn_4N compounds. None of the samples discussed here had average values of magnetic moment as large as the theoretical predictions for Mn in GaN.

For DMS behavior, the most likely region based on this study is the N-rich growth regime where a significant magnetic moment is observed. Under N-rich conditions, ferromagnetic metal accumulation and polarity reversal are avoided. The magnetic results for the N-rich grown sample are interpreted as a combination of carrier-mediated ferromagnetism with $T_C \sim 190K$ and ferromagnetic clusters with T_C much greater than room temperature. Further studies are needed to verify the possibility of carrier-mediated ferromagnetism in this sample. For slight metal-rich and metal-rich growth, accumulates are observed although the magnetizations measured for these samples were very small; so, these accumulates do not appear to be ferromagnetic. For Ga-rich growth, the observed ferromagnetism is attributed to the properties of ferromagnetic Mn-rich accumulates which are clearly visible at the surface.

Chapter 6

Room Temperature Ferromagnetism in CrGaN: Dependence on Growth Conditions in rf N-Plasma Molecular Beam Epitaxy

6.1 Introduction

Recent theoretical studies have predicted that Nitride Diluted Magnetic Semiconductors(NDMS) can exhibit ferromagnetism above room temperature.[1, 56] According to Sato *et al.*, based on first-principles calculations in the mean field approximation, CrGaN has a stable ferromagnetic state even with a Cr concentration as high as 25%.[56]

There are a number of reports about the growth and near or above room temperature ferromagnetism for CrGaN.[20, 21, 22, 23] Lee *et al.* reported ferromagnetic-like ordering for Cr doped GaN samples up to 320 K, which were prepared by ion implantation of Cr onto Mg doped MOCVD grown GaN on sapphire substrate.[20] Park *et al.* reported ferromagnetism with T_C = 280 K for Cr-doped GaN single crystals grown by sodium flux method.[21] Hashimoto *et al.* reported above room temperature ferromagnetism in their CrGaN samples grown on sapphire (0001) by electron-cyclotron-resonance plasma-assisted molecular beam epitaxy (ECR-MBE).[22] Liu *et al.* have reported the observation of ferromagnetism in Cr-GaN above 900K which was grown by reactive molecular beam epitaxy.[23]

The topic of transition-metal-doped GaN has however become very controversial, with not much being known in detail about the structural and magnetic properties and how they vary with the growth parameters. In this chapter, we report a study of CrGaN using radio frequency N-plasma molecular beam epitaxy (N-plasma MBE), where we investigate how the structural and magnetic properties depend on the the growth conditions.

6.2 Experiment

Growth of CrGaN samples was performed in a custom designed MBE chamber. Effusion cells are used for Ga and Cr while rf-plasma is used for N with N_2 as the source gas. Sapphire(0001) substrates were heated up to 900 °C and nitridated prior to growth with a plasma power of 500 Watts and N_2 flow rate of 1.1 sccm. Background pressure of the chamber was maintained at 9×10^{-6} Torr during the growth. CrGaN samples were grown at substrate temperatures of 650 and 700 °C. Prior to the growth of the main CrGaN layer, an 80nm thick GaN layer was grown under Ga-rich conditions, resulting in a smooth GaN(000$\bar{1}$) (N-polar) surface.[16] Then, $\sim$ 400nm thick CrGaN layers were grown under different Ga/N flux ratio ($R_{Ga:N}$) ranging from 0.65 to 1.0. The Cr/Ga flux ratio ($R_{Cr:Ga}$) was set to a value of 0.03 or 0.05. Growth was monitored by reflection high energy electron diffraction (RHEED) with electron energy of 20 keV.

After the growth, samples were characterized by *ex-situ* atomic force microscopy (AFM), x-ray diffraction (XRD), and Rutherford backscattering (RBS) measurements. Magnetic measurements were performed using superconducting quantum interference device (SQUID). Zero field cooled (ZFC) and field cooled (FC) measurements were performed after demagnetizing the sample. Samples were cooled to a temperature of 5K under zero magnetic field then heated slowly to a temperature of 300K in the presence of a magetic field of 100 Oe, which was applied parallel to the plane of the film. Magnetization of the sample was recorded at each interval. Then samples were cooled down to 5K in a similar fashion in the presence of the magnetic field, and magnetization was recorded.

6.3 Results

6.3.1 Structural Properties

Growth and Surface Reconstruction

First, we discuss the effect of Cr on smoothening of the surface and formation of reconstructions after the growth. It is known that GaN grown under Ga-rich conditions on sapphire(0001) substrates leads to a 3×3 Ga-adatom reconstruction after the growth and after cooling.[16, 30, 25] But under very N-rich conditions, this reconstruction is not formed after the growth due to the lack of excess Ga on the surface. Moreover, the surface of the N-rich (Ga-poor) GaN film is relatively rough compared to the Ga-rich GaN surface.[17, 63] The difference between N-rich and Ga-rich growth is seen clearly in RHEED, as shown in Fig. 6.1(a) and 6.1(b), where the N-rich RHEED pattern is spotty and the Ga-rich RHEED pattern is streaky.

This clear distinction between N-rich and Ga-rich conditions is less obvious in the case of CrGaN. RHEED patterns for CrGaN films as a function of increasing Ga-rich growth condition are shown in Figs. 6.2(a-f). The details of the growth conditions are given in Table 6.1, where the most Ga-poor growth is sample S1 and the most Ga-rich growth is sample S5. The ordering in Ga-richness of the surface is determined by looking at the surface morphology as seen in AFM images to be discussed below. The Ga-richness follows almost the Ga:N flux ratios, with the exception of sample S4, which due to its higher growth temperature actually has lower surface Ga concentration than sample S5.

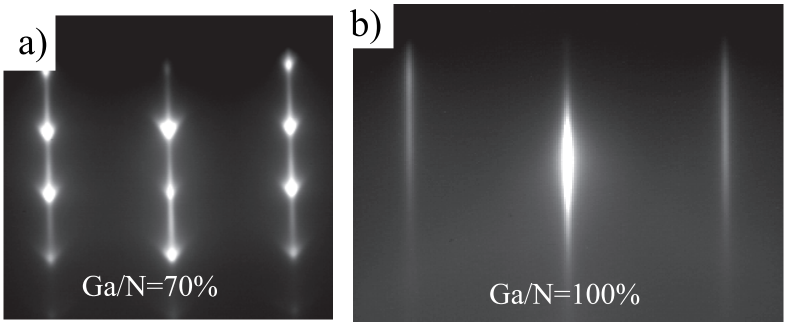

Figure 6.1: RHEED patterns along [11$\bar{2}$0] of a) N-rich GaN taken after the growth and after cooling, b) Ga-rich GaN taken during the growth.

These RHEED patterns were taken during growth near the end of the main Cr-GaN layer. Since taken at the growth temperature, all patterns show only 1×1 reconstruction.

Far from the spotty RHEED pattern of N-rich GaN [Fig. 6.1(a)], all of the growth conditions for CrGaN have fairly streaky RHEED patterns, even the most N-rich growth [Fig. 6.2(a)]. Yet none of the CrGaN RHEED patterns are quite as streaky as that of Ga-rich GaN [compare to Fig. 6.1(b)]. The result is therefore that for CrGaN growth, we should expect to find surfaces with a smoothness intermediate between Ga-rich and N-rich GaN.

Shown in Fig. 6.2(f) is the RHEED pattern of a CrGaN film grown similar to sample S3 but then annealed at 800 °C for 10 min. This RHEED pattern shows very little difference compared to that of sample S3. But, we will show that annealing does dramatically affect the surface and bulk properties of the film.

The presence of Cr on the surface appears to modify the surface structure at the atomic level. Shown in Fig. 6.3 is the RHEED pattern and its line profile for CrGaN sample S1, which was grown at the lowest Ga/N flux ratio, taken at low temperature ($\sim$ 300 K) after the growth. It is observed that the 3×3 reconstruction appears, which does not appear in the case of GaN growth, under N-rich conditions

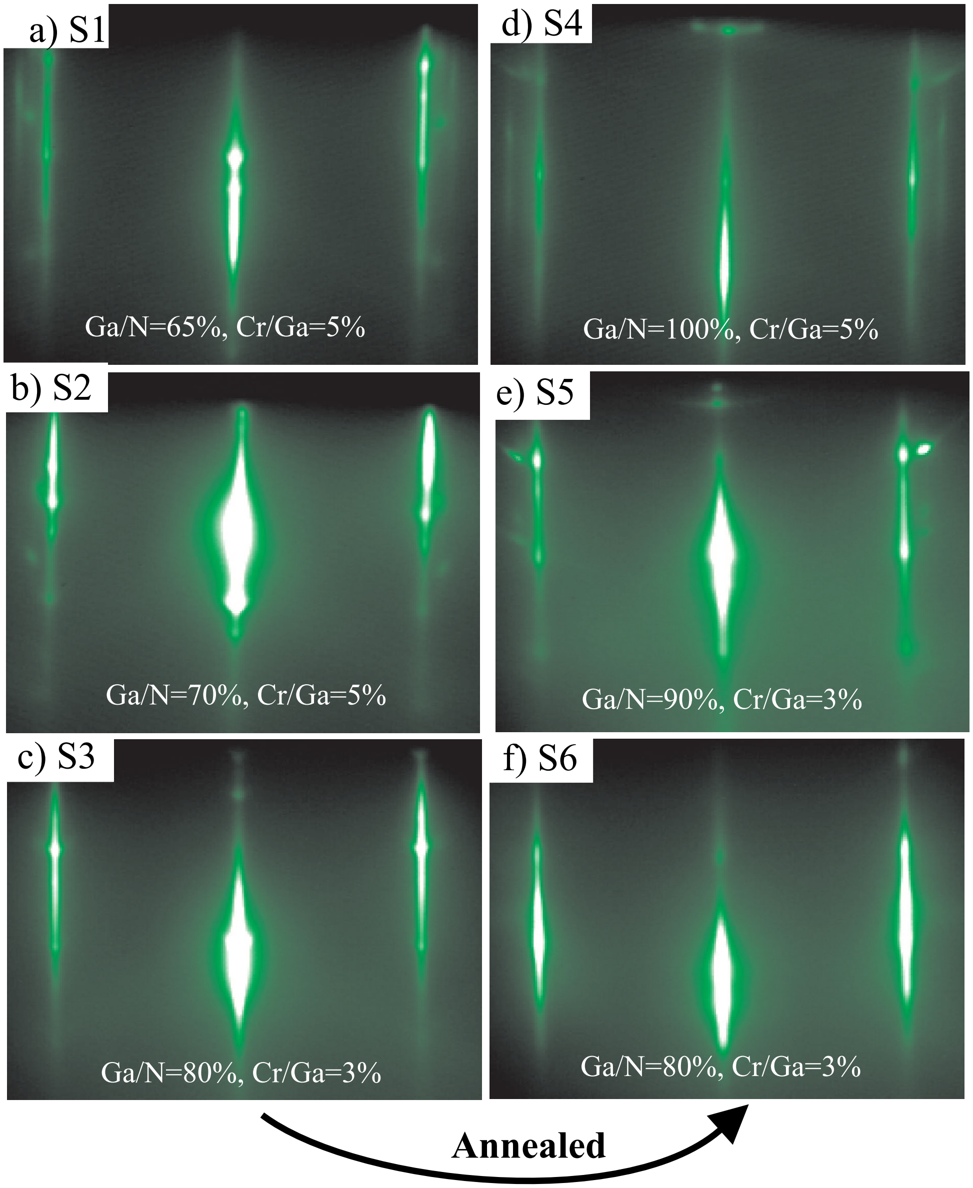

Figure 6.2: RHEED patterns along $[11\bar{2}0]$ of a) sample S1, b) sample S2, c) sample S3, d) sample S4, e) sample S5, and f) sample S6. All the RHEED patterns were taken during the growth.

Samples	$R_{Ga:N}$	$R_{Cr:Ga}$	T$_s$	Growth Condition
S1	0.65	0.05	700 °C	N-rich
S2	0.7	0.05	700 °C	N-rich
S3	0.8	0.03	650 °C	metal-rich
S4	1.0	0.05	700 °C	metal-rich
S5	0.9	0.03	650 °C	Ga-rich
S6	0.8	0.03	650 °C (annealed)	metal-rich

Table 6.1: Summary of the samples with their growth parameters

($R_{Ga:N}$=0.65). The presence of surface reconstruction shows that these surfaces have atomically smooth areas.

To test if Cr is responsible for smoothening the surface, a 150 nm thick GaN layer was grown on sapphire at T$_S$ = 650 °C and $R_{Ga:N}$ = 0.7. After the growth, no 3×3 reconstruction appeared even after cooling to low temperature, as evident from the RHEED pattern shown in Fig. 6.1(a). Then, on top of the GaN layer another layer of CrGaN was grown with the same $R_{Ga:N}$ and $R_{Cr:Ga}$ = 0.03. After the growth and after cooling to $\sim$ 370 K, a 3×3 reconstruction appeared and the RHEED pattern was more streaky, as shown in Fig. 6.4. This suggests that Cr improves the smoothness of the surface, and Cr adatoms may form the 3×3 reconstruction.

To further test if Cr adatoms form 3×3 reconstruction, a fresh GaN surface was annealed at 800°C to remove the Ga adatoms. After cooling to room temperature, a fractional monolayer of Cr was deposited, and the 3×3 reconstruction appeared. So it is likely that Cr adatoms can form a 3×3. This shows that Ga and Cr adatoms have a similar behavior on GaN(000$\bar{1}$).

For some samples, one can notice some extra diffraction spots in the RHEED patterns. This suggests some other surface structures forming, possibly CrN(111) grains. The diffraction spot spacing is approximately consistent with this, i.e. the Ga-Ga real spacing on GaN(000$\bar{1}$) is 3.189 Å,[16] while the Cr-Cr real spacing on

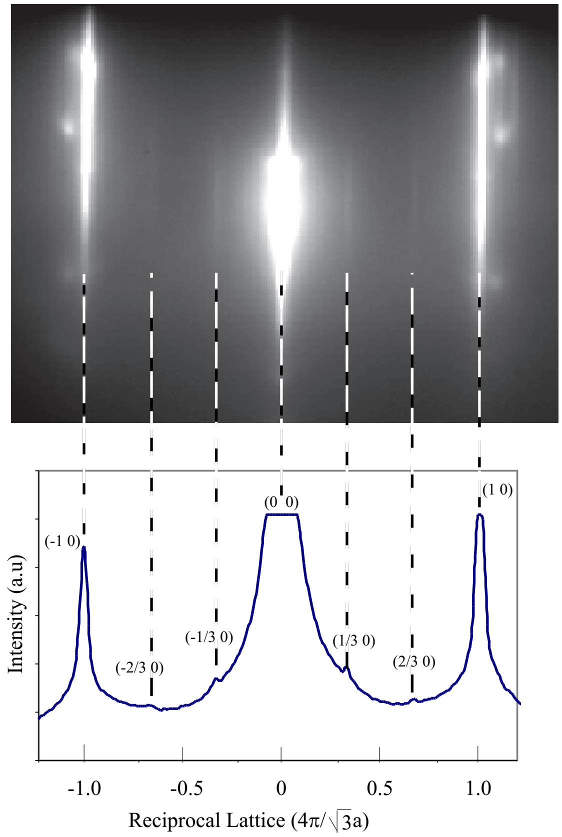

Figure 6.3: RHEED image and its line profile of sample S1, after the growth and after cooling. 1/3-order diffraction lines are shown.

CrN(111) is 2.93 Å.[64] X-ray diffraction (below) also finds in some samples very tiny CrN 222 peaks. But, the correlation between RHEED and XRD on this point is not 100%. Assuming these growth conditions lead to some tiny amount of CrN(111). It does not however seem to affect the magnetic properties; CrN is known to be antiferromagnetic at low temperature but paramagnetic at room temperature.[64]

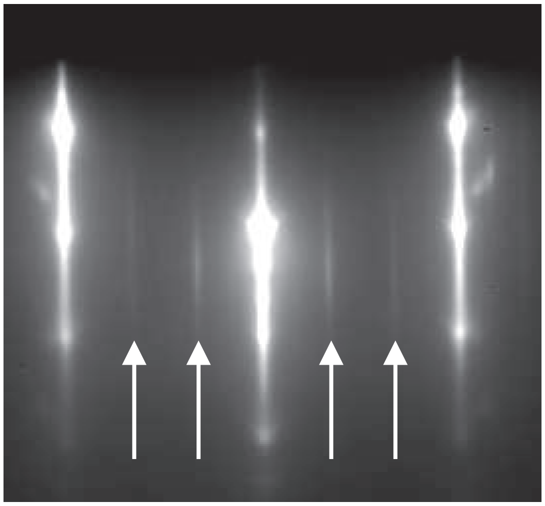

Figure 6.4: RHEED image of CrGaN layer after the growth and after cooling [Ga:N flux ratio = 0.7 and T$_S$ = 650 °C]

Surface Morphology

AFM images of size 5 μm × 5 μm of the surfaces of the samples S1-S6, are shown in Figs. 6.5(a-f). A line profile is shown below each image, which is taken along the dashed line. Root mean square values of the roughness of each surface, S1-S6, are shown at the bottom left hand corner of each image.

For CrGaN sample S1 ($R_{Ga:N} = 0.65$, T$_S$ = 700°C), plateau regions can be seen in the image and in the line profile as shown in Fig. 6.5(a). A similar result is observed for sample S2 ($R_{Ga:N} = 0.7$, T$_S$ = 700°C) as shown in Fig. 6.5(b). No apparent accumulates or precipitates are observed for samples S1 and S2.

For sample S3 ($R_{Ga:N} = 0.8$, T$_S$ = 650°C) shown in Fig. 6.5(c), the AFM image is similar to S1 and S2, although with the appearance of some larger height features marked as "A" on the image. These are typically less than 0.5 μm in size. The AFM image of S4 ($R_{Ga:N} = 1.0$, T$_S$ = 700°C) has an interconnected plateau type morphology with similar sized larger height features, labeled "B".

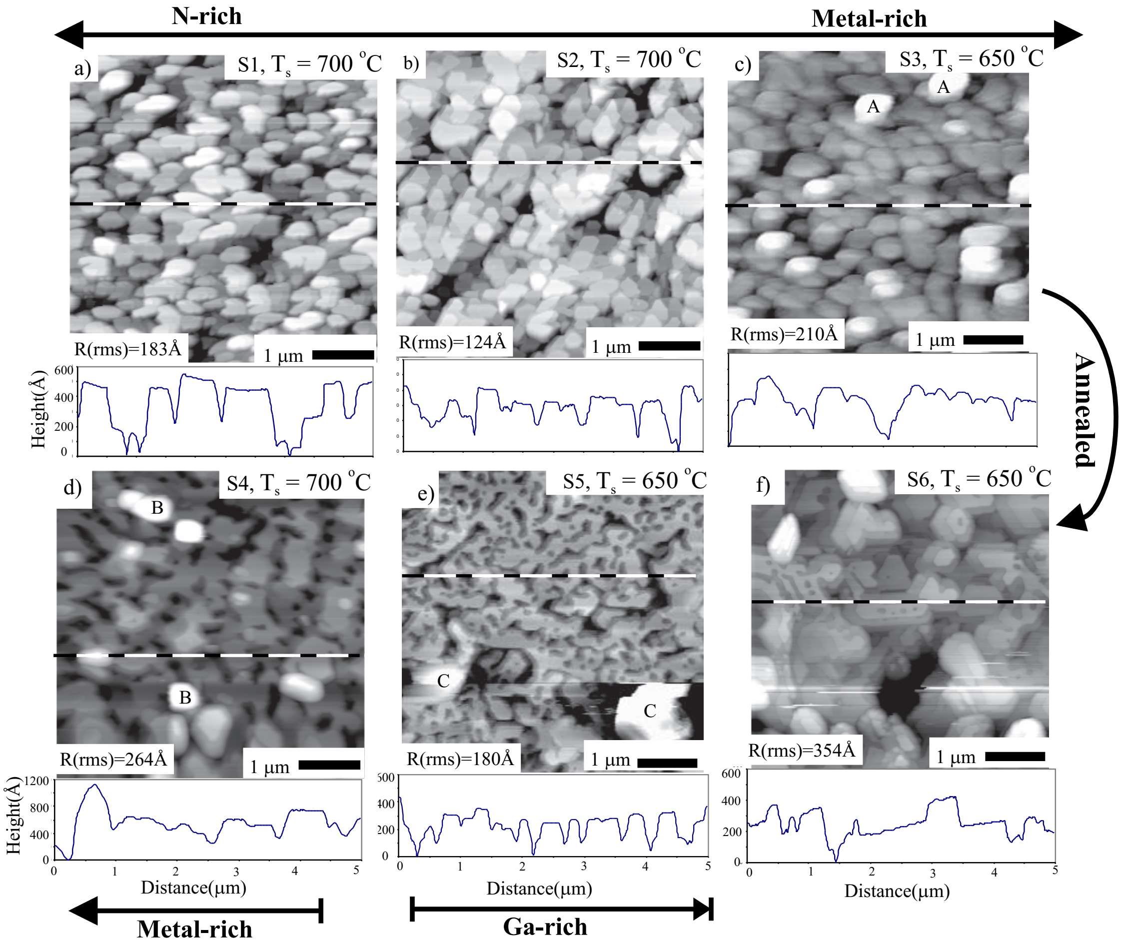

Figure 6.5: AFM images of CrGaN samples a) S1, b) S2, c) S3, d) S4, e) S5, and f) S6

For sample S5 ($R_{Ga:N}$ = 0.9, T$_S$ = 650°C) shown in Fig. 6.5(d), the surface appears as interconnected plateaus and is overall smoother than S4 with some larger height features labeled "C". We note that most of the area has the morphology of Ga-rich GaN growth surface, known from previous studies.[17] The "C" features found on the surface are $\sim 1\mu$m in size.

The AFM results show that the growth parameters do affect the morphology as expected. For almost all conditions, flat plateau-type morphology is seen, with isolated plateaus at N-rich conditions (S1,S3) and more interconnected plateaus at metal-rich and Ga-rich conditions (S3-S5). Some precipitation appears to occur at both metal-rich (S3-S4) and Ga-rich (S5) conditions but not at N-rich (S1-S2) conditions.

For sample S6 ($R_{Ga:N} = 0.8$, $T_S = 650°C$, and annealed), the AFM image also shows a plateau-type morphology with some evident precipitates as shown in Fig. 6.5(e). But the roughness is larger than for all the non-annealed samples. The annealed surface appears to have been partially decomposed, which results in some apparent pitting.

Crystallinity

XRD measurements were performed to examine the CrGaN crystallinity. Shown in Fig. 6.6(a) is the XRD spectrum of sample S3. There are CrGaN($000\overline{1}$) peaks of 2nd, 4th and 6th order along with sapphire 0006 and sapphire 00012 peaks.

These CrGaN peaks appear at the same position as GaN peaks and we did not observe any clear peak shift for samples S1-S6. The lack of significant alloy peak shift is consistent with our previous results for Ga-polar MnGaN grown on MOCVD GaN/Sapphire(0001) where Mn was shown to have been incorporated into the lattice.[60] This behavior may be related to lack of iso-crystallinity between CrN or MnN (both face-centered tetragonal, octahedral bonding) and GaN (wurtzite, tetrahedral bonding). For isocrystalline nitrides MnN and ScN, we have shown XRD peak shifts of the alloy MnScN consistent with Vegard's law.[65]

In addition, there are some CrN 111 and 222 peaks with very low intensities for sample S3. XRD spectra of samples S1, S2, S4 and S5 are very similar, also having these CrN peaks (although almost absent for S5). The largest 111 CrN peaks are for samples S1 and S2, where the intensity ratios to the GaN $000\overline{2}$ peak are $\sim 0.12\%$ and 0.17%, respectively. The CrN 111/GaN $000\overline{2}$ intensity ratios for S3, S4, and S5 are 0.05%, 0.04%, and 0.01% respectively. Since these CrN peaks are so small, we conclude that our CrGaN films are of very high crystalline quality.

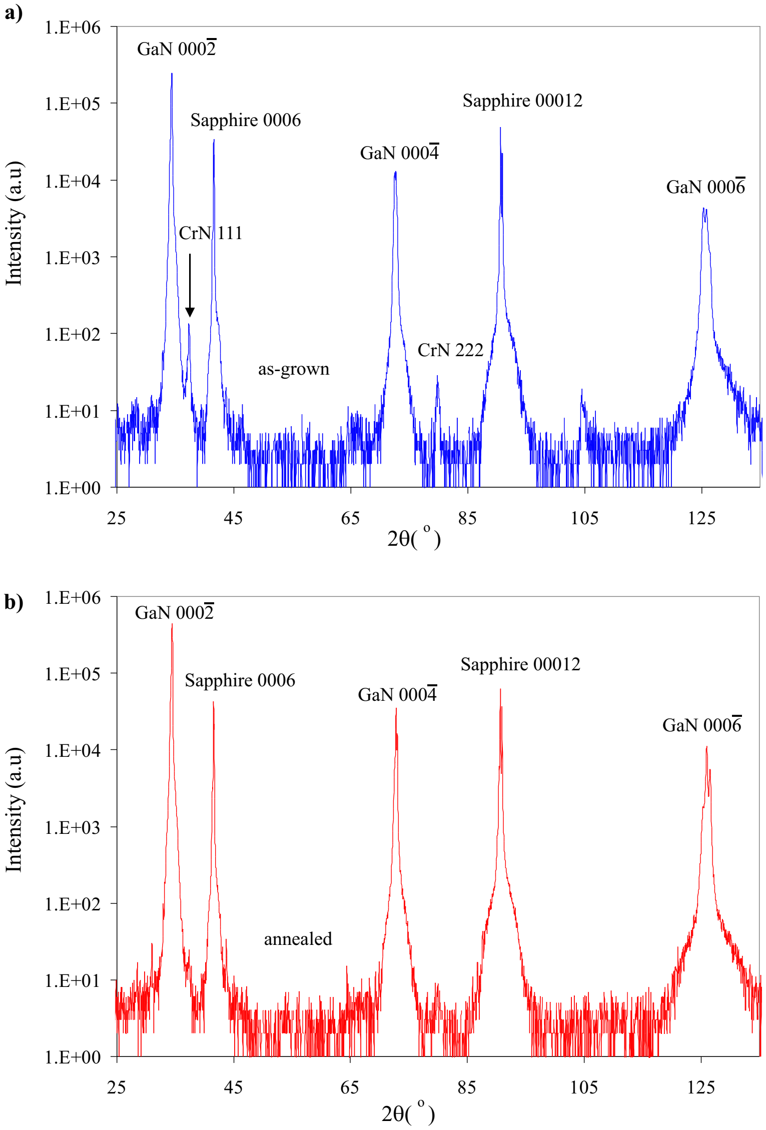

Figure 6.6: XRD 2θ spectra of a) as-grown (S3) and b) annealed (S6) samples grown at Ga/N flux ratio of 80% and Cr/Ga flux ratio of 3% at T$_S$=650 °C.

Rutherford Backscattering spectroscopy (RBS) combined with ion channeling was used to investigate the Cr incorporation. The random spectrum (incident beam misaligned with the sample normal) for sample S3 shows primarily the Ga signal which begins at energy ∼ 2.5 MeV, and a small Cr onset also starts at ∼ 2.25 MeV. The solid line is the RUMP code simulation for the random spectrum of CrGaN using parameters Cr:Ga = 3:100 and Ga:N = 91:100. Although not a perfect fit, it shows that there is Cr incorporation of ∼ 3%; the apparent total metal deficiency (6%) is much less than the total metal:N flux ratio (17% metal deficient). Also, the random spectrum of sample S3 has a rounded edge at the film/vacuum interface, which is attributed to the roughness of the sample surface. The aligned spectrum of sample S3 has a minimum de-channeling level of 17.6%. The smoothness of the aligned spectra and slight change of slope near the Cr edge are consistent with the CrGaN layer having substitutional Cr on Ga lattice sites.

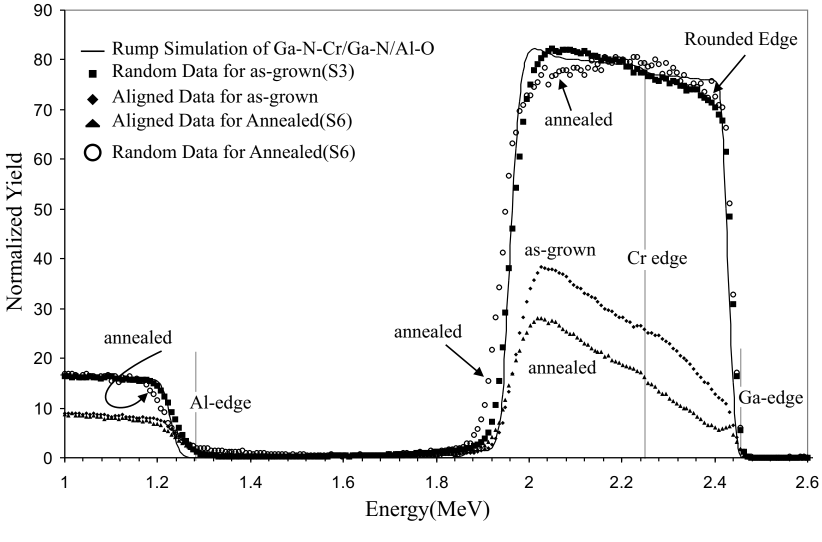

Figure 6.7: RBS results for the as-grown (S3) and annealed (S6) samples.

Shown in Fig. 6.6(b) is the XRD spectrum of the annealed sample S6, where secondary phases are less apparent, particularly the CrN phase, compared to the as-grown sample S3. The CrN 111/GaN $000\overline{2}$ intensity ratio for S6 is 0.01%. The RBS random spectrum for the annealed sample S6 shown in Fig. 6.7 has an even more rounded edge near 2.5 MeV than the as-grown sample S3, which indicates that the annealed sample has a rougher surface than the as-grown sample, in agreement with the AFM results. The rounding at the edges of the annealed sample spectrum could also indicate some diffusion of Ga and/or Cr; even the Al edge is slightly less sharp. The random spectrum for sample S6 has hardly any Cr onset. The aligned spectrum of sample S6 has a minimum de-channeling level of 8.4%, suggesting that annealing may have improved the crystallinity of the sample. Careful observation of the aligned spectrum of the annealed sample S6 reveals a small Cr peak. Overall, it can be inferred from RBS that much of the Cr for sample S6 has diffused out of the film due to annealing.

6.3.2 Magnetic Properties

Magnetic measurements (Zero field cooled (FC), field cooled (FC) and hysteresis(M-H)) were performed, using SQUID, for all of the samples S1-S6, presented above. Shown in Figs. 6.8(a-f) are the ZFC/FC measurements of samples S1, S2, S3, S4, S5 and S6 respectively, at an applied field of 100 Oe. ZFC/FC measurements were performed over the temperature range 5K-300K. Hysteresis measurements were also performed at certain temperatures (5K-300K) and the data is shown in Figs. 6.9(a-f) for samples S1-S6 respectively. Shown in Table 6.2 are the remnant magnetization values and the coercive fields at 5K(10K) and 300K for all of the samples.

Shown in Fig. 6.8(a) are the ZFC and FC magnetization of sample S1. Both ZFC and FC magnetization curves follow each other from 300K to about 140K. Below 140K ZFC curve starts to drop while FC curve increases slightly from 140K to 5K. This indicates that this sample has hysteretic magnetization below 140K. Shown in Fig. 6.9(a) are the hysteresis measurements for sample S1 at 5K and 300K. Sample exhibits hysteresis at 5K with remnant magnetization to saturation magnetization ratio (M_r/M_s) of 0.336 and coercive field of about 300 Oe. Whereas at 300K the

Samples	M_r at 300K and 5K	H_c at 300K and 5K	Richness	Magnetism
S1	(300K) 1.15 $\times 10^{-6}$ emu	5 Oe	N-rich	SPM$\geq$140K
	(5K) 5.08 $\times 10^{-5}$ emu	300 Oe		
S2	(300K) 5.36 $\times 10^{-6}$ emu	88 Oe	N-rich	FM$\geq$300K
	(5K) 1.46 $\times 10^{-5}$ emu	243 Oe		
S3	(300K) 8.52 $\times 10^{-6}$ emu	20 Oe	metal-rich	FM$\geq$300K
	(10K) 1.9 $\times 10^{-5}$ emu	36 Oe		
S4	(300K) 2.74 $\times 10^{-5}$ emu	126 Oe	metal-rich	FM$\geq$300K
	(5K) 7.69 $\times 10^{-5}$ emu	700 Oe		
S5	(300K) 2.55 $\times 10^{-6}$ emu	122 Oe	Ga-rich	SPM$\geq$130K
	(5K) 3.07 $\times 10^{-6}$ emu	150 Oe		
S6	(300K) 2.00 $\times 10^{-6}$ emu	50 Oe	metal-rich	FM$\geq$300K
	(5K) 5.41 $\times 10^{-6}$ emu	186 Oe	Annealed	

Table 6.2: Samples with their remnance, coercivity, their richness and Magnetic properties

M_r/M_s is about .007 and coercive field of about 5 Oe. This is an indication that sample exhibits superparamagnetic behavior at 300K, where coercivity and the remnance is almost zero. At lower temperature grains become blocked and single domain and hence the sample exhibits finite remnance and coercivity. From the ZFC data we can estimate that the blocking temperature is around 140K.

Shown in Fig. 6.8(b) are the ZFC and FC magnetization of sample S2. The ZFC and FC signals are distinctly separated from each other from 5K up to 300K, where the 2 curves meet. The limitations of the SQUID precluded observation above 300K. This sample exhibits hysteresis both at 5K and 300K as shown in Fig. 6.9(b). This sample has a finite remnance and finite coercivity at 300K and hence exhibits ferromagnetism at room temperature. The values for remnant magnetization and coercive field are given in Table 6.2.

Shown in Fig. 6.8(c) are the ZFC and FC magnetization of sample S3. The magnetization of this sample appears similar to that of sample S2 except for small differences in slope. The sample exhibits hysteresis both at 5K and 300K, as shown

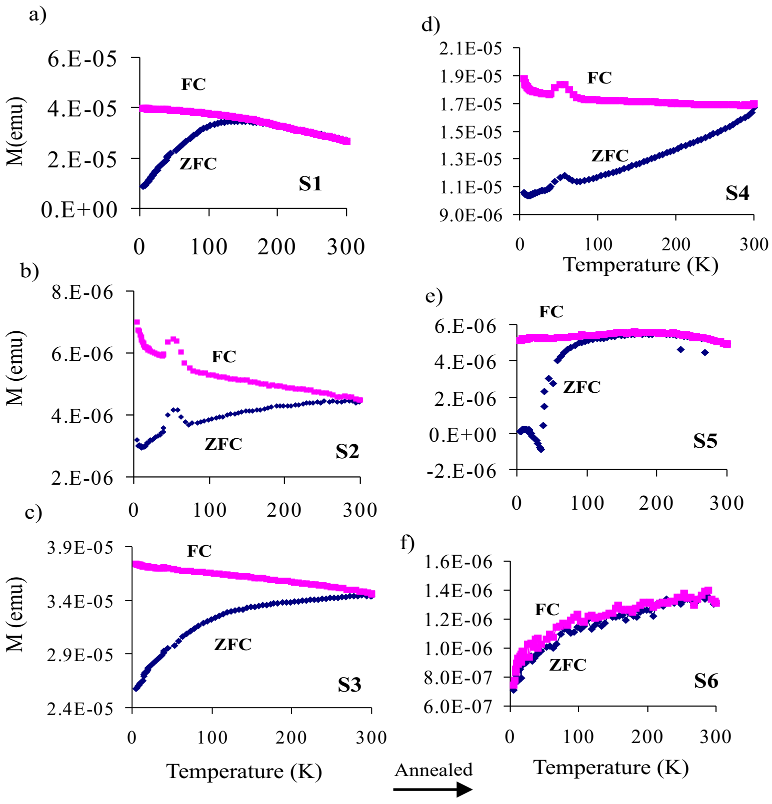

Figure 6.8: ZFC/FC magnetization curves of a) sample S1, b) Sample S2, c) Sample S3, d) Sample S4, e) Sample S5, and f) Sample S6

in Fig. 6.9(c). This sample also has non-zero remnant magnetization and coercivity at 300K which indicates that the sample is ferromagnetic at room temperature.

Shown in Fig. 6.8(d) are the ZFC and FC magnetization curves for sample S4. As with samples S2 and S3, the ZFC and FC curves are distinctly separated from each other up to 300K. This sample also shows hysteresis both at 5K and 300K as shown in Fig. 6.9(d) and hence exhibits ferromagnetism at room temperature. At 5K, the M_r/M_s ratio for this sample is about 0.55 and coercivity of 700 Oe. At 300K, the M_r/M_s ratio drops to a value of about 0.193 and the coercivity of 126 Oe. This

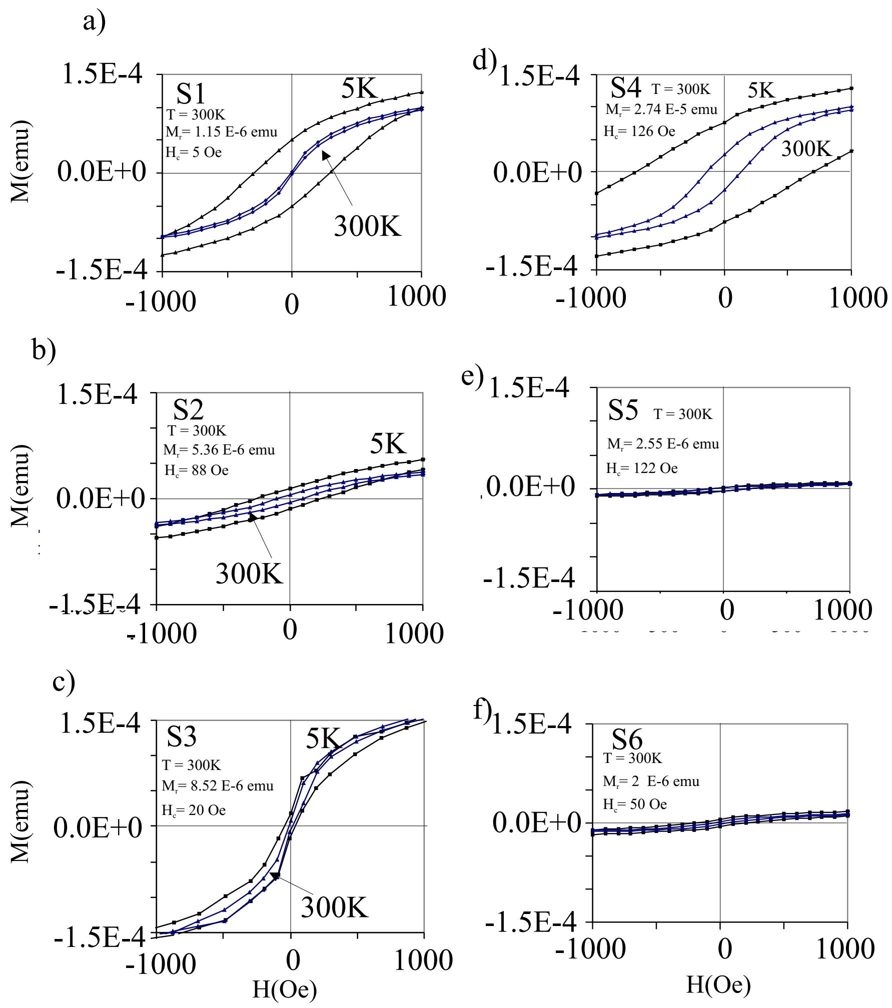

Figure 6.9: Magnetization vs applied field curves for a) sample S1, b) Sample S2, c) Sample S3, d) Sample S4, e) Sample S5, and f) Sample S6, taken at temperatures of 5K and 300K.

sample which was grown under metal-rich condition has the highest M_r/M_s ratio and coercivity at 300K of all the samples.

Shown in Fig. 6.8(e) are the ZFC and FC magnetization curves for sample S5. For S5, the magnetization is very different compared to that of S2, S3, and S4. The FC and ZFC curves are not separated except below about 130K. This sample also exhibits hysteresis both at 5K and 300K as shown by the hysteresis loops in Fig. 6.9(e). This indicates that the sample has ferromagnetism at least up to 300K. But a sharp drop in the ZFC curve also indicates the presence of superparamagnetic grains in the sample. It could be explained that the sample contains both smaller size superparamagnetic grains and the ferromagnetic grains. That is why we have observed non-zero remnance and ceorcivity above the blocking temperature which is around 200K.

ZFC and FC magnetization curves for sample S6 is shown in Fig. 6.8(f). This sample was grown under the same growth conditions as sample S3 except this was annealed at a temperature of 800 °C. The ZFC and FC data for this sample [Fig. 6.8(f)] appears completely different than for sample S3 [Fig. 6.8(c)]. In the case of sample S6, both ZFC and FC curves follow each other very closely over the whole temperature range from 5K to 300K. Moreover, M is lower at lower temperatures which is an indication of antiferromagentic alignment of the magnetic ions at lower temperature. Shown in Fig. 6.9(f) is the hysteresis measurement of the sample at 5K and 300K. This indicates that the sample is ferromagnetic at least up to room temperature. However the value of M_r is about 4 times smaller compared to the as-grown sample(S3). On the other hand at 300K the value of the coercive field for sample S6 is more than 2 times larger and at 5K it is about 5 times higher than for sample S3. RBS has suggested the removal of Cr from the film due to annealing.

These measurements demonstrate that the magnetic properties depend strongly on the MBE growth conditions, particularly the surface Ga concentration. We find that although the amount of surface Ga depends partially on the substrate temperature in addition to the Ga:N flux ratio, the substrate temperature itself does not directly control the magnetic properties of CrGaN films grown by rf plasma MBE over the window of substrate temperature studied here (650-700°C). For example, while samples S1 and S2 grew at the same sample temperature, they have totally different magnetic properties. Also, while samples S3 and S4 grew at different sample temperatures, they both show similar magnetic properties (ferromagnetic, high T_C). We also find that the Cr:Ga flux ratio, within the small window used here (3-5%), does not itself directly control the magnetic properties. For example, although samples S1 and S2 grew with the same Cr:Ga flux ratio, they have totally different magnetic properties. Similarly, while samples S3 and S4 grew with different Cr:Ga flux ratio, they have similar magnetic properties. Of course, we expect that Cr:Ga concentration may affect T_C for CrGaN samples with good magnetic properties. Lastly, we have shown that due to annealing (sample S6), remnant magnetization has reduced but the coercive field has increased.

Instead, the growth condition most responsible for directly affecting both the structural as well as the magnetic properties is the surface Ga concentration during growth. But in a ternary material, there can also be a window below Ga-rich which is metal-rich. There can then be 3 regions: N-rich, metal-rich, and Ga-rich. For N-polar GaN, one monolayer of Ga adatoms atop the Ga-terminated GaN bi-layer has been shown to be the limit in order to avoid Ga-droplet formation.[63] Growth at higher Ga flux is Ga-rich and lower Ga flux will be metal-rich and finally N-rich.

We have shown that highly N-rich conditions (S1) results in poor magnetic properties. Ga-rich conditions (S5) results also in weak magnetic properties. Whereas, an intermediate range of surface Ga coverage (S2-S4) shows good magnetic properties. We note that S2 growth conditions were actually N-rich, whereas S3 and S4 conditions are considered metal-rich, based on the surface morphology. But we also note that the magnitude of the M_r/M_s ratio of sample S4 is considerably larger than that of S2 and S3. Thus, we conclude that the conditions for the best magnetic properties of CrGaN are highly metal-rich.

Since it may be noted that the metal-rich growth conditions of samples S3 and S4 show some distinct precipitates in AFM images of Figs. 6.5(c,d), one might question if the magnetism could be attributed to those precipitates. However, several reasons argue against this. First, sample S2 grown under N-rich conditions, does not show those precipitates and yet shows good ferromagnetic properties up to at least 300K.

Second, sample S5 grown under Ga-rich conditions, also shows small precipitates in AFM [Fig. 6.5(e)] and yet has weaker magnetic properties. Thus, the observed precipitates seem not to correlate with the magnetic properties. Third, our XRD measurements do not show any second-phase peaks corresponding to known ferromagnetic Cr-containing compounds. In fact, there is only one Cr-N phase which has been thought to be ferromagnet ie - Cr_2N - but it does not appear in our XRD spectrum. Moreover, a recent paper by Liu *et al.* did not find Cr_2N to be ferromagnetic over the temperature range 10-900 K.[23] One remaining well-known Cr-containing ferromagnet is CrO_2; this oxide could theoretically form at the surface of the samples. However, if so, then we would expect that all 5 samples would show similar ferromagnetism. Therefore, we conclude that the ferromagnetism displayed in Figs. 6.9(b-d) could be due to ferromagnetic exchange interactions between magnetic Cr ions in the GaN semiconductor. Moreover, the RBS measurements support that the Cr is substitutional on Ga lattice sites.

6.4 Summary

CrGaN films were grown at substrate temperatures of 650 or 700 °C and Ga/N flux ratios from 0.65-1.0 with Cr/Ga of 0.03 or 0.05. Analysis of the results shows that both the magnetic and structural properties are dependent on the growth conditions. The growth parameter most directly affecting these properties is the surface gallium concentration, which indirectly depends on the substrate temperature as well as the incident Ga flux. We found that highly N-rich or Ga-rich conditions result in poor magnetic properties. Whereas, slightly N-rich or metal-rich conditions give ferromagnetic behavior at T at least up to 300K. Surface morphology is also strongly dependent on surface Ga concentration. N-rich conditions result in island-like plateau structure. Metal-rich conditions result in either island-like or partly interconnected plateau structure with small accumulates, and Ga-rich conditions result in interconnected plateau morphology also having accumulates. A fairly wide range of growth conditions showed good magnetic properties which are attributed not to second-phase ferromagnetic particles, but rather the observed FM behavior may be due to FM exchange interaction between magnetic Cr ions in the GaN semiconductor. Lastly, all growth conditions showed a 3×3 reconstruction upon sample cooling after growth, suggesting a smoothening effect of Cr.

Chapter 7

Scanning Tunneling Microscopy Study of Cr-doped GaN Surface Grown by RF Plasma Molecular Beam Epitaxy

7.1 Introduction

According to Sato *et al.*, based on their first-principles calculations in mean field approximation, CrGaN has a stable ferromagnetic state at a Cr concentration above 2%, provided Cr substitutes Ga in GaN lattice.[56] Cr incorporation and Cr substitution at Ga lattice site is not an easy task to investigate using bulk techniques. Scanning Tunneling Microscopy (STM) is an important tool to investigate the Cr incorporation and position in the GaN lattice at atomistic scale.

Recently a few results have been reported about the growth and bulk properties of CrGaN. Lee *et al.* have used ion implantation of Cr on Mg doped MOCVD grown GaN on sapphire substrate.[20] Park *et al.* performed the growth of Cr doped GaN single crystal by sodium flux method.[21] Hashimoto *et al.* reported the growth and above room temperature ferromagnetism in CrGaN samples which were grown on sapphire(0001) by electron-cyclotron plasma-assisted molecular beam epitaxy (MBE).[22]

In this chapter, we report the growth and *in-situ* STM study of Cr doped GaN and Cr deposition on GaN, to find out at atomistic level the position of Cr on the GaN surface.

7.2 Experimental Procedure

Growth and depositions were performed in a custom designed ultra high vacuum molecular beam epitaxy (UHV-MBE) chamber where samples can be transferred to the UHV analysis chamber, without exposing them to the air, which is equipped with the room temperature STM. Effusion cells are used for Ga and Cr sources while rf-Plasma is used for nitrogen with N_2 as the source gas. Prior to the growth, samples were heated upto 800 °C and nitridated the surface with a plasma power of 500 Watts with N_2 flow rate of 1.1 sccm . Temperature measurements were done by pyrometer and thermocouple. Background pressure of the chamber was maintained at 9×10^{-6} Torr during the growth. Growth was monitored by Reflection High Energy Electron Diffraction (RHEED) with electron energy of 20 keV.

There were three different series of experiments performed, which can be categorized as: 1)Deposition of fraction of a monolayer of Cr on N-polar GaN surface at 700 °C. 2) Deposition of fraction of a monolayer of Cr at room temperature on 1×1 N-polar GaN surface. 3) Cr doped GaN growth at substrate temperature of 700 °C. The details of the experimental procedure for all three experiments are following.

1) Cr deposition on GaN surface at 700 °C:

First Ga-rich N-polar GaN layer was grown on sapphire(0001) at a substrate temperature of 700 °C. Then growth was stopped and approximately 0.05ML of Cr was deposited on the GaN surface at 700 °C.

2) Cr deposition on 1×1 GaN at room temperature:

First approximately 2500 Å N-polar Ga-rich GaN layer was grown on sapphire(0001) substrate at a substrate temperature of 700 °C. Then sample was annealed to 800 °C for 10 minutes to remove all the Ga adatoms from the surface and achieved 1×1 surface when cooled to room temperature. Then approximately 0.1 monolayer (ML) of Cr was deposited at room temperature and subsequently STM studies were performed.

3) Cr doped GaN growth at sample temperature of 700 °C:

Ga-rich N-polar GaN layer (≈ 2500 Å) was grown on sapphire(0001) substrate at a sample temperature of 700 °C. Then Cr shutter was opened without stopping the growth. Cr/Ga flux ratio was set to ≈ 5% and growth was stopped after ≈ 3 monolayer of Cr-doped GaN was grown. Then surface was studied with *in situ* STM. In the second experiment in this series, approximately 4 ML of Cr-doped GaN was grown on MBE grown GaN surface on sapphire whereas Cr/Ga flux ratio was set to ≈ 20% and surface was studied with STM.

7.3 Results and Discussion

7.3.1 Ga-rich N-polar GaN($000\bar{1}$) Surface

N-polar Ga-rich GaN surface was scanned to observe the difference between MBE grown bare GaN surface and Cr-doped GaN surfaces. This sample was grown on sapphire(0001) substrate at sample temperature of 700 °C.

Show in Fig. 7.1(a-b) are the STM image and a schematic atomic model of the 3×3 reconstruction of N-polar GaN surface. The STM image was obtained at a sample bias of +1.5V and the tunneling current of 0.08nA. This reconstruction is commonly observed on the N-polar GaN surface and has been reported previously.[16, 25, 30] The 3×3 reconstruction is observed after the growth and after cooling the sample to below 300 °C. At higher temperatures Ga adatoms are in motion randomly and do not form a periodic 3×3 reconstructions but at lower temperature after the growth these adatoms arrange themselves in 3×3 ordering (where Ga adatoms are apart from each other by a distance three times the distance between Ga-Ga atoms of the underlying Ga adlayer (a_{Ga-Ga}).

Shown in Fig. 7.2(a-b) are the STM image and a schematic atomic model of the 6×6 reconstructions of the GaN($000\bar{1}$). The STM image was obtained at a sample bias of +2V and the tunneling current of 0.08nA. Both of these images shown in Fig. 7.1

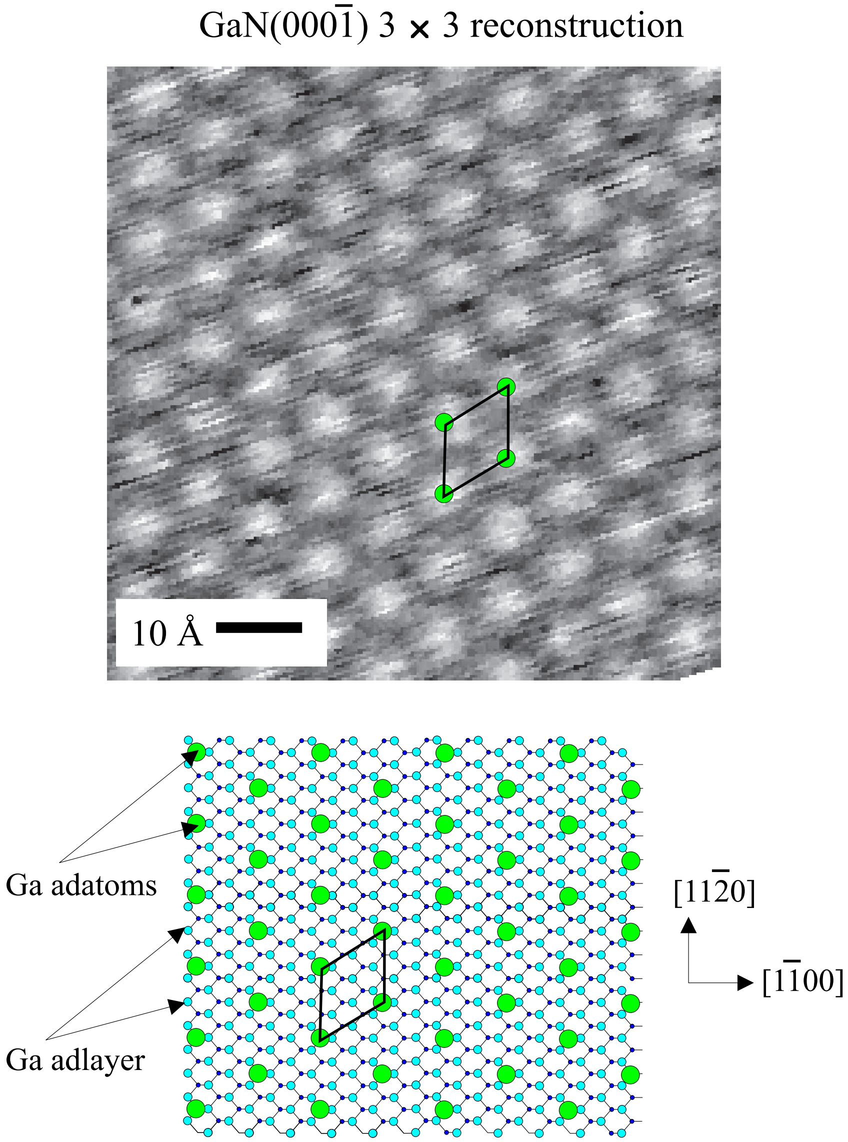

Figure 7.1: STM image of GaN(000$\bar{1}$) surface. a) 3×3 reconstruction image acquired at $V_S = +1.5$V and $I_t = 0.08$nA and b) A Schematic atomic model of 3×3 reconstruction.

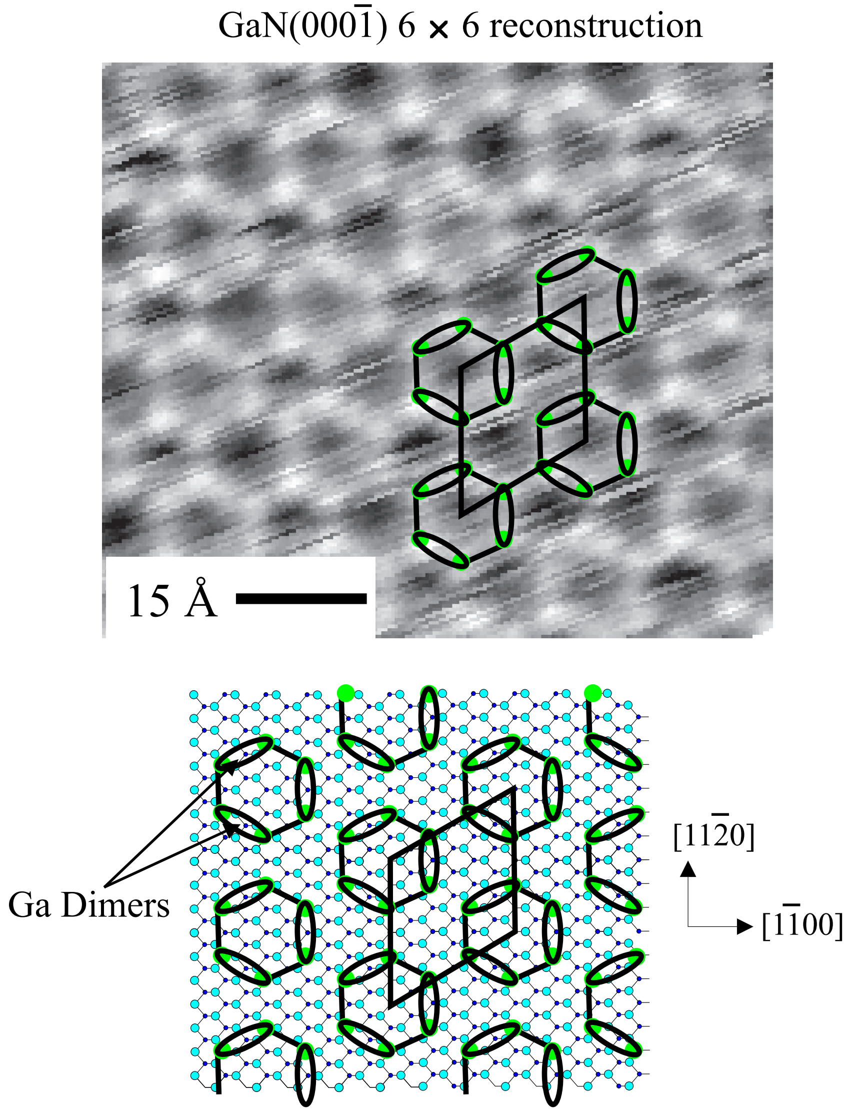

Figure 7.2: STM image of GaN(000$\bar{1}$) surface. a) 6×6 reconstruction image [V_S = +2V; I_t = 0.08nA]. and b) A Schematic atomic model of 3×3 reconstruction.

and Fig. 7.2 were obtained at the same sample surface. Some areas of the sample surface contain 3×3 and some areas contain 6×6 reconstructions. This ring like 6×6 reconstruction has also been reported extensively in the literature.[16, 25, 30]. Each ring consists of 6 Ga adatoms and each two adjacent Ga adatoms in the ring form a dimer as is shown in Fig. 7.2(b).

7.3.2 Cr deposition on GaN surface at T_s = 700 °C

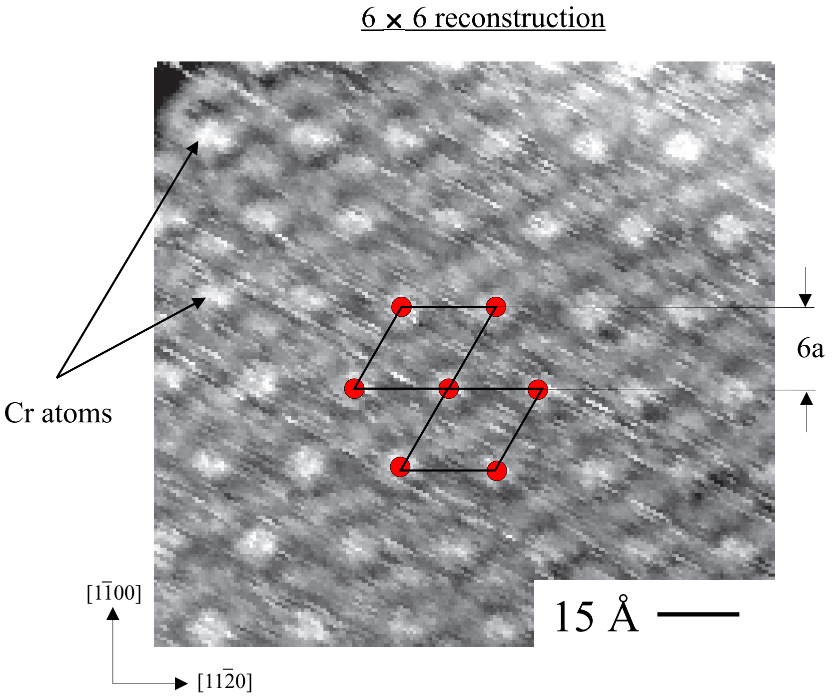

Figure 7.3: STM images of high temperature Cr deposited GaN($000\bar{1}$) surface, 6×6 reconstruction image where Cr atoms are apparent in the image [V_S = -1.5V; I_t = 0.08nA]

In this experiment, approximately 0.05ML of Cr was deposited on Ga-rich grown GaN surface at sample temperature of 700 °C. Shown in Fig. 7.3 is the room temperature STM image of the surface. This image was obtained at a sample bias of -1.5V and tunneling current of 0.08nA.

This reconstruction shown in Fig. 7.3 is a ring like reconstruction where these rings have a periodicity of 6a$_{Ga-Ga}$ hence forming a 6×6 reconstruction, which looks very similar to the GaN(000$\bar{1}$) 6×6 reconstruction. However, one of the 6 protrusions in the ring like structure appears brighter than the other 5 protrusions. As this unusual effect was not observed in the GaN 6×6 reconstruction so it can be inferred that this brighter protrusion is due to Cr atom which is substituting Ga position in this 6×6 arrangement of Ga adatoms.

We can conclude that Cr substitutes Ga lattice positions on the surface when deposited at sample temperature of 700 °C on Ga-rich GaN(000$\bar{1}$) surface.

7.3.3 Cr deposition on 1×1 GaN(000$\bar{1}$) adlayer at room temperature

In this experiment Ga-rich GaN was grown on sapphire(0001) at substrate temperature of 700 °C then growth was stopped and sample was annealed at 800 °C to remove all the Ga ad-atoms forming 3×3 and 6×6 reconstructions. When sample was cooled down to room temperature only 1×1 RHEED streaks were observed. Then Cr was deposited at room temperature on this 1×1 GaN adlayer.

Shown in Fig. 7.4 is the RHEED scan acquired in real time. As it can be seen from the RHEED pattern shown in Fig. 7.4 that before the Cr shutter was opened there was only 1×1 streaks of the GaN(000$\bar{1}$) surface. These streaks are due to the 1×1Ga ad-layer on the GaN surface. Then Cr shutter was opened for a very short time to deposit approximately 0.1 ML of Cr. As it can be seen that during the Cr deposition 3×3 streaks appear and these streaks stay on the surface even after the Cr shutter was closed. This is a direct evidence that this 3×3 reconstruction was formed by Cr atoms. Thus it can be inferred that Cr substitutes Ga atoms at least on the GaN surface.

The 3×3 reconstruction was observed when Cr deposition was performed at room temperature and disappears when temperature is slightly (above 100 °C) increased.

Moreover, this 3×3 reconstruction is irreversible, because when the temperature is reduced to room temperature then this reconstruction is not recovered. On the other hand, if we deposit more Cr then 3×3 appears again. So this is in a metastable state and when temperature is increased then either the Cr atoms form themselves into 1×1 reconstruction or simply accumulate and form clusters on the surface.

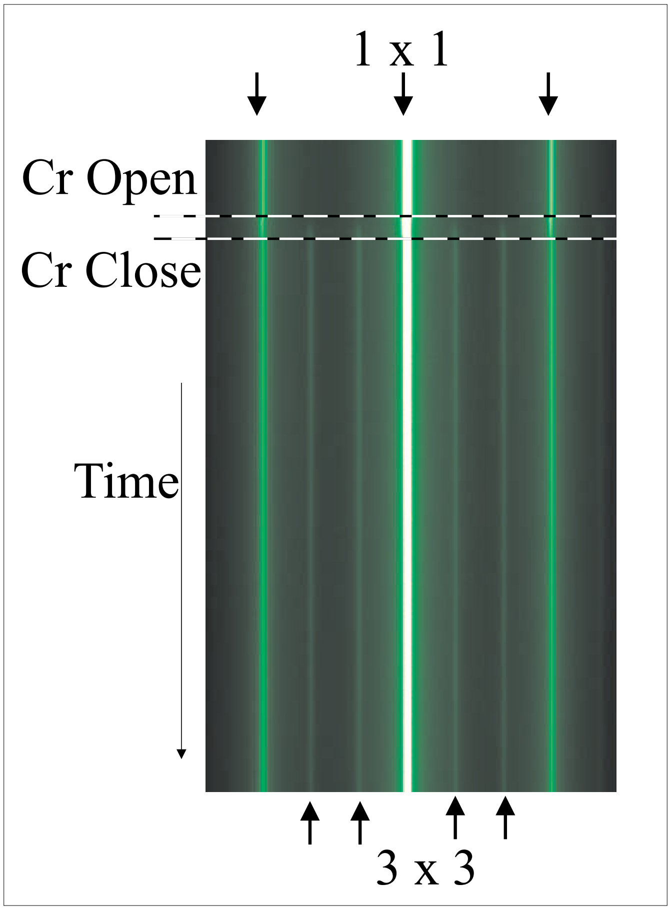

Figure 7.4: RHEED scan acquired during Cr deposition on 1×1 GaN surface at room temperature.

STM study was performed on this surface. Shown in Fig. 7.5 is the STM image of the 0.03 ML of Cr deposited GaN($000\bar{1}$) surface. This image shows 3×3 reconstruction. The image was obtained at a sample voltage of -1V and tunneling current was set to 0.09nA. This image is a clear proof in the real space of the 3×3 reconstruction observed in the RHEED pattern. Some bright spots on the surface can be attributed to some impurities which were deposited on the surface in the growth chamber, as the Cr deposition was performed at room temperature.

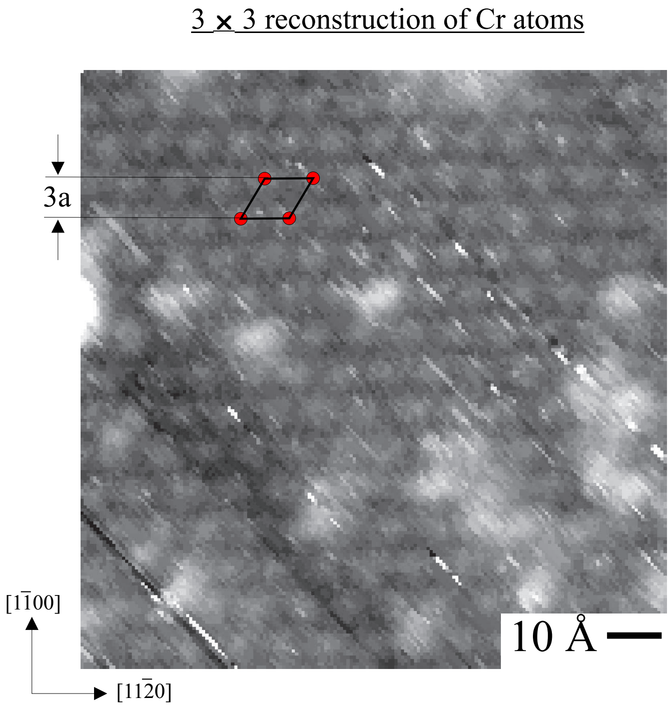

Figure 7.5: STM image of room temperature Cr deposited GaN(000$\bar{1}$) surface showing 3×3 surface reconstruction.[V_S = -1V; I_t = 0.09nA]

7.3.4 Cr-doped GaN(000$\bar{1}$)

Cr-doped GaN (CrGaN) sample was grown at Cr/Ga flux ratio of approximately 5% and substrate temperature of 700 °C. Shown in Fig. 7.6 is an STM image of the Cr-doped GaN surface. This image was obtained at sample bias of +1V and tunneling current of 0.08nA. This STM image shows 3×3 arrangement of atoms. This STM image appears similar to the GaN surface shown in Fig. 7.1(a) except there are some bright protrusions, which are highlighted by the circles around them. In the 3×3 reconstruction on the GaN surface, all the atomic protrusions have similar height and hence they appear equally bright. So this can be inferred that the bright protrusions appearing on the Cr-doped GaN surface are actually Cr atoms. These Cr atoms appear at the position of Ga atoms. This means that at least on the surface Cr occupies Ga lattice site in CrGaN growth.

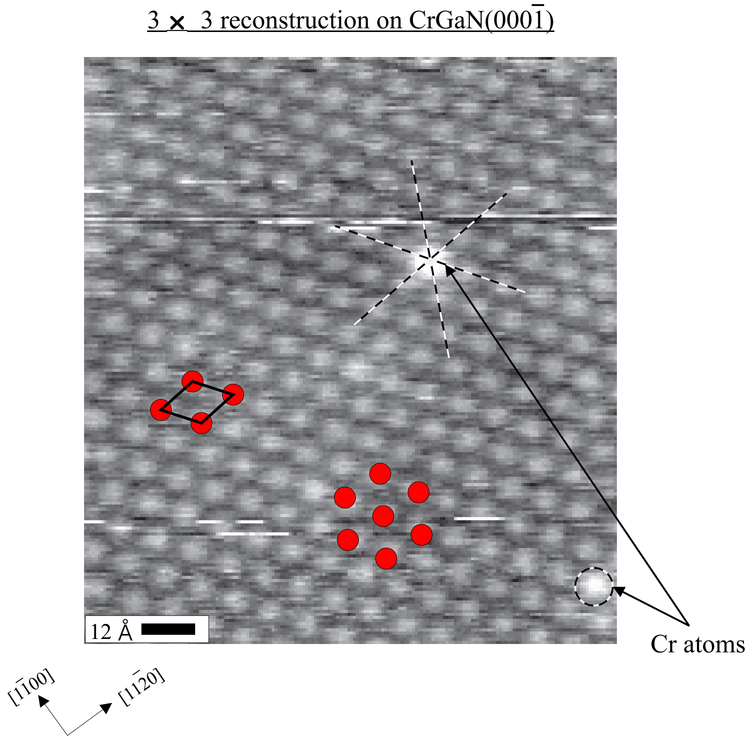

Figure 7.6: STM image of 5% Cr-doped GaN(000$\bar{1}$) surface, showing 3×3 reconstruction with apparent substitutional Cr atoms [$V_S = +1V$; $I_t = 0.08nA$]

As it can be seen from the STM image shown in Fig. 7.6 that there are fewer Cr atoms appearing in the image than the Cr/Ga flux ratio. Concentration of Cr was set to 5% of the Ga but this number is based on the Cr/Ga flux ratios. As CrGaN was grown at high temperature (700 °C) and at this temperature sticking coefficient of Cr is not equal to 1, i,e all of the Cr evaporated does not stick to the surface but some of it desorbs from the surface during the growth. Hence actual Cr/Ga ratio on the surface is smaller than their flux ratios.

7.3.5 STM studies of 20% Cr-doped GaN surface

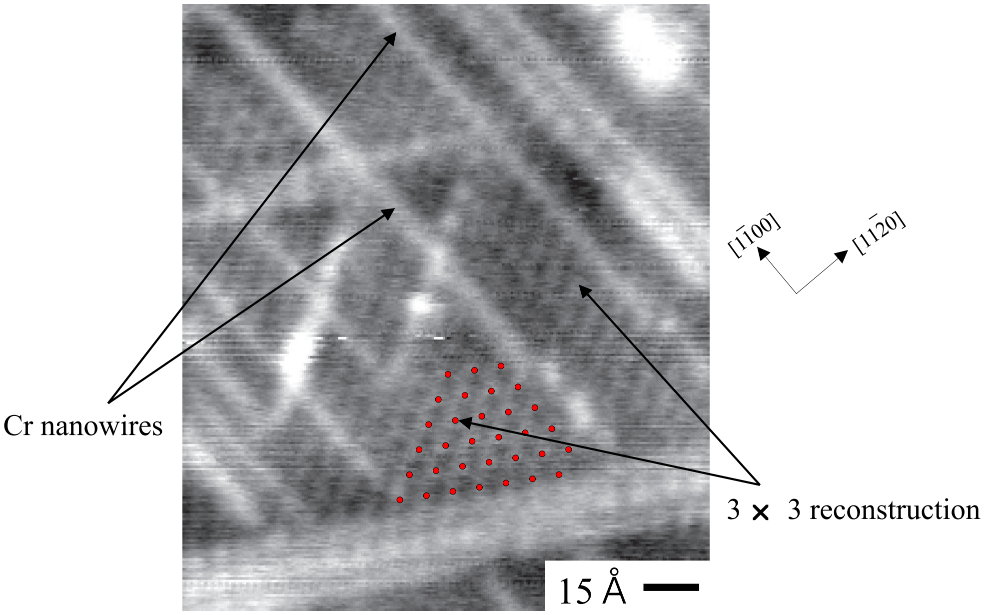

Figure 7.7: STM image of 20% Cr-doped GaN(000$\bar{1}$) surface, showing Cr nanowires [V_S = -1V; I_t = 0.08nA], with a schematic model of 3×3 reconstruction superimposed on the STM image.

In this experiment, about 4ML of CrGaN was grown on Ga-rich MBE grown GaN at sample temperature of 700 °C. Cr/Ga flux ratio was set to approximately 20%. Shown in Fig. 7.7 is the STM image of the surface. This image was obtained at a sample bias of -1V and tunneling current of 0.08nA. Cr segregation can clearly be seen on the surface in this image. Cr atoms arrange themselves in linear features, forming Cr nanowires. As shown in Fig. 7.7 these Cr nano linear features are formed along the high symmetry lines in the 3×3 reconstruction surface. In this study we could not determine conclusively that whether this 3×3 reconstruction observed on the surface was also formed by Cr atoms or Ga atoms. But the linear features formed on the surface are definitely a result of higher Cr concentration as these kind of features can not be found on the bare GaN surface regardless of the Ga/N flux ratio.

A schematic atomic model of the 3×3 reconstruction is superimposed on the STM image. It can be seen from this STM image that most of the Cr nanowires in the upper part of the image consist of single Cr atoms aligned linearly. Most of the Cr atoms forming these nanowires are commensurate with the perfect 3×3 reconstruction but some are displaced about a single lattice constant from the perfect 3×3 reconstruction. Most of these nanowires are several hundred Angstroms long.

7.4 Summary

It has been found that Cr substitutes Ga site at least on the surface of GaN lattice when Cr/Ga flux ratio is kept 5% and below. When Cr was deposited on the 1×1 GaN surface, Cr forms 3×3 reconstruction on the surface. At higher Cr/Ga concentration of 20%, Cr starts to form nano linear features on the surface of CrGaN layer.

Chapter 8

Conclusions

MnGaN thin films were grown on MOCVD GaN(0001)/Sapphire(0001) substrate at sample temperature of 550 °C by rf plasma molecular beam epitaxy. We have found that depending on the Ga/N flux ratio, MnGaN can be grown under three different growth conditions: 1) N-rich, 2) metal-rich, and 3) Ga-rich. Ga-rich growth condition result in microscopic precipitates and chemical inhomogeneity whereas N-rich growth conditions result in uniform Mn incorporation without precipitates. Although Mn is incorporated in metal-rich growth conditions but excess metal precipitates on the surface. Mn incorporation was estimated to be about 5% for N-rich and slight metal-rich growth conditions.

We have thus shown that either metal-rich or N-rich conditions are necessary for achieving substitutional Mn incorporation on the Ga sites. Metal-rich conditions result in films with better crystallinity compared with N-rich conditions, as determined by RBS channeling. This is presumed to be related to increased surface diffusion for the metal-rich case. Moreover, our AFM study finds that the smoothest surface morphologies occur for either Ga-rich conditions (not including the precipitates) or for slightly metal-rich conditions. Therefore, in order to provide both Mn incorporation on Ga sites and the smoothest surface morphology, it is concluded that the optimal growth conditions for Ga-polar MnGaN by rf N-plasma MBE are in the slightly metal-rich regime.

We also found that the Ga-polarity is maintained for N-rich, slightly metal-rich, and Ga-rich conditions. However, for increasingly metal-rich conditions (but not Ga-rich), the polarity is flipped, resulting in N-polarity. This is attributed to Mn building up and forming a Mn-rich surface atomic layer which leads to the inversion.

Magnetic properties of the MnGaN samples strongly depend on the growth conditions. N-rich growth results in two fairly large magnetic components, one of which has a transition temperature which exceeds 300K and the other is at $\sim$ 190 K. Slight metal-rich growth results in a single very small magnetic component with transition above 300K. Metal-rich growth results in a film with almost zero magnetization at 300K. Finally, Ga-rich growth results in a significant magnetization which is attributed to Mn_xGa_y or Mn_4N compounds. None of the samples discussed here had average values of magnetic moment as large as the theoretical predictions for Mn in GaN.

For DMS behavior, the most likely region based on this study is the N-rich growth regime where a significant magnetic moment is observed. Under N-rich conditions, ferromagnetic metal accumulation and polarity reversal are avoided. The magnetic results for the N-rich grown sample are interpreted as a combination of carrier-mediated ferromagnetism with $T_C \sim$ 190K and ferromagnetic clusters with T_C much greater than room temperature. Further studies are needed to verify the possibility of carrier-mediated ferromagnetism in this sample. For slight metal-rich and metal-rich growth, accumulates are observed although the magnetizations measured for these samples were very small; so, these accumulates do not appear to be ferromagnetic. For Ga-rich growth, the observed ferromagnetism is attributed to the properties of ferromagnetic Mn-rich accumulates which are clearly visible at the surface

CrGaN films were grown at substrate temperatures of 650 or 700 °C and Ga/N flux ratios from 0.65-1.0 with Cr/Ga of 0.03 or 0.05. Analysis of the results shows that both the magnetic and structural properties are dependent on the growth conditions. The growth parameter most directly affecting these properties is the surface gallium concentration, which indirectly depends on the substrate temperature as well as the incident Ga flux. We found that highly N-rich or Ga-rich conditions result in poor magnetic properties. Whereas, slightly N-rich or metal-rich conditions give ferromagnetic behavior at T at least up to 300K. Surface morphology is also strongly dependent on surface Ga concentration. N-rich conditions result in island-like plateau structure. Metal-rich conditions result in either island-like or partly interconnected plateau structure with small accumulates, and Ga-rich conditions result in interconnected plateau morphology also having accumulates. A fairly wide range of growth conditions showed good magnetic properties which are attributed not to second-phase ferromagnetic particles, but rather the observed FM behavior may be due to FM exchange interaction between magnetic Cr ions in the GaN semiconductor. Lastly, all growth conditions showed a 3×3 reconstruction upon sample cooling after growth, suggesting a smoothening effect of Cr.

Cubic GaN(001) has been grown under Ga-rich growth conditions on MgO(001) using rf N-plasma MBE. A family of surface reconstructions c(4×12), 4×7, c(4×16), 4×9, c(4×20), and 4×11, with Ga adatoms coverage of 0.208ML, 0.214ML, 0.219ML, 0.222ML, 0.225ML, and 0.227Ml respectively, were observed on Ga-rich grown c-GaN(001). Due to the fact that our MBE chamber is free of group V elements except N, these are intrinsic c-GaN(001) reconstructions. STM and STS shows that c-GaN(001)-c(4×16) and other reconstructions have metallic surface.

Bibliography

[1] T. Dietl, H. Ohno, F. Matsukura, J. Cibert, and D. Ferrand, Science **287**, 1019 (2000).

[2] T. Zhang, N. Takahashi, M. Spangenberg, T.-H. Shen, E. A. Seddon, D. Greig, and J. A. D. Matthew, Surf. Sci. **193**, 217 (2002).

[3] A. Filipe, A. Schuhl, and P. Galtier, Appl. Phys. Lett. **70**, 129 (1997).

[4] A. Filipe, and A. Schuhl, J. Appl. Phys. **81**, 4359 (1997).

[5] S. Sonoda, S. Shimizu, T. Sasaki, Y. Yamamoto, and H. Hori, J. Crystal Growth **237**, 1358 (2002).

[6] M. L. Reed, N. A. El-Masry, H. H. Stadelmaier, M. K. Ritums, M. J. Reed, C. A. Parker, J. C. Roberts, and S. M. Bedair, Appl. Phys. Lett. **79**, 3473 (2001).

[7] G. T. Thaler, M. E. Overberg, B. Gila, R. Frazier, C. R. Abernathy, S. J. Pearton, J. S. Lee, S. Y. Lee, Y. D. Park, Z. G. Khim, J. Kim, and F. Ren, Appl. Phys. Lett. **80**, 3964 (2002).

[8] M. E. Overberg, C. R. Abernathy, S. J. Pearton, N. A. Theodoropoulou, K. T. McCarthy, and A. F. Hebard, Appl. Phy. Lett. **79**, 1312 (2001).

[9] Y. Cui and L. Li, Appl. Phys. Lett. **80**, 4139 (2002).

[10] H. Yang, H. Al-Brithen, A. R. Smith, J.A. Borchers, R.L.Cappelletti, and M.D. Vaudin, **78**, 3860 (2001).

[11] G. Kreiner and H. Jacobs, J. Alloys Compd. **183**, 345 (1992).

[12] A. Leineweber, R. Niewa, H. Jacobs, and W. Kockelm Ann, J. Mater. Chem. **10**, 2827 (2000).

[13] M. Tabuchi, M. Takahashi, and F. Kanamaru, J. Alloys Compd. **210**, 143 (1994).

[14] H. Yang, H. Al-Brithen, A. R. Smith, E. Trifan, and D. C. Ingram, J. Apply. Phys. **91**, 1053 (2002).

[15] R. Held, D. E. Crawford, A. M. Johnson, A. M. Dabiran, and P. I. Cohen, J. Electron. Mater. **26**, 272 (1997).

[16] A. R. Smith, R. M. Feenstra, D. W. Greve, J. Neugebauer, and J. E. Northrup, Phys. Rev. Lett. **79**, 3934 (1997).

[17] R. M. Feenstra, H. Chen, V. Ramachandran, C. D. Lee, A. R. Smith, J. E. Northrup, T. Zywietz, J. Neugebauer, and D. W. Greve, Surface Rev. Lett. **7**, 601 (2000).

[18] J. E. Northrup, J. Neugebauer, R. M. Feenstra, and A. R. Smith, Phys. Rev. B **61**, 9932 (2000).

[19] Kazunori Sato, and Hiroshi Katayama-Yoshida, Jpn. J. appl. Phys. **40**, L485 (2001).

[20] J. S. Lee, J. D. Lim, Z. G. Khim, and Y. D. Park, J. Appl. Phys. **93**, 4512 (2003).

[21] S. E. Park, H. J. Lee, Y. C. cho, and S. Y. Jeong, Appl. Phys. Lett. **80**, 4187 (2002).

[22] M. Hashimoto, Y. K. Zhou, M. Kanamura, H. Katayama-Yoshida, and H. Asahi, J. Crystal Growth **251**, 327 (2003).

[23] H. X. Liu, S. Y. Wu, R. K. Singh, L. Gu, N. R. Dilley, L. Montes, and M. B. Simmonds, Appl. Phys. Lett. **85**, 4076 (2004).

[24] R. M. Feenstra, Phys. Rev. B50(7), (1994) 4561.

[25] A. R. Smith, V. Ramachandran, R. M. Feenstra, D. W. Greve, M.-S. Shin, M. Skowronski, J. Neugebauer, and J. E. Northrup, J. Vac. Sci. Technol. A **16**, 1641 (1998).

[26] E. J. Tarsa, B. Heying, X. H. Wu, P. Fini, S. P. DenBaars, and J. S. Speck, J. Appl. Phys. **82**, 5472 (1997).

[27] R. A. Held, G. Nowak, B. E. Ishaug, S. M. Seutter, A. Parkhomovsky, A. M. Dabiran, P. I. Cohen, I. Grzegory, and S. Porowski, J. Appl. Phys. **85**, 7697 (1999).

[28] B. Heying, E. J. Tarsa, C. R. Elsass, P. DenBaars, and J. S. Speck, J. Appl. Phys. 85 (1999) 6470 .

[29] T. Zywietz, J. Neugebauer, and M. Scheffler, Appl. Phys. Lett. **73(4)**, 487 (1998).

[30] A. R. Smith, R. M. Feenstra, D. W. Greve, J. Neugebauer, and J. E. Northrup, Appl. Phys. A **66**, S947 (1998).

[31] S. Strite, J. Ruan, Z. Li, A. Salvador, H. Chen, David J. Smith, W. J. Choyke, and H. Morkoç, J. Vac. Sci. Technol. **B** 9 (4), Jul/Aug (1991) 1924.

[32] O. Brandt, H. Yang, B. Jenichen, Y. Suzuki, L. Däweritz, and K. H. Ploog, Phys. Rev. B 52 (1995) R2253.

[33] Akihiko Kikuchi, Hiroyuki Hoshi, and Katsumi Kishino, Jpn. J. Appl. Phys. 34 (1995) 1153.

[34] H. Okumura, K. Ohta, G. Feuillet, K. Balakrishnan, S. Chichibu, H. Hamaguchi, P. Hacke, and S. Yoshida, J. Cryst. Growth 178 (1997) 113.

[35] M. Wassermeier, A. Yamada, H. Yang, O. Brandt, J. Behrend, and K. H. Ploog, Surf. Sci. 385 (1997) 178.

[36] M. Wassermeier, H. Yang, O. Brandt, A. Yamada, J. Behrend, and K. H. Ploog, Appl. Surf. Sci. 123/124 (1998) 181.

[37] D. Wang, S. Yoshida, and M. Ichikawa, Appl. Phys. Lett **80** (2002) 2472.

[38] G. Feuillet, H. Hamaguchi, K. Ohta, P. Hacke, H. Okumura, and S. Yoshida, Appl. Phys. Lett. **70** (1997) 1025.

[39] G. Feuillet, H. Hamaguchi, H. Okumura, and S. Yoshida, Mat. Sci. Engi. **B**59 (1999) 80.

[40] Min-Ho Kim, F. S. Juang, Y. G. Hong, C. W. Tu, and Seong-Ju Park, J. Crystal Growth, 251 (2003) 465.

[41] R. C. Powell, N.-E. Lee, Y.-W. Kim, and J. E. Greene, J. Appl. Phys. **73** (1992) 189.

[42] J. Neugebauer, T. Zywietz, M. Scheffler, J. E, Northrup, and C. G. Van de Walle, Phys. Rev. Lett. 80 (1998) 3097.

[43] B. K. Rao and P. Jena, Phys. Rev. Lett. **89(18)**, 185504 (2002).

[44] E. Kulatov, H. Nakayama, H. Mariette, H. Ohta, and Y. A. Uspenskii, Phys. Rev. B **66**, 045203 (2002).

[45] L. Kronik, M. Jain, and J. R. Chelikowsky, Phys. Rev. B **66**, 041203(R) (2002).

[46] S. Kuwabara, K. Ishii, S. Haneda, T. Kondo, and H. Munekata, Physica E **10**, 233 (2001).

[47] M. Zając, J. Gosk, M. Kamińska, A. Twardowski, T. Szyszko, and S. Podsiadło, Appl. Phy. Lett. **79**, 2432 (2001).

[48] M. Zając, R. Doradziński, J. Gosk, J. Szczytko, M. Lefeld-Sosnowska, M. Kamińska, A. Twardowski, M. Palczewska, E. Grzanka, and W. Gębicki, Appl. Phy. Lett. **78**, 1276 (2001).

[49] S. Kuwabara, T. Kondo, T. Chikyow, P. Ahmet, and H. Munekata, Jpn. J. Appl. Phys. **40**, L724 (2001).

[50] S. Sonoda, H. Hori, Y. Yamamoto, T. Sasaki, M. Sato, S. Shimizu, K.-I. Suga, and K. Kindo, IEEE Trans. on Mag. **38(5)**, 2859 (2002).

[51] A. R. Smith, R. M. Feenstra, D. W. Greve, M.-S. Shin, M. Skowronski, J. Neugebauer, and J. E. Northrup, Surf. Sci. **423**, 70 (1999).

[52] A. R. Smith, R. M. Feenstra, D. W. Greve, M.-S. Shin, M. Skowronski, J. Neugebauer, and J. E. Northrup, Appl. Phys. Lett. **72(17)**, 2114 (1998).

[53] V. Ramachandran, R. M. Feenstra, W. L. Sarney, L. Salamanca-Riba, J. E. Northrup, L. T. Romano, and D. W. Greve, Appl. Phys. Lett. **75**, 808 (1999).

[54] L. R. Doolittle, Nucl. Inst. Meth. **B9**, 334 (1985).

[55] National Compound Semiconductor Roadmap, http://ncsr.csci-va.com.

[56] K. Sato and H. Katayama-Yoshida, Semicond. Sci. Technol. **17**, 367 (2002).

[57] M. Tanaka, J. P. Harbison, T. Sands, B. Philips, T. L. Cheeks, J. De Boeck, L. T. Florez, and V. G. Keramidas, Appl. Phys. Lett. **63(5)**, 696 (1993).

[58] K.-M. Ching, W.-D. Chang, and T.-S. Chin, Appl. Surf. Sci. **92**, 471 (1996).

[59] H. Ohno, Science **281**, 951 (1998).

[60] M. B. Haider, C. Constantin, H. Al-Brithen, H. Yang, E. Trifan, D. Ingram, A. R. Smith, C. V. Kelly and Y. Ijiri, J. Appl. Phys. **93**, 5274 (2003).

[61] G. P. Das, B. K. Rao, and P. Jena, Phys. Rev. B, **68**, 035207-1(2003)

[62] K. H. Ploog, S. Dhar, and A. Trampert, J. Vac. Sci. Technol. B **21**(4), 1756(2003)

[63] E. Monroy, E. Sarigiannidou, F. Fossard, N. Gogneau, E. Bellet-Amalric, J.-L. Rouvire, S. Monnoye, H. Mank, and B. Daudin , Appl. Phys. Lett. **84**, 3684 (2004).

[64] C. Constantin, M. B. Haider, A. R. Smith, Appl. Phys. Lett. **85**, 6371 (2004).

[65] H. Al-Brithen, H. Yang, A. R. Smith, J. Appl. Phys. **96**, 3787 (2004).

[66] M. B. Haider, H. Al-Brithen, R. Yang, C. Constantin, D. Ingram, and A. R. Smith, accepted for publication in J. Crystal Growth (2005).

Appendix A

List of Publications

- Room Temperature Ferromagnetism in CrGaN: Dependence on Growth Condition in rf N-Plasma Molecular Beam Epitaxy., **Muhammad B. Haider**, Hamad Al-Brithen, Rong Yang , Costel Constantin, David Ingram, and Arthur R. Smith, Accepted in Journal of Crystal Growth: August, (2005)
- Scanning Tunneling Microscopy and Surface Simulation of Zinc-blend GaN(001) Intrinsic 4× reconstruction: Linear Gallium Tetramers? , Hamad A. AL-Brithen, Rong Yang, **Muhammad B. Haider**, Costel Constantin, Erdong Lu, Nancy Sandler, Arthur R. Smith, and Pablo Ordejon. Accepted in Phys. Rev. Lett. August, (2005)
- Dependence of Magnetic Properties on the Growth Conditions of MnGaN Grown by rf N Plasma Molecular Beam Epitaxy., **Muhammad B. Haider**, Costel Constantin, Hamad Al-Brithen, Gabriel Caruntu, Charles J. O'Connor, and Arthur R. Smith, Physica Status Solidi (a) 202, 1135-1144 (2005).
- Scanning Tunneling Microscopy Study of the Structural Phase Transformation in Manganese Nitride: θ-MnN to η-Mn_3N_2, Rong Yang, **Muhammad B. Haider**, Haiqiang Yang, Hamad Al-Brithen, and Arthur R. Smith. Applied Physics A 81, 695 (2005)
- ScGaN Alloy Growth by Molecular Beam Epitaxy: Evidence for a Metastable Layered Hexagonal Phase., Costel Constantin, Hamad Al-Brithen, **Muham-**

mad B. Haider, David Ingram, and Arthur R. Smith, Phys. Rev. B. 70, 193309 (2004)

- Metal/Semiconductor Phase Transition in Chromium Nitride(001) grown by rf-plasma assisted Molecular Beam Epitaxy., Costel Constantin, **Muhammad B. Haider**, David Ingram, and Arthur R. Smith, Applied Physics Letter: 85, 6371 (2004).

- Mixing Rocksalt and Wurtzite Structure Binary Nitrides to Form Novel Ternary Alloys ScGaN and MnGaN., Costel Constantin, Hamad Al-Brithen, **Muhammad B. Haider**, David Ingram, and Arthur R. Smith, Material Research Society Symposium Proceedings. 799, Z9.5.1-Z9.5.6, (2004)

- Ga/N flux ratio influence on Mn incorporation, surface morphology, and lattice polarity during radio frequency molecular-beam epitaxy of (Ga,Mn)N, **Muhammad B. Haider**, Costel Constantin, Hamad Al-Brithen, Haiqiang Yang, Eugen Trifan, David Ingram, Arthur R. Smith, C.V. Kelly and Y. Ijiri, J. Appl. Phys. 93, 5274, (2003)

Appendix B

List of Contributed Talks and Posters in Conferences

- Scanning Tunneling Microscopy Study of GaCrN Grown by MBE, **Poster Presentation** AVS 51st Internation Symposium and Exhibition, Anaheim, CA, Nov 2004,
- Molecular Beam Epitaxial Growth and Surface Analysis using Scanning Probe Microscopy of GaCrN, **Oral Presentation**, International Workshop on Nitride Semiconductors (IWN-04), Pittsburgh, PA, Jul 2004
- Scanning Tunneling Microscopy Study of III-V Dilute Magnetic Semiconductor (Ga,Cr)N, **Oral Presentation**, 9th joint MMM/InterMag, Anaheim, CA, Jan 2004.
- Growth Regimes of (Ga,Mn)N during rf MBE and their effect on the Alloy Formation, **Oral Presentation**, APS March Meeting, Austin, TX, March 2003.
- Advantage of Nitrogen-Rich Growth for Incorporation of Manganese into GaN using RF-Molecular Beam Epitaxy, **Oral Presentation**, 47th Magnetism and Magnetic Materials Conference (MMM), Tampa, FL, NOV 2002.

- Scanning Tunneling Microscopy Study of III-V Dilute Magnetic Semiconductor (Ga,Cr)N, **Oral Presentation**, 9th joint MMM/InterMag, Anaheim, CA, Jan 2004.